Chapter – 6

Novel substituted isoindolinones derived from Lawsone: Synthesis, Characterization, DFT and biological studies

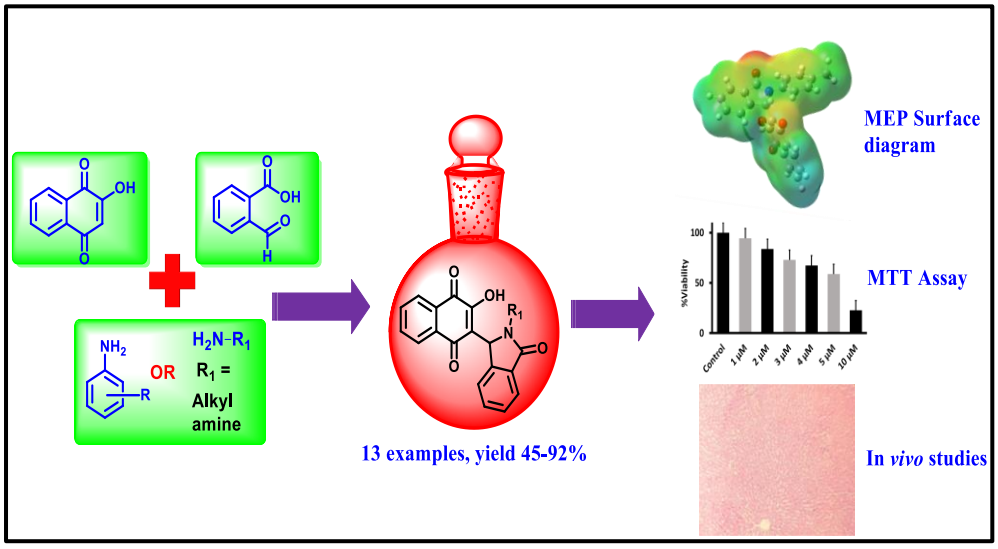

Published in *J. Mol. Struct.*, 2022, *50*, 1267, 133601

6.1 Introduction

Isoindolinone skeleton is ubiquitous in many natural and synthetic products with various biological activities as shown in figure **1** [1–3]. These isoindolinone scaffolds tend to possess a broad range of biological activities such as antihypertensive, anti-inflammatory, anesthetic, antiviral, and anticancer [4–9]. Inspired by this fact, the synthesis of isoindolinone derivatives has attracted much attention during the past few decades. The traditional methods to synthesize substituted isoindolinone derivatives are mainly restricted to use of Wittig reaction, Grignard reagents, Heck cyclization, reduction process, Gabriel approach, lithiation process, Dies alder approach, and various enantioselective methods **(scheme 6.1)** [10–16]. These methods are generally associated with several drawbacks such as multistep procedures, high temperature, use of expensive noble metal catalysts, and toxic or inflammable solvents. Therefore, the development of a simple, efficient, and environmentally friendly protocol for the synthesis of isoindolinone is highly desirable [17].

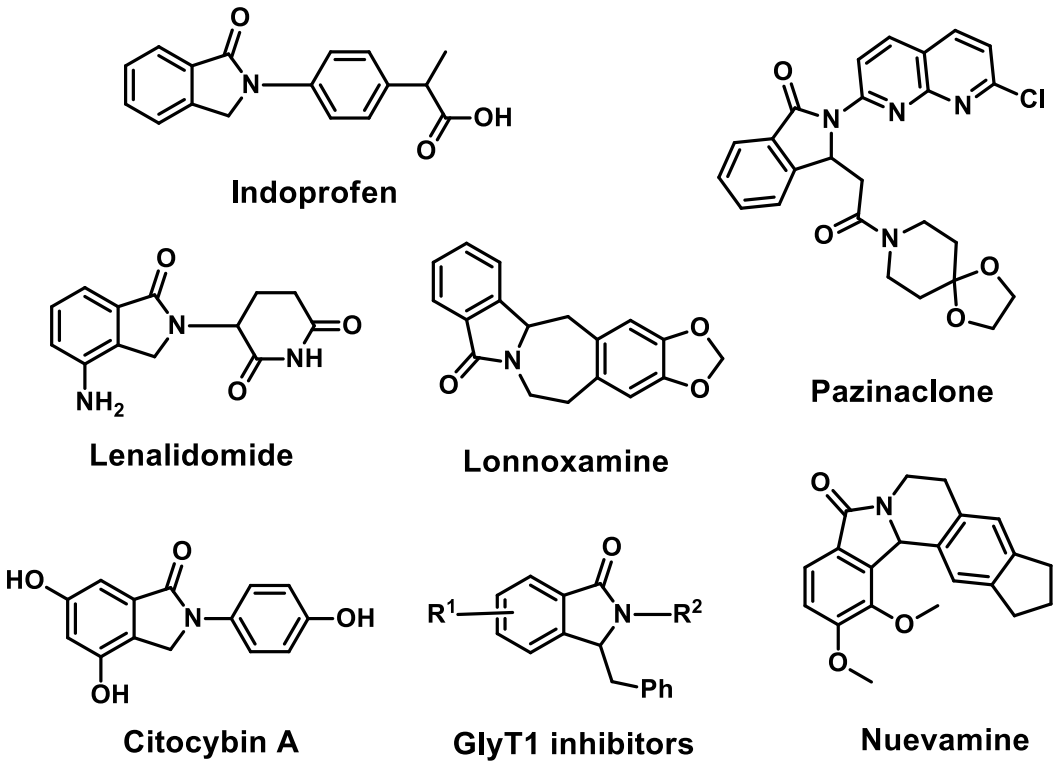

Figure 6.1 Examples of natural and synthetic biologically active isoindolinone motifs.

The multicomponent reaction strategy has recently attracted increasing attention for organic synthesis and pharmaceutical industries for the construction of complex molecules [18,19]. A similar one pot three-component reaction of 2-formyl benzoic acid with a variety of nucleophiles and primary amines also provides a direct approach toward the synthesis of isoindolinone derivatives as shown in **scheme 6.1.** However**,** these methods report the use of high temperatures, expensive catalysts, or microwave heating [16,17,20,21].

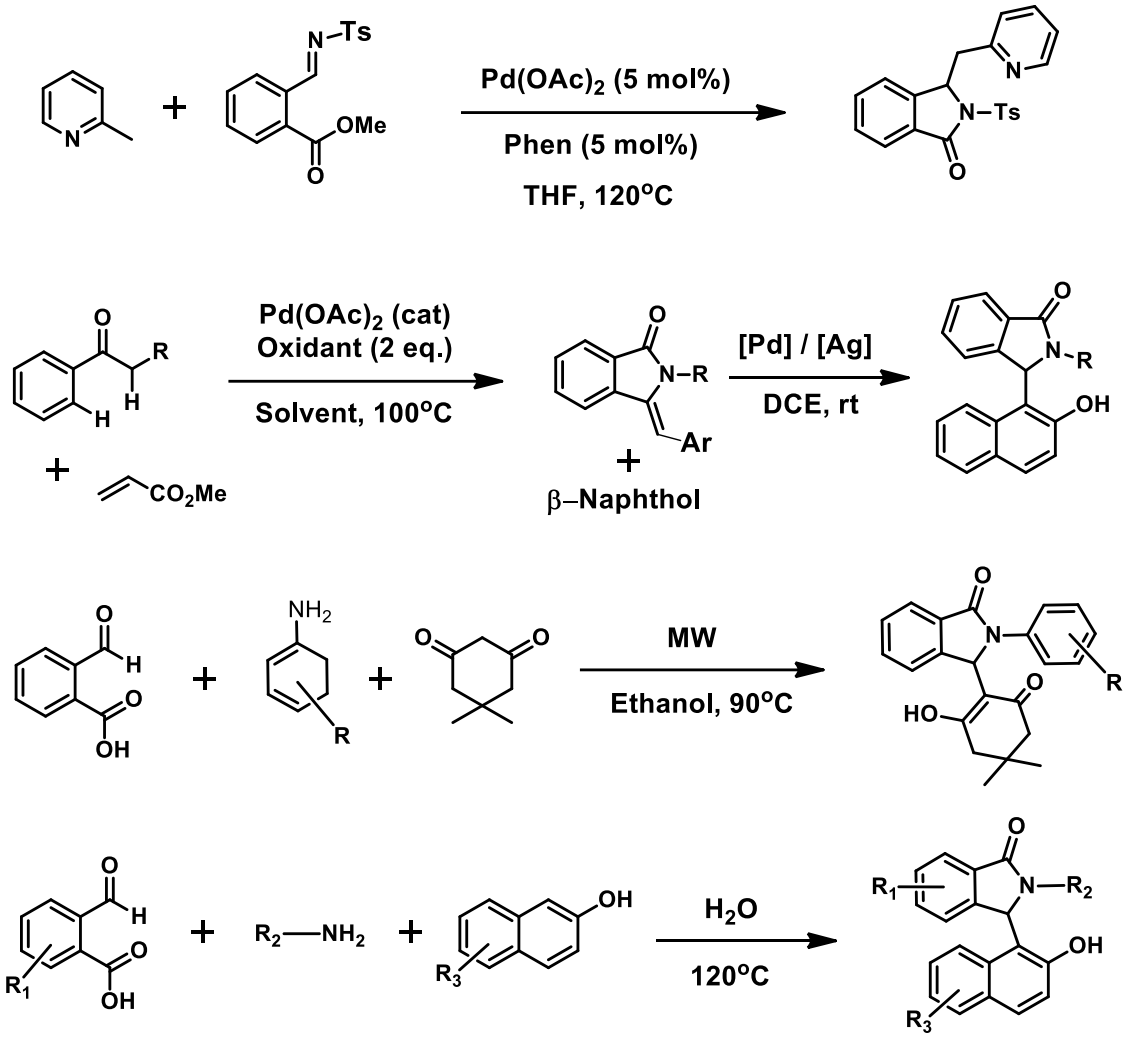

Scheme 6.1 Synthetic approaches to substituted isoindolinones.

Recently we have reported mannich bases synthesized derived from biologically important 2-hydroxy-1,4-naphthoquinone (Lawsone), using multicomponent reaction, for potential anticancer activity on HepG2 cell lines (Human liver cancer cell line) [22,23]. Given the importance of the isoindolinone skeleton, it is desirable to establish a practical method to synthesize isoindolinone derived from lawsone employing environment-friendly reaction media and investigating their biological activity.

In recent days, computational methods have been promoted as a valid tool for the prediction of pharmacokinetic parameters such as adsorption, distribution, metabolism, and excretion (ADME) when chemical structures are numerous [24]. Density function theory (DFT) is a powerful computing tool for revealing the complete molecular structure, stability, and global reactivity parameters of biomolecules such as dipole moment, electrophilicity (ω), electronegativity (χ), chemical potential (μ), softness (S), hardness (η), and electron affinity (A) [25–27]. The DFT calculations of title compounds have not yet been reported.

Herein we report the synthesis of substituted isoindolinone derivatives via a three-component Mannich-cascade cyclization reaction of lawsone, 2-formyl benzoic acid, and primary amines in presence of acetic acid as a catalyst at room temperature with moderate to high yields. The formation of desired product was confirmed by various analytical techniques such as ^{1}H NMR, ^{13}C NMR, FT-IR, and Mass spectroscopy. In addition, DFT calculations of synthesized compounds were performed to determine molecular structure, dipole moment, Molecular Electrostatic Potential (MEP) maps, and global reactivity parameters. Further, in *vitro* anticancer activity of selected compounds was evaluated against HepG2 (Human liver carcinoma cell lines) employing MTT assay. The compounds with promising activity were further investigated by molecular docking on Alpha fetoprotein (AFP), and finally, by in *vivo* studies.

6.2 Results and Discussions

6.2.1 Synthesis of isoindolinones

Lawsone **1** (1.0 mmol), 4-methyl aniline **2a** (1.1 mmol), and 2-formyl benzoic acid **3** (1.0 mmol) was used as the model substrates to prepare desired substituted isoindolinone **4a.** As shown in **table 6.1**, the reaction proceeded smoothly at room temperature affording the desired product 4a in 80% isolated yield without using a catalyst **(table 6.1, entry 1).** Encouraged by this result, we further screened different common organic solvents such as methanol, tetrahydrofuran, dichloromethane, chloroform, acetone, and acetonitrile to find a suitable solvent to promote the model reaction. Lower isolated yields of 4a were obtained when the reaction was performed in these solvents **(table 6.1, entry 2-7).** When water was used instead of organic solvents to synthesize 4a, only a trace amount of product was isolated **(table 6.1, entry 8).** When reaction was carried out under reflux conditions, the isolated yield of compound **4a** was decreased to 56%, even on extending

the reaction time up to 24 h **(Table 6.1, entry 9).** Furthermore, it was observed that when 5 mol% acetic acid was added to the reaction mixture, the yield of corresponding isoindolinone **4a** significantly increases to 92% **(table 6.1, entry 10).** There was no improvement in yield when 5 mol% PTSA was added to the reaction mixture **(table 6.1, entry 11)**. Thus optimized reaction conditions are as follows: lawsone **1** (1.0 mmol), 4-methyl aniline **2a** (1.1 mmol), and 2-formyl benzoic acid **3** (1.0 mmol) in ethanol at room temperature for 20 h in presence of 5 mol% acetic acid **(table 6.1, entry 10).**

Table 6.1 Optimization of reaction conditions[a]

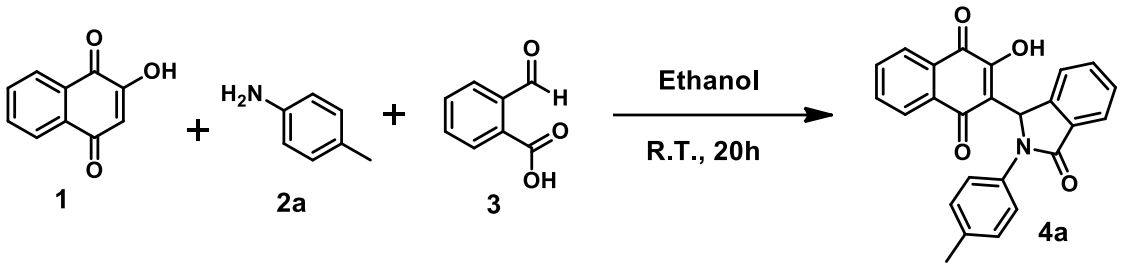

Entry	Solvent	Time (h)	Yield (%)[b]
1	Ethanol	20	81
2	Methanol	20	61
3	Tetrahydrofuran	22	51
4	Dichloromethane	24	72
5	Chloroform	24	70
6	Acetone	21	16
7	Acetonitrile	22	41
8	Water	24	Trace
9	Ethanol[c]	24	56
10	**Ethanol[d]**	**20**	**92**
11	Ethanol[e]	20	79

[a] Reaction conditions: Lawsone (**1**) (1.0 mmol), 4-methyl aniline (**2a)** (1.1 mmol), 2-formyl benzoic acid **(3)** (1.0 mmol), Solvent (5 mL) at room temperature

[b] Yield of isolated product.

[c] Reaction was performed under reflux condition.

[d] Acetic acid (5 mol%) was used as a catalyst.

[e] PTSA (5 mol%) was used as a catalyst.

Isoindolin-1-yl-naphthalene-1,4-dione **4a** was characterized using various spectral studies. The yellow solid showed a molecular ion peak at 396.17 in the ESI-MS spectrum, consistent with molecular formula $C_{25}H_{17}NO_4$. The FT-IR spectrum of **4a** showed bands for hydroxyl and conjugated carbonyl functional groups at 3399 cm^{-1} and 1680 cm^{-1} respectively. While the bands for carbonyl of isoindolinone and naphthoquinone was observed at 1625 cm^{-1} and 1680 cm^{-1} respectively.

^{1}H NMR spectrum indicates one methyl group at δ 2.63 ppm. A singlet was also observed at δ 6.86 ppm due new bond formed between aldehyde, amine, and lawsone. The eight protons of naphthoquinone and aromatic aldehyde appear in δ 7.1-8.3 ppm region as double doublet (dd), and triplet of doublet (td). They were confirmed by their coupling constant values (J) as reported in the literature [23]. The ^{13}C NMR spectra showed three peaks at δ 168.01, 180.48, and 184.01 corresponding to the isoindolinone and naphthoquinone carbonyl group. The methyl group was observed at δ 20.91 ppm, while one aliphatic tertiary carbon near to amide nitrogen was observed at δ 55.58 ppm. All other aromatic carbons were observed in aromatic region δ 118 to 154 ppm. On the spectral evidence, **4a** was confirms to be 2-hydroxy-3-(3-oxo-2-(p-tolyl)isoindolin-1-yl)naphthalene-1,4-dione**.** Similar trend was observed for all other compounds.

After determining optimized reaction conditions, we next examined a range of primary amines **2a-2m** to test the scope of one pot three-component reaction with Lawsone **(1)** and 2-formyl benzoic acid **(3).** As shown in t**able 6.2**, various primary amines including substituted aryl amines, heteroaryl-alkylamines, and alkyl amines were for reaction. Aryl amine substituted with methyl, chloro, bromo, and fluoro groups **(table 6.2, entry 1-7)** provided the corresponding isoindolinone products **4a-4g** in good to excellent yield (79-92%). Apart from aryl amines, benzyl amine, 2-furfuryl amine, tryptamine, and thiophene-2-ethyl amine **(table 6.2, entry 8-11)** also successfully afforded the corresponding isoindolinone **4i-4k** good to high yields (62-78%). We further examined the reaction with common aliphatic amines like n-butyl amine and n-octylamine **(table 6.2, entry 12 & 13).** These amines successfully gave desired product **4l** and **4m** respectively. However, the reaction of n-butyl amine gave corresponding product **4l** in only 45% yield **(table 6.2, entry 12).** When 2-picolyl amine and 2-amino pyridine were used as a substrate, the desired product was not observed even on reflux conditions **(table 6.2, entries 14 & 15).**

Table 6.2 Scope of amines[a]

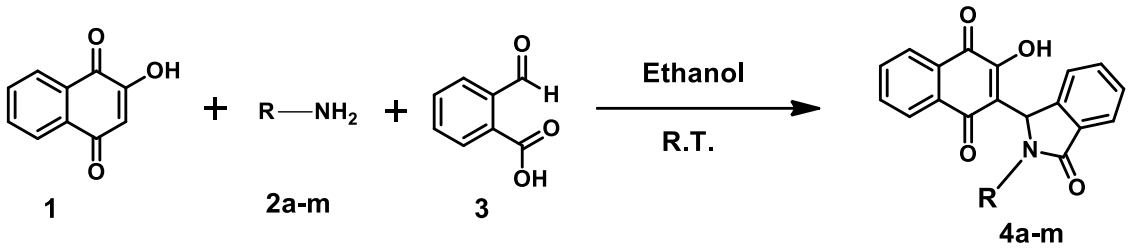

Entry	R	Product	Yield (%)[b,c]
1	4-MeC_6H_5	4a	92 ± 0.60
2	4-MeOC_6H_5	4b	91 ± 0.85
3	C_6H_5	4c	80 ± 1.1
4	4-ClC_6H_5	4d	83 ± 1.2
5	4-BrC_6H_5	4e	79 ± 1.4
6	3-Cl-4F-C_6H_5	4f	83 ± 1.2
7	3,4-$(Me)_2C_6H_5$	4g	81 ± 1.5
8	$C_6H_5CH_2$	4h	78 ± 1.8
9	Furfuryl	4i	62 ± 1.7
10	Tryptamine	4j	65 ± 0.90
11	Thiophene-2-ethyl	4k	68 ± 1.5
12	n-butyl	4l	75 ± 2.1
13	n-octyl	4m	70 ± 1.3
14	2-picolyl [d]	-	0
15	2-pyridinyl [d]	-	0

[a] Reaction conditions: Lawsone (**1**) (1.0 mmol), 4-methylaniline (**2a)** (1.1 mmol), 2-formyl benzoic acid **(3)** (1.0 mmol), Solvent (5 mL), Acetic acid (5 mol%) at room temperature

[b] Yield of isolated product.

[c] n = 3 (experiments were performed in triplicates).

[d] At reflux (80 ^oC).

Based on the literature precedents, a plausible reaction mechanism was proposed and shown in **scheme 6.2**. Initially 2-formyl benzoic acid **3** condensed with amine **2a** to generate intermediate **A,** followed by Mannich type reaction of Lawsone with activated

iminium intermediate **A,** to give intermediate **B**. It further undergoes subsequent re-aromatization and intramolecular cyclization to form final product **4a.**

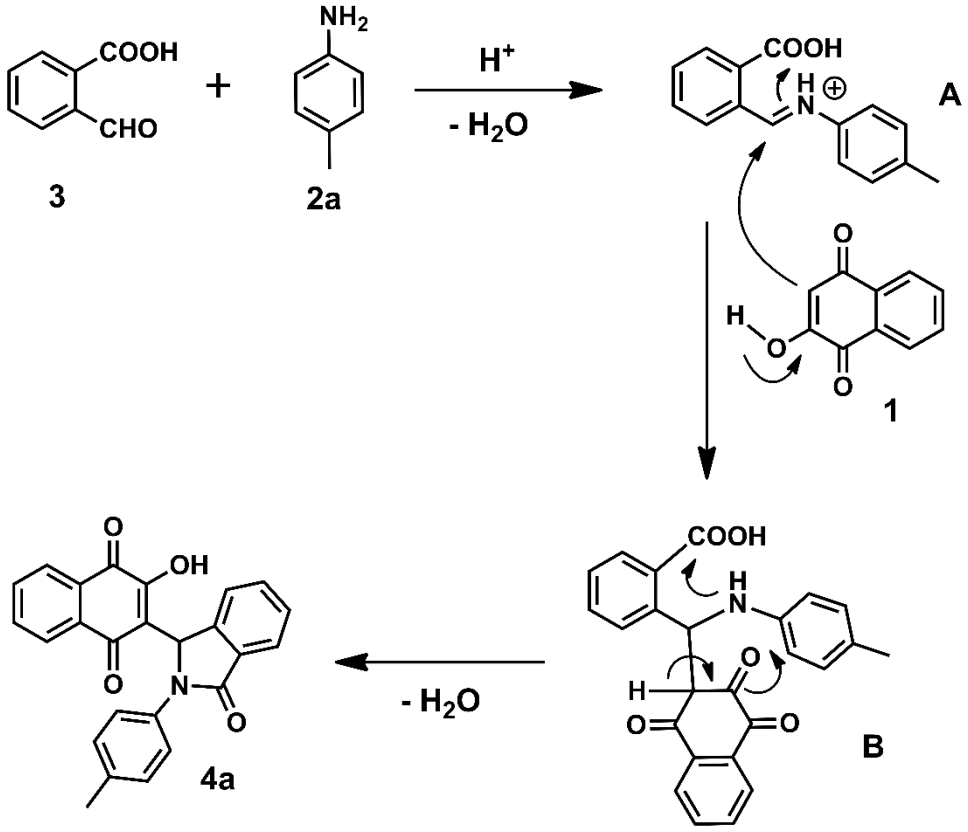

Scheme 6.2 Proposed plausible reaction pathway for synthesis of isoindolinones.

6.2.3 Theoretical studies

The impact of Frontier molecular orbital (FMO) is indispensable in the determination of electronic, optical activity, chemical stability, biological activity, and molecule reactivity. Recently, many reports showed the correlation between FMOs and several biological properties such as antimicrobial, anticancer, antifungal, and cytotoxic activities,[28–35]. There are numerous methods to determine the excitation energies of the molecule (FMO) is the most popular method to determine the gap between the highest occupied molecular orbital (HOMO) and the lowest occupied molecular orbital (LUMO) of a neutral molecule.

The energy gap between HOMO-LUMO can be measured by the excitability of the compound and reports the nature of the molecular system. The higher energy gap between HOMO-LUMO is responsible for low chemical reactivity and high kinetic

stability. Since the energy is unfavourable to high lying LUMO to add electron and low lying HOMO to remove an electron, which forms the activated complex of any possible chemical reaction [36–38]. The global reactivity parameters such as dipole moment, electrophilicity (ω), electronegativity (χ), chemical potential (μ), softness (S), hardness (η), and electron affinity (A) provide useful information to understand the pharmacological activity of the compounds in drug modelling by using HOMO-LUMO energies [27,39–42].

Table 6.3 HOMO, LUMO, energy gap, global electronegativity, global hardness and softness, global electrophilicity index, and dipole moment of compound 4a.

Parameters	B3LYP/6-31G (d, p) (eV)
HOMO	-5.549
LUMO	-3.402
ΔE	2.147
Ionization potential (I)	5.549
Electron affinity (A)	3.402
Chemical potential (μ)	-4.475
Hardness (η)	1.073
Electronegativity (χ)	4.475
Softness (σ)	0.536
Electrophilicity index (ω)	9.329
Dipole moment (Debye)	6.195

The HOMO-LUMO values of compound **4a** are shown in **table 6.3.** The HOMO and LUMO gap of compound **4a** is -2.147 eV. The electron transition alignments for the electron transfer from ground state to the excited state are mainly responsible for electron excitation from HOMO-LUMO. The compositions of atomic orbitals of **4a** derived from FMOs along with optimized structure are shown in **figures 2a** and **2b.** The molecular structure optimization and HOMO-LUMO gap of remaining compounds **4b-4m** were calculated using similar basic sets of function (i.e. B3LYP/6-31G (d, p) shown in **table S6.1**. The compound **4b** showed the lowest (-1.859 eV) while **4l** showed the highest (-2.833 eV) HOMO-LUMO energy gap. The data tabulated in **table S6.1** indicated that the values of ionization potential are higher that electron affinity, which disclose that all the

compounds have better capability to accept electrons. Electrophilicity index (ω) is one of the main quantum chemical descriptors for evaluation of biological activity. Compound **4h, 4i, 4k,** and **4m** possess higher electrophilicity (16.28, 14.39, 16.12, and 16.05) among synthesized compounds. Which denotes that they are stronger electrophiles. As a result, **4i** has lesser energy gap so, making it more polarizable, least kinetic stable and high reactivity making it soft molecule. Furthermore dipole moment of **4i** is low (5.72) and electronegativity ($\chi = 4.65$) is high makes stables and effects biological activity [26,27].

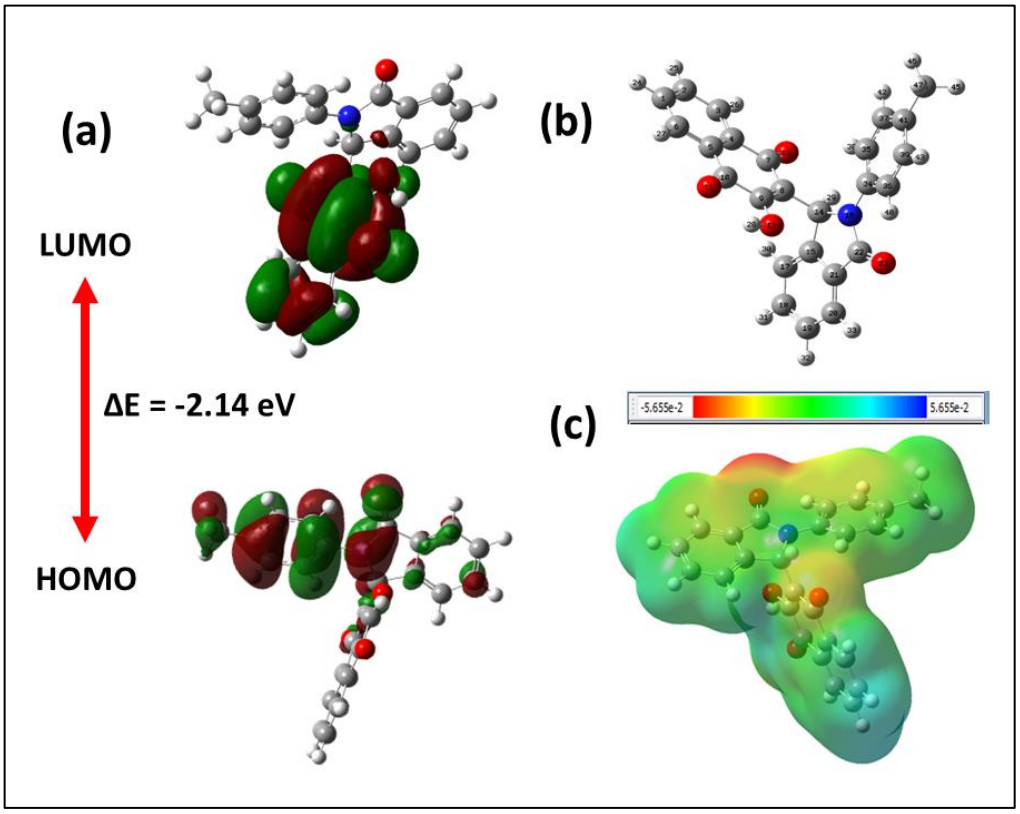

Figure 6.2 (a) Surface plot showing the frontier molecular orbitals, (b) optimized structure with atom labeling, and (c) MEP surface diagram of compound 4a.

The molecular electrostatic potential (MEP) surface is very important to determine electrophilic and nucleophilic sites based on the electrostatic potential distribution [43]. The MEP surface of compound **4a** was drawn by DFT/B3LYP method and shown in **figure 6.2c.** The electrostatic values are visualized in terms of color coding. The negative and positive potential regions are shown by red and blue color respectively. While zero and neutral potential regions are shown by green and yellow color respectively. As shown in **figure 6.2c** the major negative potential appears over O23 atom due to isoindolinone C=O group, while considerably lower negative potential than O23 atom observed near

O12 atom of naphthoquinone C=O group. The positive potential is surrounded near phenolic oxygen O13 atom due to nearby hydrogen atoms, which indicates the occurrence of O-H----O interaction [44]. Similar behavior was observed in other compounds **4b-4m** as shown in **figure S6.53**. In case of compound **4j,** the positive potential was observed near the nitrogen atom of indole ring as shown in **figure S6.53** due to the presence of the NH group. These data suggest that carbonyl oxygen of isoindolinone and naphthoquinone has a higher electron density and it plays an important role in the biological activity through hydrogen bonding with the target.

The potential of new molecule as new drug can be evaluated by forecasting in silico physicochemical attributes, drug likeness, or adsorption, distribution, metabolism, excretion (ADME) traits. Topological polar surface area (TPSA), an attribute that is explored to forecast the passive molecular transport trait of drugs, was also appraised. The physicochemical properties are shown in **table S6.2.** The physicochemical properties are in good agreement with the applied criteria. It is expected to have good bioavailability score as all the compounds have TPSA $\leq$ 110 Å. Theoretical data of in silico pharmacokinetic/ADME evaluations are presented in **table S6.3.** The following predictions can be made based on this. All the compounds showed high gastrointestinal absorptions (GI). All the compounds are P-gp (p- glycoprotein) non inhibitors except **4m,** while half of compounds have no BBB (blood brain barrier) permeability. All the synthesized compounds were tested for inhibition of the Cytochrome P450 isomers, that is, CYP1A2, CYP2C19, CYP2C9, CYP2D6, and CYP3A4. It was found that all compounds are inhibitor of CYP2C9, CYP3A4 and non-inhibitor of CYP2D6. Most of the compounds are CYP1A2 inhibitors except **4b, 4g** and **4m**. All the tested compounds are inhibitors of CYP2C19 with the exception of compound **4b** and **4i.** The predictions show that they satisfy the Lipinski rule of five [45], Veber rule [46] as well as Egan rule [47] suggesting good bioavailability.

6.3 Biological evaluation

6.3.1 Cytotoxicity

To investigate the cytotoxic potential of isoindolinone derivatives, some compounds were considered for in vitro cytotoxicity studies on Human liver cancer cells (HepG2 cell lines) based on information obtained from DFT and ADME predictions. The compounds

were screened at 1 to 10 μM concentrations for 48h for cell viability assay (by MTT) and their IC_{50} values were obtained.

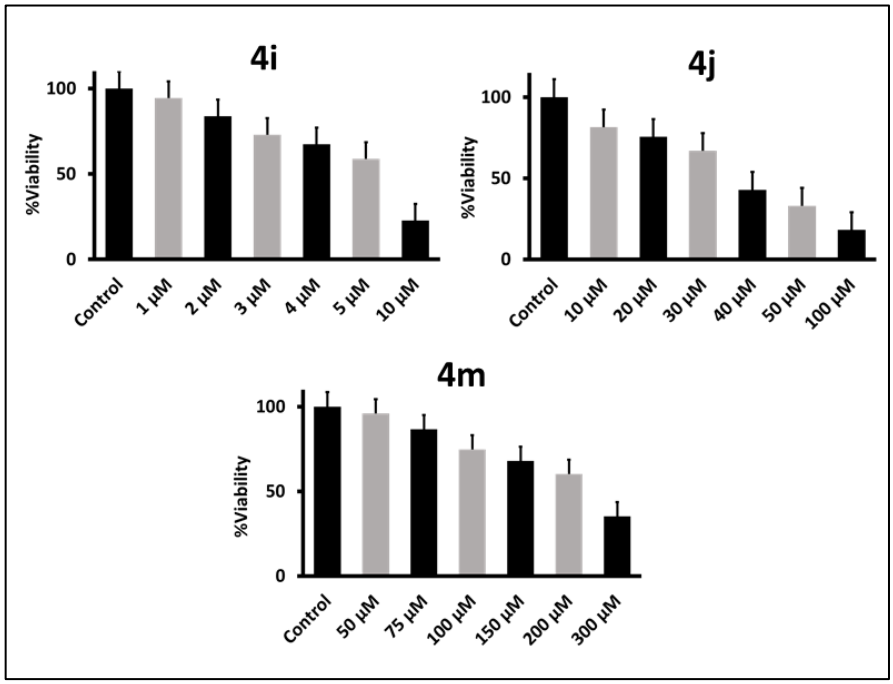

Figure 6.3 Graph of %viability against concentration for MTT assay of compound 4i, 4j, and 4m.

The compounds **4j** and **4m** were screened at higher concentrations to determine their IC_{50} values as they showed low cytotoxicity at lower concentrations. The plot of % viability *vs* concentration of compound obtained is shown in **figure 6.3.** The IC_{50} values of compounds **4i, 4j,** and **4m** were also calculated and are 5.29**,** 39.35, 265.25 μM, respectively. Among all, **c**ompound **4i** showed the lowest IC_{50} value which was also in comparable range with standard drug Dox (IC_{50} 1.30 μM) [48]. While compound **4m** showed high IC_{50} value. Overall the isoindolinone skeleton derived from lawsone with heterocyclic aromatic ring showed high cytotoxicity (i.e. **4i and 4j**) while the compound with long chain showed low cytotoxicity against HepG2 cell lines.

6.3.2 Molecular Docking

The molecular docking of active compounds (**4i**, and **4j**) with the target protein Alpha fetoprotein (PDB ID: 2DA2) a liver cancer-associated protein. As alpha Fetoproteins (APF) is most widely used and accepted serum marker for Hepatocellular carcinoma (HCC) [49–51]. The molecular docking study disclosed that compounds are promising

candidates for further studies, which is justified by low binding energy -7.6 and -7.1 kcal/mol for **4i** and **4j** respectively with AFP.

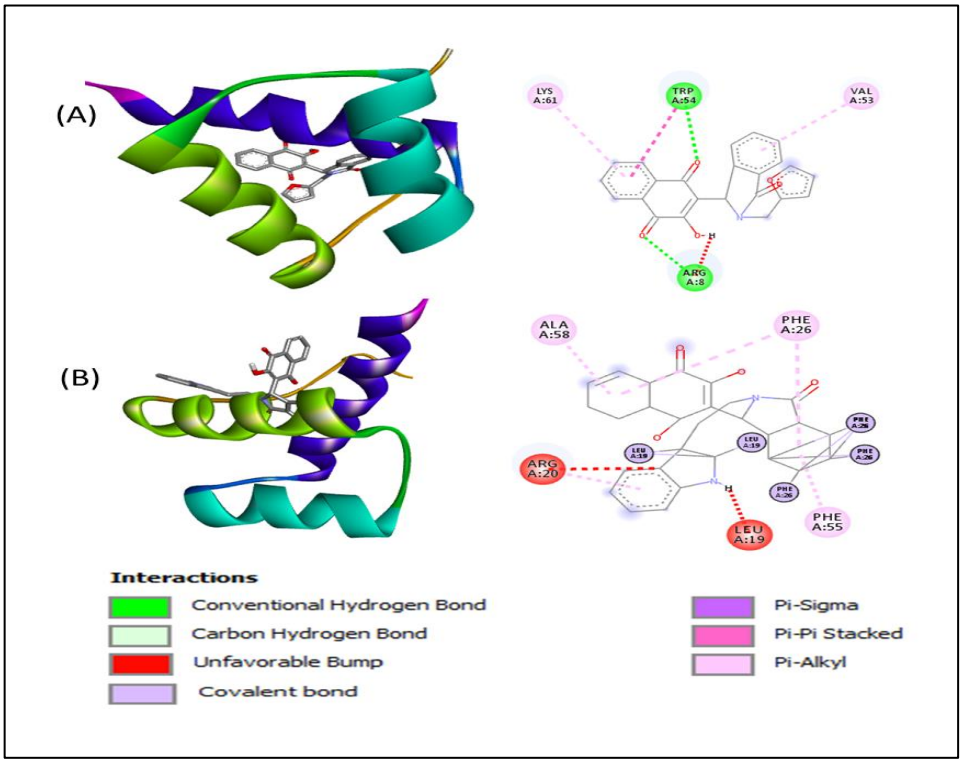

Figure 6.4 In silico docking model of AFP protein with (A) 4i, and (B) 4j. 3D and 2D images generated with Biovia Discovery Studio Visualizer

Docking and 2D diagrams illustrating protein ligand interaction are shown in **figure 6.4A and 6.4B.** The different interactions were shown by compounds at molecular level such as, hydrogen bond, covalent bond, pi-sigma bond, pi-pi stacked bond. Compound **4i** displayed various binding interactions including hydrogen bonding with residue TRP A54 and ARG A8. It also displayed pi-alkyl bonding with residue VAL A53 and LYS A61. Compounds 4j was involved in binding interactions involves pi-alkyl with PHE A55, PHE A26, and ALA A58. Thus, the minimum binding energies and hydrogen bond interactions of compound **4i** with AFP might be one of the justifications for good in vitro activity.

6.3.3 In vivo studies

Hepatocellular carcinoma (HCC) is the most common form of liver cancer and causes prominent cancer death worldwide [52]. The anticancer potential of one of the synthesized compounds was assessed for the treatment of liver cancer on nude mice model. The tumor

regression observed in the animals dosed with **4i** was compared with the animal treated with a well-known anticancer drug doxorubicin. The changes in body weight and weight of liver in animals revealed that reduction of tumor after treatment with compound **4i.** The tumor induced group showed the most significant decline in body weight **(figure S6.54A)**. While, no change in body weight was observed after treatment with compound **4i**. As per the **figure S6.54B** the increase in weight of the liver suggest tumor growth, which got reversed following treatment.

The liver functioning was analyzed by testing the serum SGOT and SGPT levels. Both SGOT and SGPT levels were found to be increased in the HCC induced untreated group as shown in **figure 6.5A**. Upon treatment with DOX and **4i** the levels were observed to attain normal state with **4i** showing anticancer potential comparable to DOX **(figure 6.5A)**. The circulating levels of Alpha Fetoproteins (APF) is an important biomarker accessed to monitor presence and progress of HCC. The AFP level was found to be significantly elevated in HCC induced group **(figure S6.54C)**. It is interesting to note that compound **4i** showed lower AFP value than standard drug doxorubicin validates efficacy of isoindolinone derivatives.

The tumor progression and angiogenesis was monitored by analyzing the levels of cancer specific biomarkers, matrix metallopeptidase (MMP) 2 and 9 [53,54]. The results showed an increment in the levels of MMP-2 and 9 in the plasma that marks the beginning of hepatic tumor development **(figure 5B)**. The group of animals treated with **4i** showed decrement the levels of both these biomarkers. The results were comparable to the animals treated with DOX. The liver tissues were examined post H&E staining, the untreated group demonstrated severe distortions in the liver lobes and a de-arrangement of hepatic code as well as canaliculi **(figure 6.5C (i))** [55]. However, after treatment with compound **4i** the distorted histoarchitecture was restored and showed a morphology that is similar to the animals of control group **(figure 6.5C (iii))**. Overall, in vivo studies provided valuable insight on the efficiency of substituted isoindolinone derived from Lawsone **(compound 4i)** for the prevention of tumor progression.

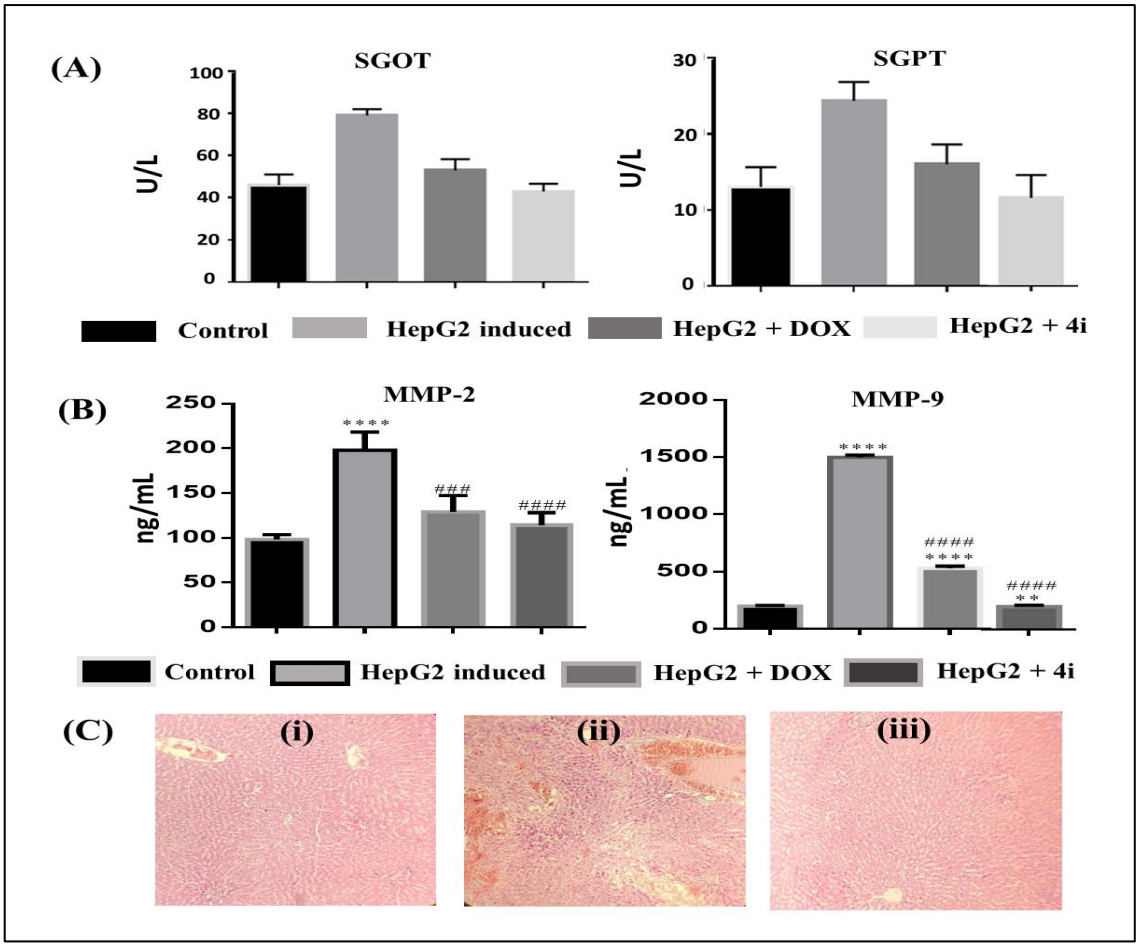

Figure 6.5 (A) Serum SGOT and SGPT profile, (B) MMP-2 and MMP-9 profile, (C) histoarchitecture of (i) Control and animals dosed with (ii) HepG2 and (iii) HepG2 + 4i.

6.4 Experimental

6.4.1 Material and methods

Lawsone and 2-formyl benzoic acid was purchased from Sigma Aldrich, India. All other reagents Amines were purchased from Sigma-Aldrich, Spectrochem, and SRL chemicals, Mumbai, India. All the reagents were used without further purification. The reaction progress was monitored by TLC in ultraviolet light. Merck TLC plates were used to monitor the reaction progress. All melting points were recorded by the scientific open capillary method and are uncorrected. FT-IR spectra were recorded on Bruker Alpha FT-IR Spectrometer by using KBr pellets. ^{1}H & ^{13}C NMR spectra were recorded on Bruker Avance (400 MHz) spectrometer in $CDCL_3$ or DMSO-d_6 solvent. Chemical shift are reported in parts per million (ppm) downfield from

TMS and coupling constants (*J*) is reported in Hertz (Hz). Proton count multiplicities are reported as singlet (s), doublet (d), triplet (t), multiplet (m), doublet of doublet (dd), and triplet of doublet (td). Mass spectra were determined by water acquity ultra-performance LC with SQ detector.

6.4.2 General procedure for synthesis of substituted isoindolinones (4a-4m)

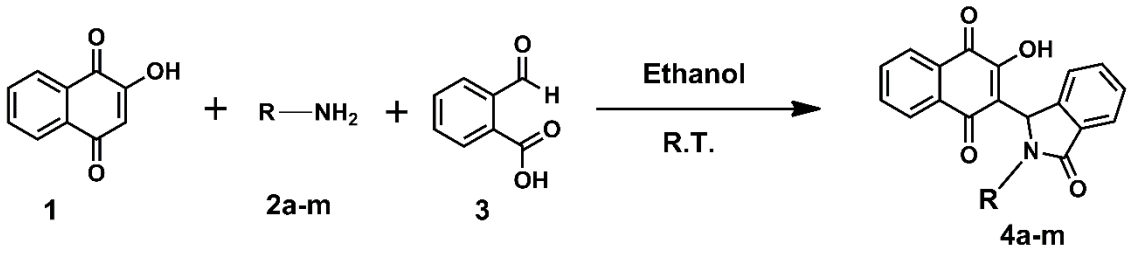

Scheme 6.3 General schematic for synthesis of substituted isoindolinones.

The compounds from **4a-4m** were synthesized following the optimized reaction conditions. Briefly, a mixture of 2-formyl benzoic acid (1 mmol) in ethanol (5 mL), respective amine (1.1 mmol), and Lawsone (1 mmol) were mixed in 25 mL round bottom flask at room temperature in presence of 5 mol% of acetic acid until the reaction was completed. The progress of reaction was monitored by TLC. After completion of the reaction, the obtained solid was filtered and washed by ethanol. Isolated crude product was recrystallized in acetic acid and dried under vacuum. General schematic for synthesis is shown in **scheme 6.3.**

2-hydroxy-3-(3-oxo-2-(p-tolyl)isoindolin-1-yl)naphthalene-1,4-dione (4a)

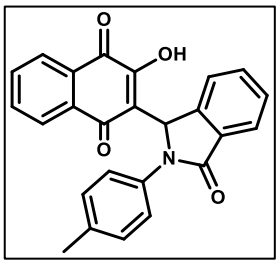

Yellow solid; Yield: 92%; M.P: 210 ^{o}C -212 ^{o}C

^{1}H NMR ($CDCL_3$, 400 MHz) δ (ppm): 2.63 (s, 1H), 6.86 (s, 1H), 7.12 (d, 2H, *J*=8.4 Hz), 7.36 (dd, 1H, *J*=8.4 Hz), 7.54 (m, 4H), 7.72 (td, 1H, *J*=7.6 Hz, *J*=1.2 Hz), 7.84 (td, 1H, *J*=8.2 Hz, *J*=1.2 Hz), 7.95 (dd, 1H, *J*=7.6 Hz, *J*=1.2 Hz), 8.03 (dd, 1H, *J*=8.8 Hz, *J*=1.2 Hz), 8.24 (dd, 1H, *J*=8.8 Hz, *J*=1.2 Hz). **^{13}C NMR** ($CDCL_3$, 100 MHz) δ (ppm): 20.91, 55.58, 118.16, 121.86, 122.23, 122.32, 123.76, 126.58, 127.12, 128.54, 129.43, 132.17,

133.02, 133.46, 134.79, 134.86, 135.30, 135.40, 142.82, 154.52, 168.01, 180.48, 184.01. **IR (KBr) cm^{-1}**: 3399 (O-H), 3073 (=C-H), 2913 (C-H), 1680 (C=O), 1625 (C=O, amide), 1592 (C=C), 1272 (C-N), 1048 (C-O). **ESI/MS** 396.17 $[M+1]^+$ calculated for $C_{25}H_{17}NO_4$. Anal. Calculated for: C, 75.94; H, 4.33; N, 3.54; O, 16.19; Found C, 75.90; H, 4.35; N, 3.52.

2-hydroxy-3-(2-(4-methoxyphenyl)-3-oxoisoindolin-1-yl)naphthalene-1,4-dione(4b)

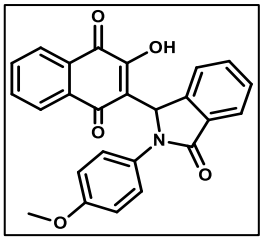

Orange solid; Yield: 91%; M.P: 200 ^oC

^{1}H NMR ($CDCL_3$, 400 MHz) δ (ppm): 3.75 (s, 1H), 6.82 (d, 1H), 6.85 (d, 2H, *J*=4 Hz), 7.37 (d, 1H, *J*=7.2 Hz), 7.54 (m, 4H), 7.72 (td, 1H, *J*=8.2 Hz, *J*=1.2 Hz), 7.83 (td, 1H, *J*=8.2 Hz, *J*=1.2 Hz), 7.94 (d, 1H, *J*=6.8), 8.04 (dd, 1H, *J*=6.4 Hz, *J*=4.4 Hz), 8.25 (dd, 1H, *J*=7.2 Hz, *J*=4.4 Hz). **^{13}C NMR** ($CDCL_3$, 100 MHz) δ (ppm): 55.36, 55.80, 114.19, 118.12, 122.31, 123.74, 123.80, 126.64, 127.19, 128.57, 128.68, 129.31, 130.38, 132.09, 132.20, 133.01, 133.12, 133.51, 135.56, 142.74, 154.13, 156.96, 167.89, 180.47, 183.93. **IR (KBr) cm^{-1}**: 3237 (O-H), 3024 (=C-H), 2962 (C-H), 1671 (C=O), 1639 (C=O, amide), 1586 (C=C), 1273 (C-N), 1049 (C-O). **ESI/MS** 396.17 $[M+1]^+$ calculated for $C_{25}H_{17}NO_4$. Anal. Calculated for: C, 72.99; H, 4.16; N, 3.40; O, 19.14; Found C, 72.95; H, 4.18; N, 3.42.

2-hydroxy-3-(3-oxo-2-phenylisoindolin-1-yl)naphthalene-1,4-dione (4c)

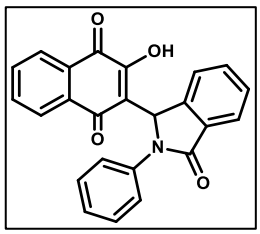

Yellow solid; Yield: 80%; M.P: 208-210 ^oC

^{1}H NMR ($CDCL_3$, 400 MHz) δ (ppm): 6.90 (s, 1H), 7.11 (q, 1H, *J*=8.0 Hz), 7.33 (t, 2H, *J*=9 Hz), 7.37 (d, 1H, *J*=6.8 Hz), 7.55 (m, 2H), 7.68 (dd, 2H, *J*=4.8 Hz), 7.72 (td, 1H, *J*=8.2 Hz, *J*=1.2 Hz), 7.84 (td, 1H, *J*=8.2 Hz, *J*=1.2 Hz), 7.96 (dd, 1H, *J*=8.0), 8.03 (dd, 1H, Hz, *J*=4.4 Hz), 8.27 (dd, 1H, *J*=4.2). **^{13}C NMR** ($CDCL_3$, 100 MHz) δ (ppm): 20.75,

55.41, 118.16, 121.70, 122.07, 122.34, 123.92, 125.03, 126.66, 127.223, 128.67, 128.99, 129.26, 132.17, 132.37, 132.87, 133.56, 135.48, 137.48, 142.66, 154.03, 168.03, 176.68, 180.45, 183.95. **IR (KBr) cm^{-1}**: 3384 (O-H), 3017 (=C-H), 1706, 1678 (C=O), 1641 (C=O, amide), 1594 (C=C), 1275 (C-N), 1047 (C-O). **ESI/MS** 382.16 $[M+1]^+$ calculated for $C_{24}H_{15}NO_4$. Anal. Calculated for: C, 78.58; H, 3.96; N, 3.58; O, 16.78; Found C, 78.60; H, 3.95; N, 3.56.

2-(2-(4-chlorophenyl)-3-oxoisoindolin-1-yl)-3-hydroxynaphthalene-1,4-dione (4d)

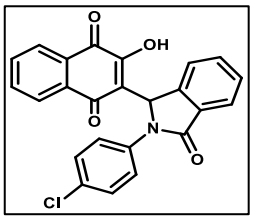

Yellow solid; Yield: 83%; M.P: 212-214 ^oC

^{1}H NMR ($CDCL_3$, 400 MHz) δ (ppm): 6.85 (s, 1H), 7.26 (d, 1H, *J*=2.0 Hz), 7.38 (dd, 1H, *J*=7.6 Hz), 7.56 (td, 2H, *J*=8.8 Hz), 7.62 (d, 1H), 7.64 (d, 1H), 7.74 (td, 1H, *J*=16.4 Hz), 7.86 (td, 1H, *J*=16.4 Hz), 7.94 (d, 1H), 8.04 (dd, 1H, Hz, *J*=4.2 Hz), 8.26 (dd, 1H, *J*=4.2). **^{13}C NMR** ($CDCL_3$, 100 MHz) δ (ppm):55.43, 117.73, 122.40, 122.86, 123.12, 123.92, 126.74, 127.24, 128.75, 129.07, 129.31, 130.22, 132.08, 132.57, 133.66, 135.52, 136.06, 142.59, 154.29, 168.07, 180.34, 183.97. **IR (KBr) cm^{-1}**: 3404 (O-H), 3061 (=C-H), 2914 (C-H), 1692, 1667 (C=O), 1650 (C=O, amide), 1590 (C=C), 1277 (C-N), 1038 (C-O). **ESI/MS** 416.70 $[M+1]^+$ calculated for $C_{24}H_{14}ClNO_4$. Anal. Calculated for: C, 69.32; H, 3.39; N, 3.37; O, 15.39; Cl, 8.53; Found C, 69.34; H, 3.42; N, 3.36.

2-(2-(4-bromophenyl)-3-oxoisoindolin-1-yl)-3-hydroxynaphthalene-1,4-dione (4e)

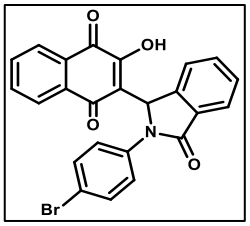

Yellow solid; Yield: 80%; M.P: 232-236 ^oC

^{1}H NMR ($CDCL_3$, 400 MHz) δ (ppm): 6.85 (s, 1H), 7.42 (m, 3H), 7.56 (m, 4H), 7.75 (td, 2H, *J*=8.2 Hz, *J*=1.2 Hz), 7.46 (d, 1H), 8.04 (dd, 1H, Hz, *J*=4.4 Hz, *J*=1.2 Hz), 8.28 (dd, 1H, *J*=4.2 Hz, *J*=1.2 Hz). **^{13}C NMR** ($CDCL_3$, 100 MHz) δ (ppm):30.98, 55.33, 117.73, 118.02, 122.41, 123.10, 123.38, 123.93, 126.75, 127.25, 128.76, 129.30, 132.09, 132.35, 132.56, 132.59, 133.67, 135.53, 136.60, 142.55, 154.26, 168.02, 180.33, 183.97.

IR (KBr) cm^{-1}: 3403 (O-H), 3061 (=C-H), 1691 1667 (C=O), 1650 (C=O, amide), 1584 (C=C), 1277 (C-N), 1037 (C-O). **ESI/MS** 462.83 $[M+1]^+$ calculated for $C_{24}H_{14}BrNO_4$. Anal. Calculated for: C, 62.63; H, 3.07; N, 3.04; O, 13.90; Br, 17.36; Found C, 62.60; H, 3.05; N, 3.06.

2-(2-(3-chloro-4-fluorophenyl)-3-oxoisoindolin-1-yl)-3-hydroxynaphthalene-1,4-dione (4f)

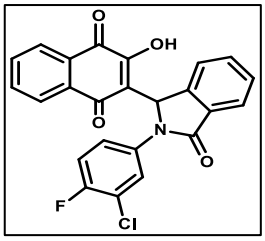

Yellow solid; Yield: 83%; M.P: 174-178 ^oC

^{1}H NMR ($CDCL_3$, 400 MHz) δ (ppm): 6.88 (s, 1H), 7.07 (t, 1H, *J*=8.6 Hz), 7.36 (dd, 1H, *J*=7.6 Hz), 7.56 (dd, 1H, *J*=5.8 Hz), 7.59 (td, 1H, *J*=8.0 Hz, *J*=1.2 Hz), 7.75 (td, 1H, *J*=8.2 Hz, *J*=1.2 Hz), 7.78 (dd, 1H, *J*=8.0 Hz, *J*=1.2 Hz), 7.93 (t, 2H, *J*=9.4 Hz), 8.07 (dd, 1H, Hz, *J*=4.2 Hz), 8.23 (dd, 1H, *J*=4.2). **^{13}C NMR** ($CDCL_3$, 100 MHz) δ (ppm): 55.45, 116.53, 117.54, 120.97, 121.89, 122.41, 124.01, 124.12, 126.80, 127.33, 128.87, 129.21, 132.08, 132.30, 134.14, 142.43, 154.07, 167.89, 180.32, 183.92. **19F NMR** (CDCL3, 400 MHz) δ (ppm): -119.48 (s). **IR (KBr) cm^{-1}**: 3389 (O-H), 3088 (=C-H), 2940 (C-H), 1675 (C=O), 1634 (C=O, amide), 1593 (C=C), 1275 (C-N), 1047 (C-O). **ESI/MS** 434.71 $[M+1]^+$ calculated for $C_{24}H_{13}ClFNO_4$. Anal. Calculated for: C, 66.45; H, 3.02; N, 3.23; O, 14.75; Cl, 8.17; F, 4.38; Found C, 66.47; H, 3.04; N, 3.21.

2-(2-(3,4-dimethylphenyl)-3-oxoisoindolin-1-yl)-3-hydroxynaphthalene-1,4-dione (4g)

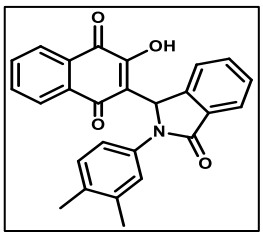

Yellow solid; Yield: 81%; M.P: 180-184 ^oC

^{1}H NMR ($CDCL_3$, 400 MHz) δ (ppm): 2.17 (s, 3H), 2.23 (s, 3H), 6.86 (s, 1H), 7.05 (d, 1H, *J*=8.0 Hz), 7.29 (dd, 1H, *J*=5.2 Hz), 7.36 (d, 1H, *J*=7.2 Hz), 7.52-7.55 (m, 3H), 7.72 (td, 1H, *J*=8.0 Hz, *J*=1.2 Hz), 7.84 (td, 1H, *J*=8.2 Hz, *J*=1.2 Hz), 7.94 (dd, 1H, *J*=4.2

Hz), 8.03 (dd, 1H, Hz, *J*=4.4 Hz), 8.26 (dd, 1H, *J*=4.2). **^{13}C NMR** ($CDCL_3$, 100 MHz) δ (ppm):20.05, 19.26, 55.66, 118.25, 119.39, 121.75, 123.49, 123.77, 124.22, 126.57, 127.12, 128.55, 129.43, 129.94, 132.11, 132.23, 133.09, 133.44, 135.31, 137.16, 142.85, 154.48, 168.08, 180.50, 183.97. **IR (KBr) cm^{-1}**: 3340 (O-H), 3036 (=C-H), 2913 (C-H), 1679 (C=O), 1641 (C=O, amide), 1593 (C=C), 1271 (C-N), 1044 (C-O). **ESI/MS** 410.77 $[M+1]^+$ calculated for $C_{26}H_{19}NO_4$. Anal. Calculated for: C, 76.27; H, 4.68; N, 3.42; O, 15.63; Found C, 76.30; H, 4.66; N, 3.44.

2-(2-benzyl-3-oxoisoindolin-1-yl)-3-hydroxynaphthalene-1,4-dione (4h)

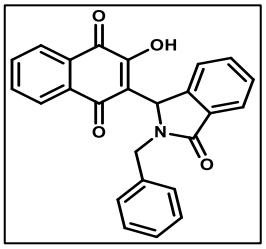

Light yellow solid; Yield: 78%; M.P: 174-178 ^oC

^{1}H NMR ($CDCL_3$, 400 MHz) δ (ppm): 4.52 (d, 1H, *J*=14.8 Hz), 4.89 (d, 1H, *J*=14.8 Hz), 6.10 (s, 1H), 7.11 (m, 3H), 7.23 (m, 4H), 7.47 (m, 2H), 7.47 (m, 2H), 7.75 (td, 1H, *J*=8.2 Hz, *J*=1.2 Hz), 7.86 (m, 2H), 8.06 (dd, 1H, *J*=4.4 Hz), 8.23 (dd, 1H, *J*=4.2). **^{13}C NMR** ($CDCL_3$, 100 MHz) δ (ppm):45.27, 54.52, 117.29, 122.27, 123.63, 126.63, 126.47, 127.08, 127.60, 128.26, 128.34, 128.40, 128.54, 128.60, 129.28, 131.68, 132.556, 133.44, 135.35, 135.46, 136.78, 143.83, 154.07, 169.17, 180.42, 183.87. **IR (KBr) cm^{-1}**: 3465 (O-H), 3034 (=C-H), 2917 (C-H), 1664 (C=O), 1652 (C=O, amide), 1592 (C=C), 1272 (C-N), 1037 (C-O). **ESI/MS** 396.20 $[M+1]^+$ calculated for $C_{25}H_{17}NO_4$. Anal. Calculated for: C, 75.94; H, 4.33; N, 3.54; O, 16.19; Found C, 75.90; H, 4.35; N, 3.55.

2-(2-(furan-2-ylmethyl)-3-oxoisoindolin-1-yl)-3-hydroxynaphthalene-1,4-dione (4i)

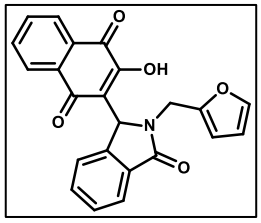

Light yellow solid; Yield: 65%; M.P: 200-204 ^oC

^{1}H NMR ($CDCL_3$, 400 MHz) δ (ppm): 4.56 (d, 1H, *J*=15.6 Hz), 4.86 (d, 1H, *J*=15.6 Hz), 6.08 (d, 1H, *J*=3.2 Hz), 6.12 (d, 2H, *J*=14.4 Hz), 7.11 (s, 1H), 7.47 (m, 2H), 7.26 (s, 1H),

7.47 (q, 2H, *J*=15.6 Hz), 7.76 (t, 1H, *J*=15.2 Hz), 8.10 (d, 1H, *J*=7.6 Hz), 8.26 (d, 1H, *J*=8.0 Hz). **^{13}C NMR** ($CDCL_3$, 100 MHz) δ (ppm): 37.62, 54.64, 109.08, 110.55, 117.25, 122.32, 123.62, 126.51, 127.08, 128.27, 129.41, 131.77, 132.38, 133.45, 135.36, 142.36, 143.75, 150.27, 168.85, 180.63, 183.92. **IR (KBr) cm^{-1}**: 3408 (O-H), 3068 (=C-H), 1670 (C=O), 1641 (C=O, amide), 1592 (C=C), 1272 (C-N), 1045 (C-O). **ESI/MS** 386.68 $[M+1]^+$ calculated for $C_{23}H_{15}NO_5$. Anal. Calculated for: C, 71.68; H, 3.92; N, 3.63; O, 20.76; Found C, 71.70; H, 3.94; N, 3.60.

2-(2-(2-(1H-indol-3-yl)ethyl)-3-oxoisoindolin-1-yl)-3-hydroxynaphthalene-1,4 dione (4j)

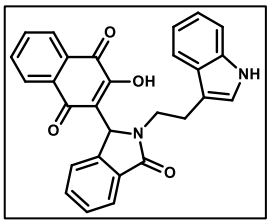

Reddish brown solid; Yield: 65%; M.P: 204-206 ^oC

^{1}H NMR ($CDCL_3$, 400 MHz) δ (ppm): 3.08 (q, 1H, *J*=14.0 Hz), 3.20 (q, 1H, *J*=14.0 Hz), 3.47 (q, 1H, *J*=13.2 Hz, *J*=6.8 Hz), 4.24 (q, 1H, *J*=13.2 Hz, *J*=6.8 Hz), 6.84 (t, 1H, *J*=7.4 Hz), 6.96 (t, 1H, *J*=7.2 Hz), 7.02 (d, 1H), 7.17-7.22 (m, 2H), 7.42-7.46 (m, 3H), 7.74 (td, 1H, *J*=8.0 Hz, *J*=1.2 Hz), 7.82-7.86 (m, 2H), 7.99 (s, 1H broad), 8.04 (dd, 1H, *J*=7.2 Hz, *J*=0.8 Hz), 8.16 (d, 1H, *J*=7.6 Hz). **^{13}C NMR** ($CDCL_3$, 100 MHz) δ (ppm): 24.28, 54.12, 55.23, 111.58, 111.83, 116.22, 116.66, 118.47, 118.59, 121.35, 122.89, 123.01, 123.11, 126.37, 127.45, 128.27, 130.66, 132.28, 135.27, 136.80, 145.02, 145.63, 168.15, 181, 183.19, 184.67. **IR (KBr) cm^{-1}**: 3447 (O-H), 3054 (=C-H), 1679 (C=O), 1650 (C=O, amide), 1594 (C=C), 1277 (C-N), 1039 (C-O). **ESI/MS** 449.86 $[M+1]^+$ calculated for $C_{28}H_{20}N_2O_4$. Anal. Calculated for: C, 74.99; H, 4.50; N, 6.25; O, 14.27; Found C, 74.95; H, 4.55; N, 6.27

2-hydroxy-3-(3-oxo-2-(2-(thiophen-3-yl)ethyl)isoindolin-1-yl)naphthalene-1,4-dione (4k)

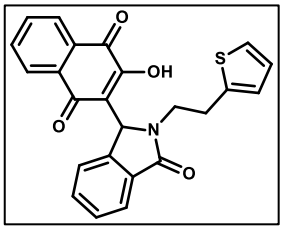

Yellow solid; Yield: 68%; M.P: 182 ^{o}C

^{1}H NMR ($CDCL_3$, 400 MHz) δ (ppm): 3.12 (m, 2H), 3.27 (t, 1H, *J*=13.6 Hz), 4.25 (q, 1H, *J*=12.6), 6.12 (s, 1H), 6.81 (q, 2H, *J*=5.2 Hz), 7.03 (dd, 1H, *J*=6 Hz, *J*=1.2 Hz), 7.26 (s, 1H), 7.47 (td, 2H, *J*=7.6 Hz), 7.80 (td, 1H, *J*=7.6), 7.84-7.91 (m, 2H), 8.134 (dd, 1H, *J*=6.8 Hz), 8.28 (dd, 1H, *J*=6.8 Hz). **^{13}C NMR** ($CDCL_3$, 100 MHz) δ (ppm):28.72, 20.59, 42.63, 54.85, 117.04, 122.37, 123.37, 123.93, 125.40, 126.69, 127.05, 127.22, 128.30, 129.37, 131.69, 132.35, 132.57, 133.60, 135.53, 141.06, 143.62, 154.22, 169.41, 180.60, 184.10. **IR (KBr) cm^{-1}**: 3430 (O-H), 2924 (C-H), 1668 (C=O), 1635 (C=O, amide), 1592 (C=C), 1273 (C-N), 1044 (C-O). **ESI/MS** 416.70 $[M+1]^+$ calculated for $C_{24}H_{27}NO_4S$. Anal. Calculated for: C, 69.38; H, 4.12; N, 3.37; O, 15.40; S, 7.72; Found C, 69.35; H, 4.16; N, 3.39.

2-(2-butyl-3-oxoisoindolin-1-yl)-3-hydroxynaphthalene-1,4-dione (4l)

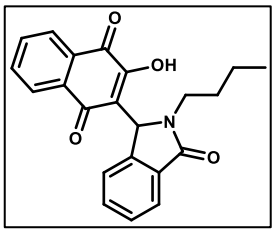

Yellow solid; Yield: 67%; M.P: 174 ^{o}C

^{1}H NMR ($CDCL_3$, 400 MHz) δ (ppm): 0.905 (q, 3H), 1.58 (q, 2H), 1.37 (q, 2H), 2.83 (q, 1H, *J*=13.6 Hz), 3.99 (q, 1H, *J*=15.2 Hz), 7.31 (d, 1H, *J*=8.4 Hz), 7.41 (d, 1H, *J*=7.6 Hz), 7.47 (td, 1H, *J*=8 Hz), 7.73 (d, 1H, *J*=7.6 Hz), 7.79 (td, 1H, *J*=7.6 Hz), 7.88 (td, 1H, *J*=7.6), 8.13 (dd, 1H, *J*=7.6 Hz), 8.29 (dd, 1H, *J*=7.6 Hz). **^{13}C NMR** ($CDCL_3$, 100 MHz) δ (ppm): 13.76, 20.08, 30.26, 40.20, 54.39, 117.14, 122.26, 123.26, 126.71, 127.06, 128.16, 129.65, 131.40, 132.35, 132.90, 133.53, 135.31, 143.86, 155.16, 169.53, 180.68, 184.35. **IR (KBr) cm^{-1}**: 3408 (O-H), 2958 (C-H), 1668 (C=O), 1638 (C=O, amide), 1593 (C=C), 1273 (C-N), 1046 (C-O). **ESI/MS** 362.67 $[M+1]^+$ calculated for $C_{22}H_{19}NO_4$. Anal. Calculated for: C, 73.12; H, 5.30; N, 3.38; O, 17.70; Found C, 73.10; H, 5.32; N, 3.39.

2-hydroxy-3-(2-octyl-3-oxoisoindolin-1-yl)naphthalene-1,4-dione (4m)

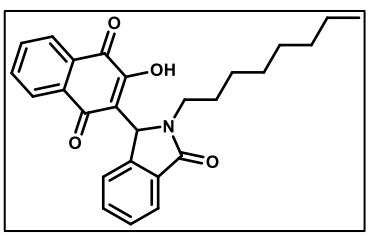

Yellow solid; Yield: 70%; M.P: 152 ^{o}C

^{1}H NMR ($CDCL_3$, 400 MHz) δ (ppm): 0.85 (t, 3H), 1.25 (s, 12H, broad), 2.81 (s, 1H, *J*=13.8 Hz), 3.97 (s, 1H, *J*=15 Hz), 7.30 (d, 1H, *J*=7.6 Hz), 7.43 (t, 1H, *J*=7.2 Hz), 7.47 (dd, 1H, *J*=8.4 Hz), 7.78 (td, 2H, *J*=10.4 Hz), 7.88 (td, 1H, *J*=9.2), 8.15 (dd, 1H, *J*=8.4 Hz, *J*=1.2 Hz), 8.29 (dd, 1H, *J*=8.8 Hz). **^{13}C NMR** ($CDCL_3$, 100 MHz) δ (ppm): 14.10, 22.62, 26.88, 28.16, 29.16, 31.77, 40.51, 54.38, 117.17, 122.26, 123.27, 126.44, 126.71, 127.04, 127.10, 128.17, 129.63, 131.39, 132.35, 133.21, 133.53, 135.32, 143.66, 155.08, 169.08, 180.68, 164.33. **IR (KBr) cm^{-1}**: 3432 (O-H), 2925 (C-H), 1668 (C=O), 1639 (C=O, amide), 1592 (C=C), 1273 (C-N), 1045 (C-O). **ESI/MS** 418.4 $[M+1]^+$ calculated for $C_{26}H_{27}NO_4$. Anal. Calculated for: C, 74.80; H, 6.52; N, 3.35; O, 15.33; Found C, 74.82; H, 6.50; N, 3.38.

6.4.3 Computational Studies

The Gaussian 16 software was used to carry out all theoretical calculations. Density functional theory (DFT) calculation was assigned to optimize the geometry of substituted isoindolinones **(4a-4m)** using B3LYP/6-311G (d,p) basis sets [56]. Gauss View 6 visualization program was used to determine frontier molecular orbitals and HOMO-LUMO energy gap of isoindolinones **(4a-4m)**. Molecular electrostatic potential was performed using a similar set of theoretical calculations and designed with GaussView 6 [22]. Various ADME traits were forcasted employing SwissADME online tool [24].

All computation related to docking were performed on AutodockVina software [57]. The structure of ligand was optimized using Gaussian 16 software. The target protein Alpha fetoprotein (AFP) was extracted from protein databank (PDB ID: 2DA2). The PDB file of selected protein was processed by deleteing ligands and non proteins using discovery studio visualizer v20.1.0.19295. Further, the protein structure was prepared by removing water molecules and then the addition of Kollman charges and polar hydrogen atoms. Next, the ligands were processed by merging Gastiger charges to their structures [58]. Finally, both ligand and protein structures were converted to pdbqt file using AutoDock Tools 1.5.6. Autodock Vina v1.1.2 carried out docking calculations. The dimension for grid used for protein was kept 40 × 60 × 60 Å and separated by 0.375 Å. The exhaustiveness for the docking run was set to the default value of eight. The ligand's binding energy was calculated using the default Lamarckian genetic algorithm of the

AutoDock Vina software package [58]. Biovia Discovery Studio Visuliser v20.1.0.19295 generated the representative 2D and 3D structure showing protein-ligand structures.

6.4.4 In vitro studies

IC_{50} values of the synthesized compounds were determined using MTT assay on HepG2 cell line. HepG2 cells (10^4 cells/well) were seeded in 96 well plate in 10% DMEM media. 0.1% dimethyl sulfoxide was used to dissolve lawsone and its isoindolinone derivatives. Untreated cells were taken as positive control. Dilutions of the compounds were prepared in incomplete DMEM media. Dosing was done at about 70% confluency. After 48h incubation 3-(4, 5-dimethylthiazol-2-yl)-2, 5-diphenyltetrazoliumbromide (MTT; 5 mg/ml) was added for 4h. At the end of incubation MTT was removed from the wells and 150 μL/well of DMSO was added and incubated till formazan crystals dissolved completely. Reading was taken at 570 nm in synergy HTX multimode reader.

6.4.5 In vivo studies

In vivo studies were carried out using our previously reported protocol [59]. Laboratory animals (Balbc mice 28–30 g, n = 24, male/female) were procured from Zydus Research Center, Ahmedabad. Ethical clearance for animal experimentation was obtained from Institutional Animal Committee (IAEC) and CPCSEA. Animals were housed under standard conditions of LD 12:12 with food and water ad libitium. The animals were divided in various treatment groups as follows: the experiment consisted of 4 groups of animals with n=6 mice per group. The animals in group 1 were dosed only with double distilled water and it was considered as control group. Various physiological parameters determined in this group were considered as the standard values for tumor free condition. The animals in the remaining groups (2 to 4) were administered intraperitoneal injections of HePG2 cells for the induction of hepatic tumor (HCC). Post successful tumor induction the animals of group 2 were dosed with only PBS and this was considered as untreated group. The treatment groups comprised of group 3 dosed only with DOX.HCl group 4 dosed with compound **4i**.

The experiment continued for 14 days and at the end, body weights were recorded. Blood was collected by retro-orbital sinus puncture and serum was separated in the cold centrifuge (3000 rpm). Hepatic markers for liver function (SGPT and SGOT) were assessed using standard kits (Reckon diagnostics Ltd., Vadodara, India). Markers

of matrix modulation (MMP-2 and 9) were assessed by ELISA kits (Krishgen Biosystems, Mumbai, India). Animals were sacrificed under mild ether anesthesia and the liver autopsy was conducted. Pieces of liver tissue obtained from control and experimental groups were stored in RNA later solution. Forward and reverse primers of genes controlling immunity (TLR-2 and 4) were procured from Eurofins Scientific, New Delhi, India. RNA extraction was done by Trizol reagent and cDNA was synthesized using iscript™ cDNA kit (BIORAD, California,USA). Quantitative RT- PCR was performed using SYBR select master mix (Applied Biosystems in Quant Studio 12 K (Life Technologies) real time PCR machine.

6.5 Conclusion

To summarize, we have developed an efficient method towards the synthesis of biologically active substituted isoindolinone via multi-component Mannich reaction using naturally occurring Lawsone, 2-formyl benzoic acid, and various primary amines. This approach offers the advantage such as the use of environmentally benign solvent, acetic acid as catalyst, column chromatography free workup procedure. The HOMO-LUMO energy gap (ΔE) and MEP surface diagram were also determined using a theoretical DFT study. The compound **4b** with 4-methoxybenzene substitution showed the lowest (-1.859 eV) while compound **4l** with n-butyl substitution showed the highest (-2.833 eV) HOMO-LUMO energy gap. The electrostatic potential data derived from MEP surface diagram revealed that carbonyl oxygen of isoindolinone and naphthoquinone has a higher electron density and it plays an important role in the biological activity through hydrogen bonding with the target and was supported by a description of global reactivity parameters. The ADME parameters revealed that compounds have good bioavailability. The IC_{50} value for cytotoxic activity of compound **4i** was found to be 5.29 μM on the HepG2 cell line, which is comparable with the standard drug. Furthermore, molecular docking studies on Alpha fetoprotein (AFP), confirm the minimum binding energy with protein and interaction via hydrogen bonding. In addition, in vivo studies corroborate with in-vitro data. The cancer-induced Balb mice demonstrated noteworthy decrement in levels of biomarkers MMP-2 and MMP-9 indicating significant tumor regression when compound **4i** was injected into animals. It was also evident in the histoarchitecture of the liver. Thus isoindolinone derived from lawsone can be effective as an anticancer drug

6.7 Spectra

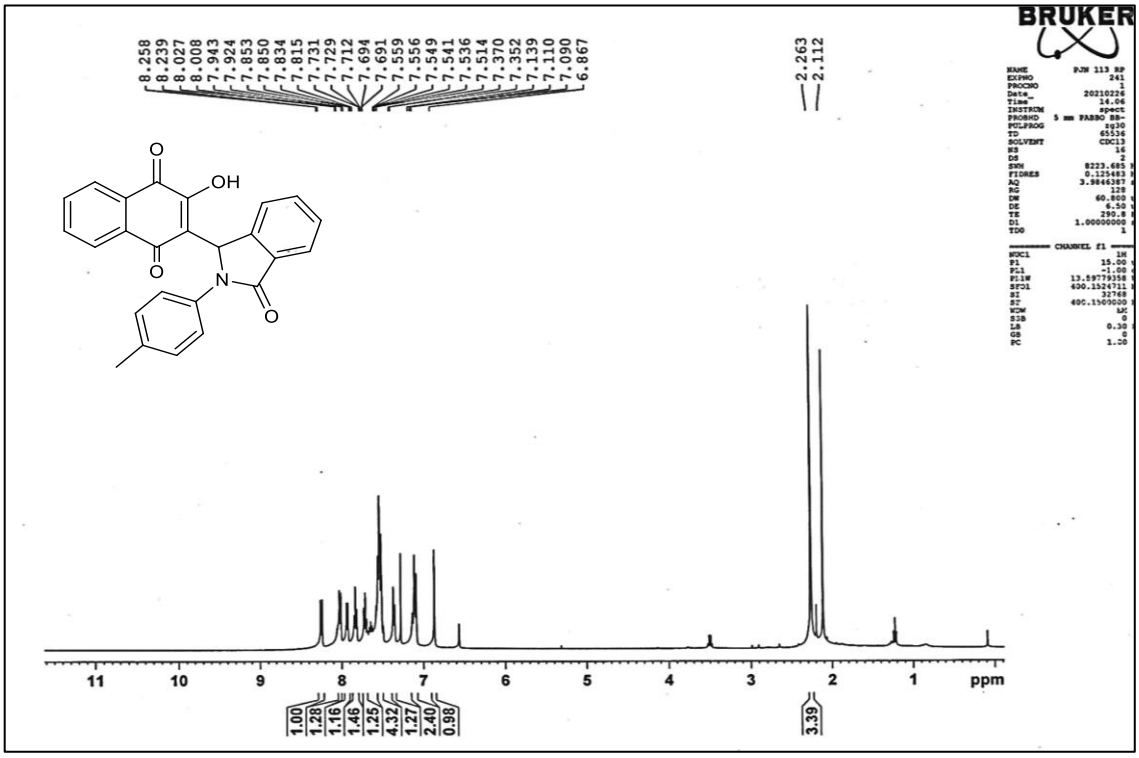

Figure S6.1 ^{1}H NMR spectra of 4a

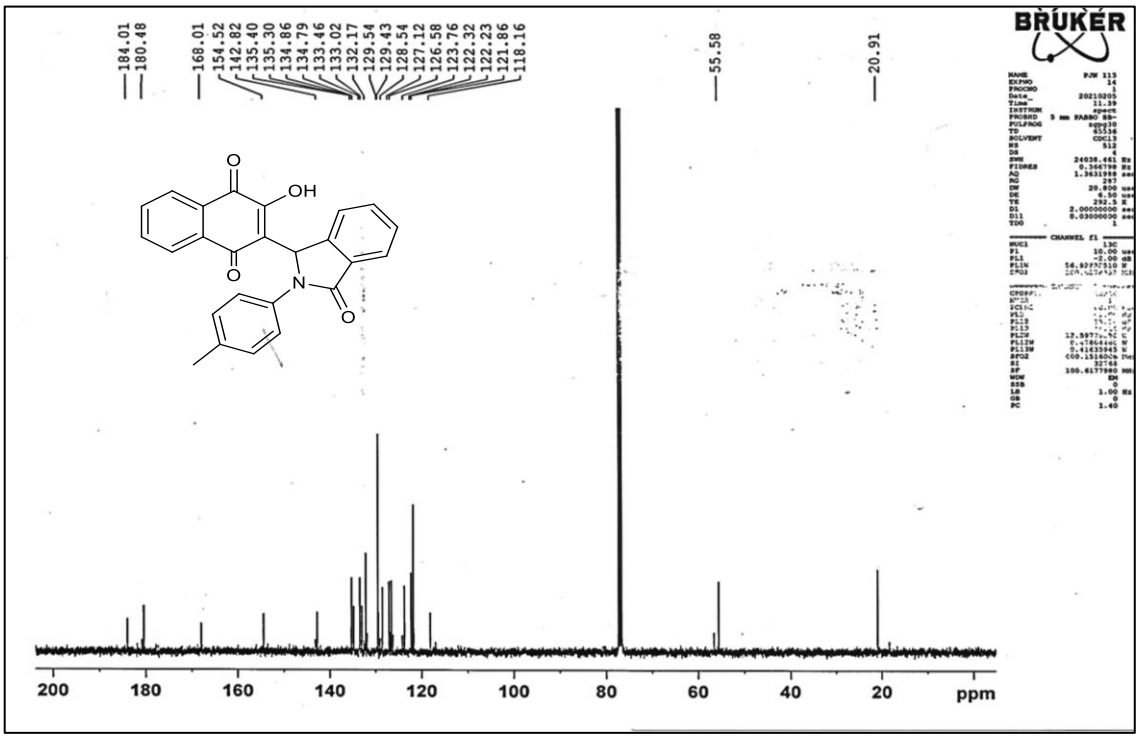

Figure S6.2 ^{13}C NMR spectra of 4a

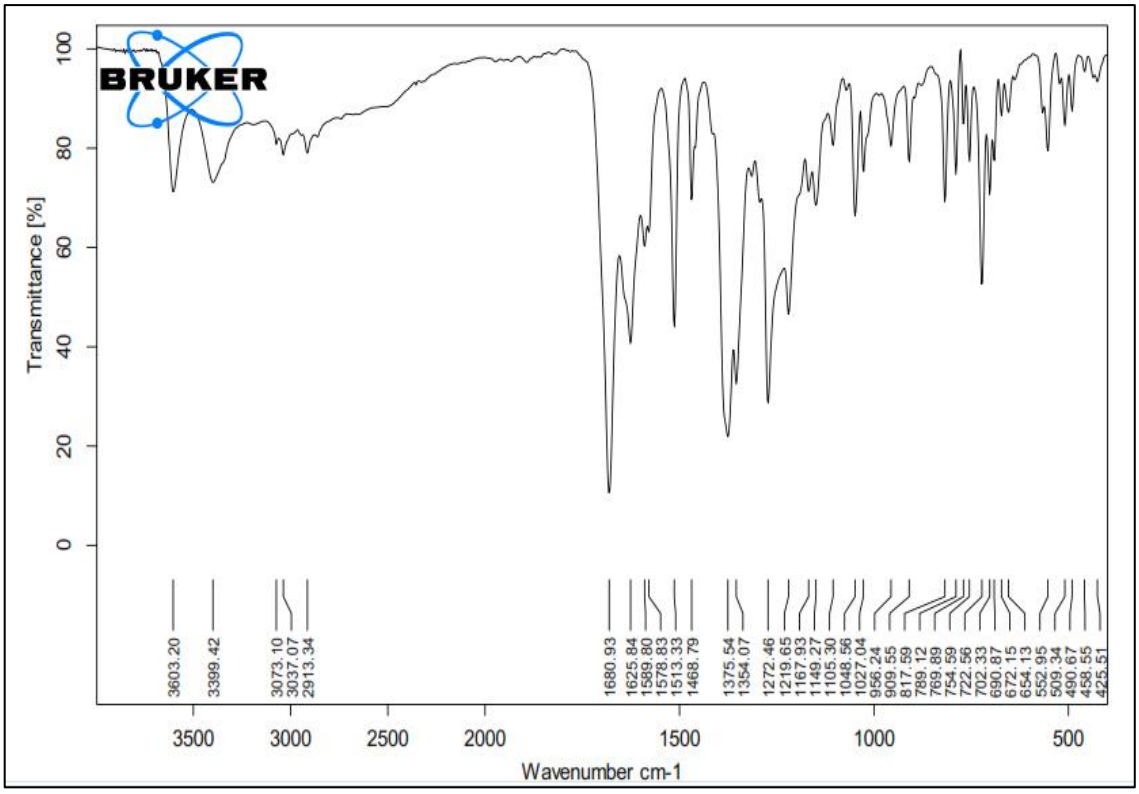

Figure S6.3 FT-IR spectra of 4a

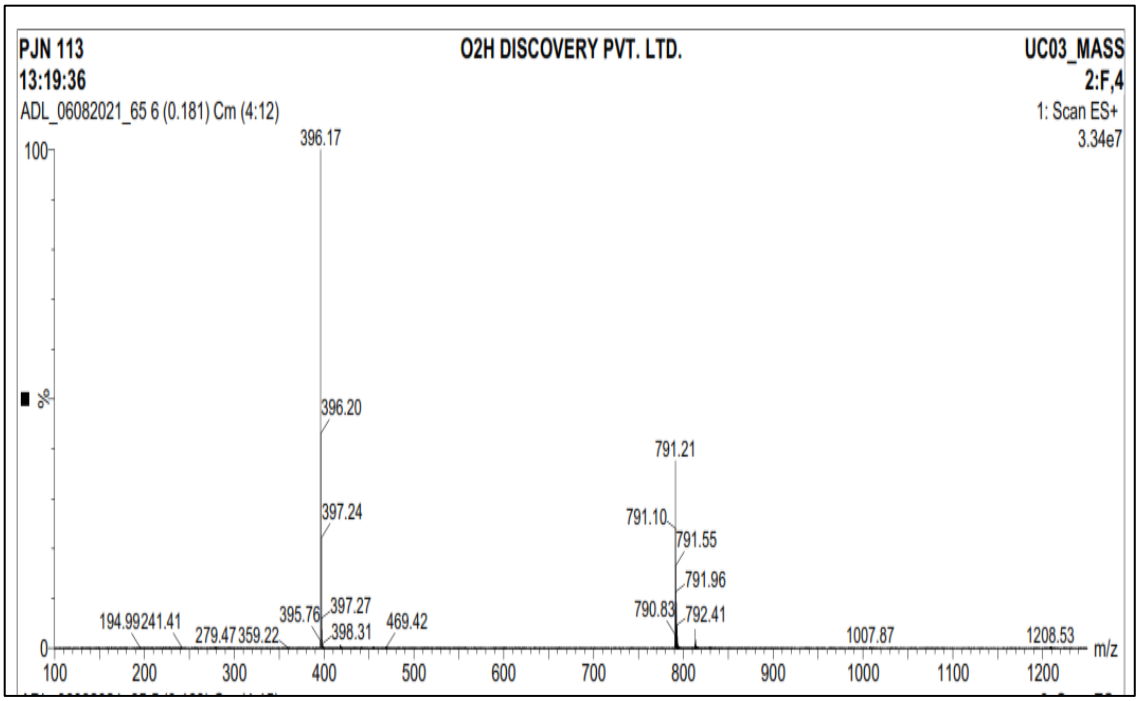

Figure S6.4 ESI-MS spectra of 4a

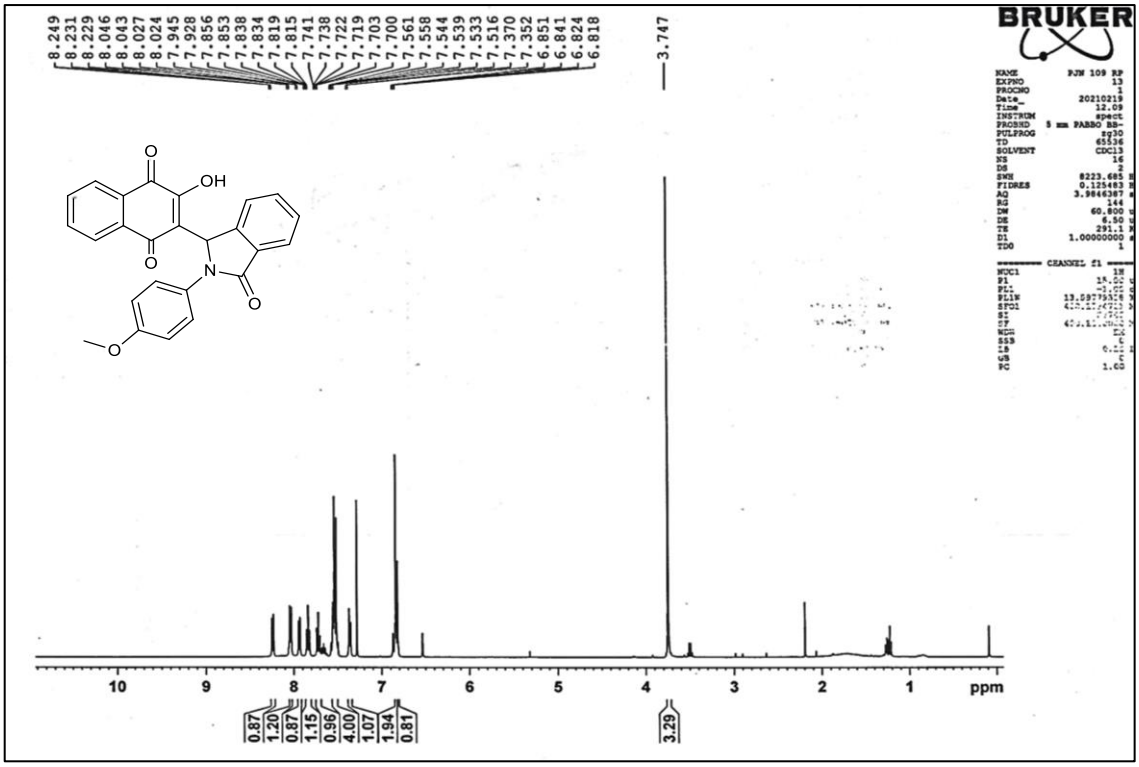

Figure S6.5 ^{1}H NMR spectra of (4b)

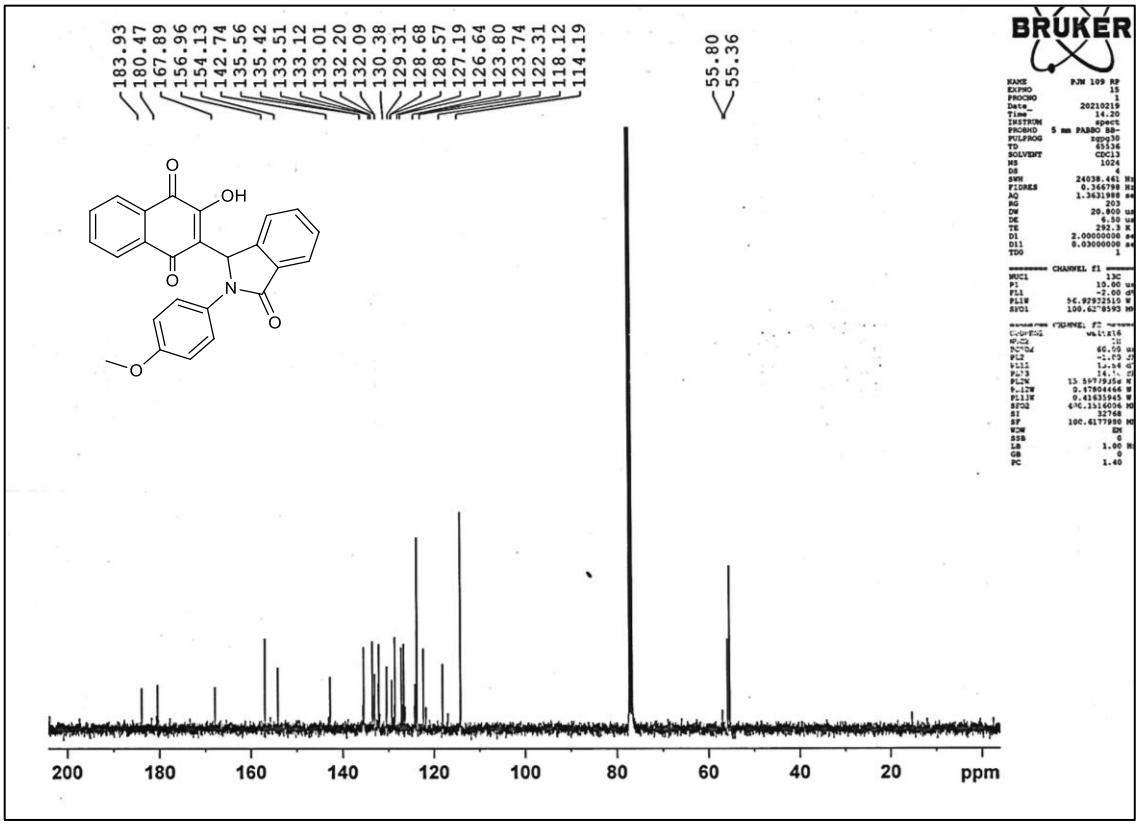

Figure S6.6 ^{13}C NMR spectra of (4b)

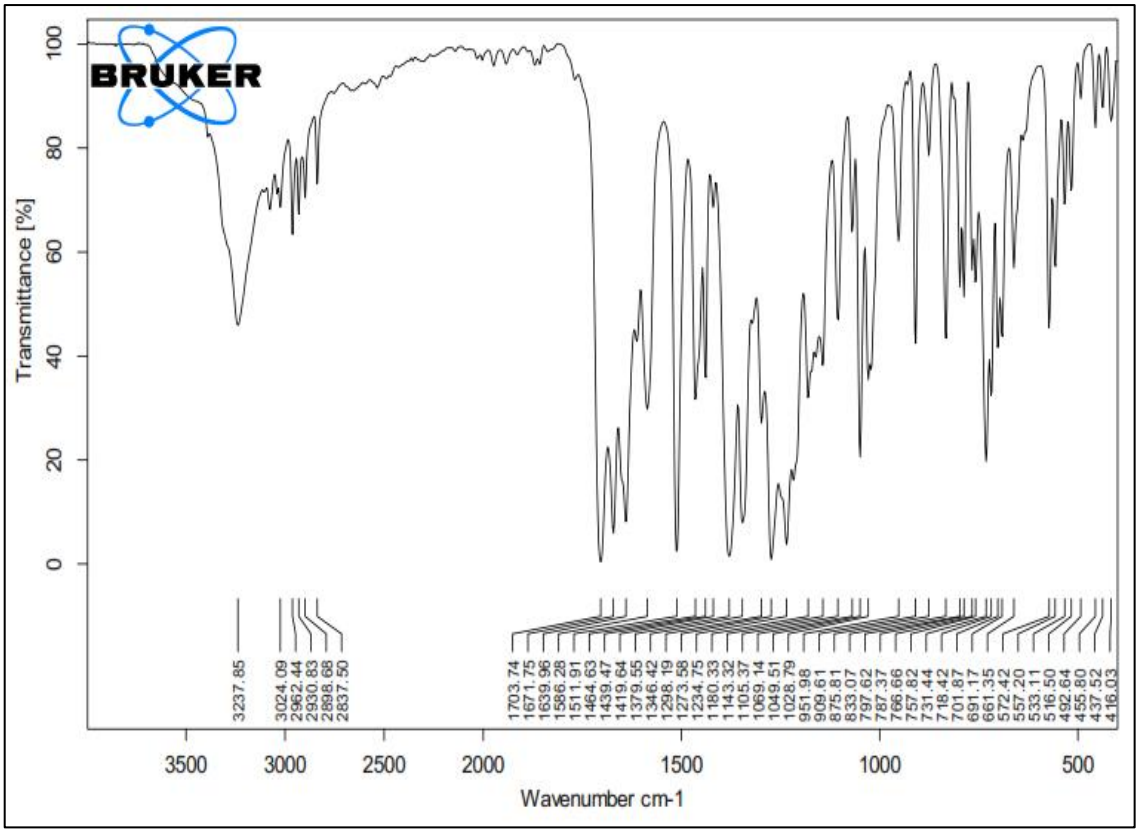

Figure S6.7 FT-IR spectra of 4b

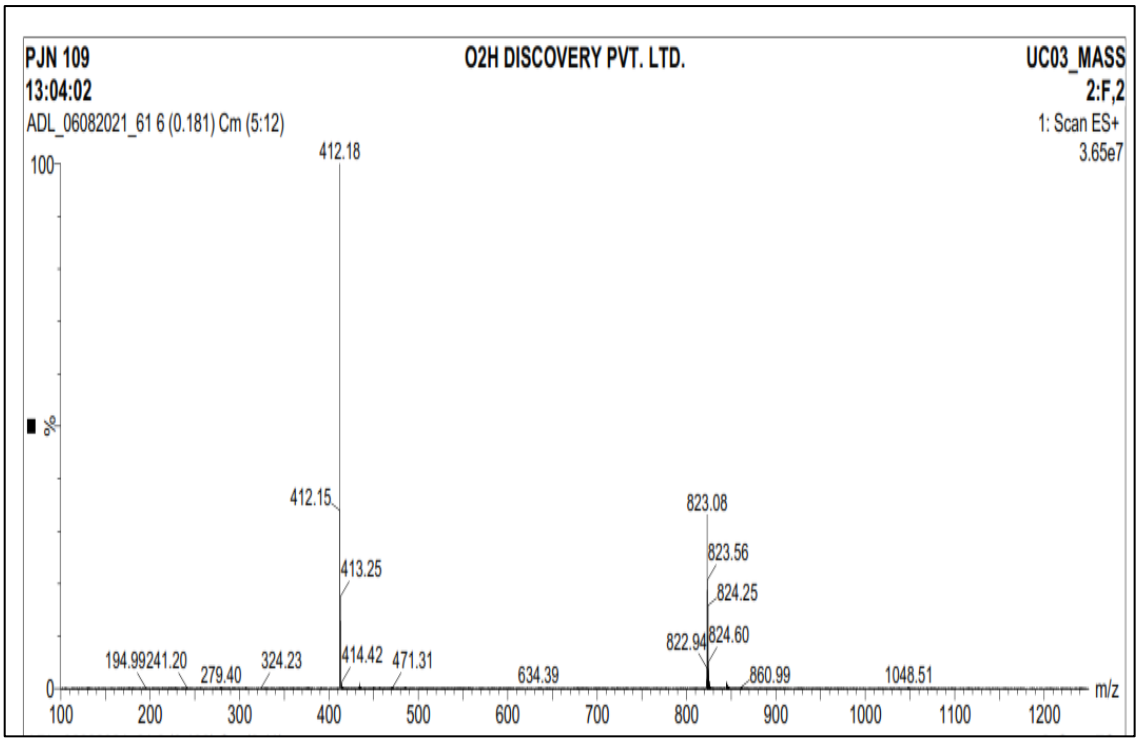

Figure S6.8 ESI-MS spectra of 4b

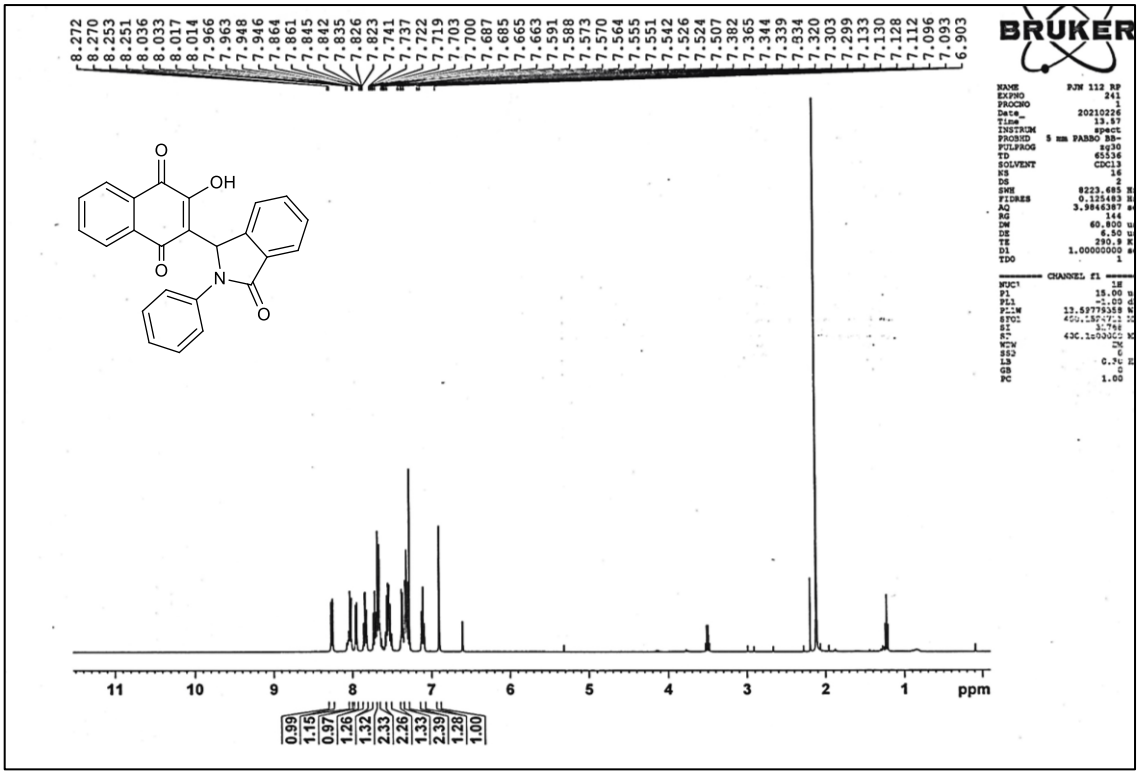

Figure S6.9 ^{1}H NMR spectra of 4c

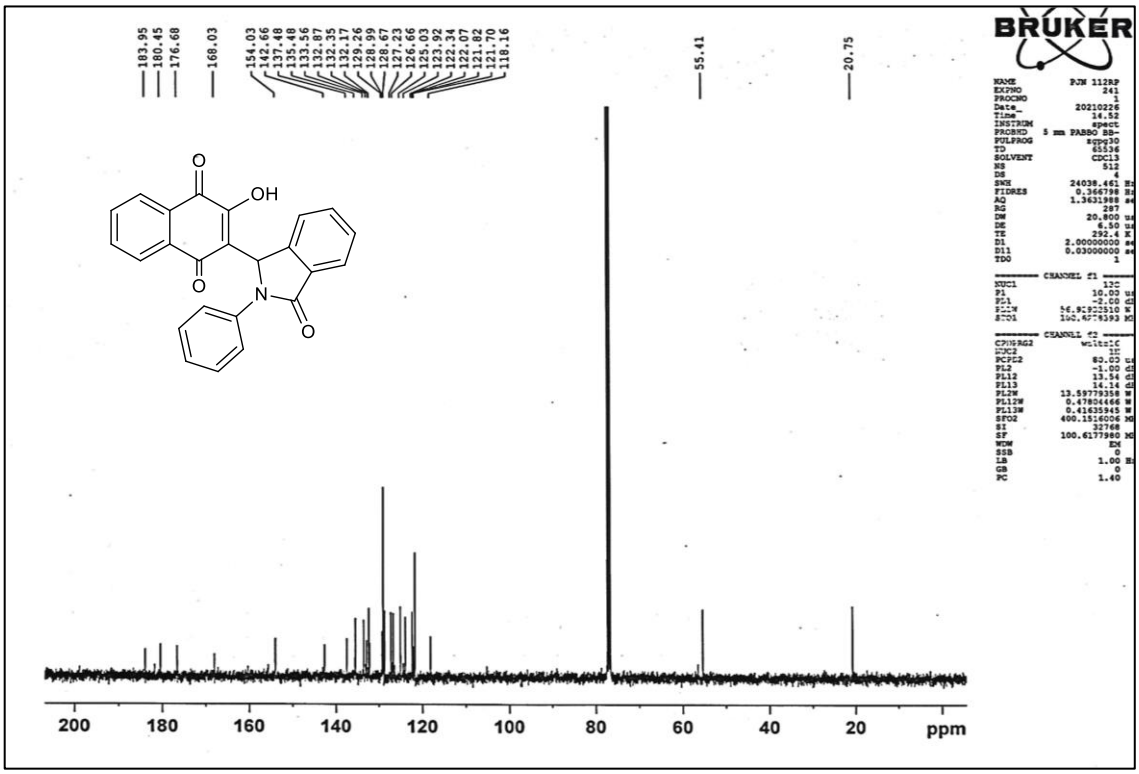

Figure S6.10 ^{13}C NMR spectra of 4c

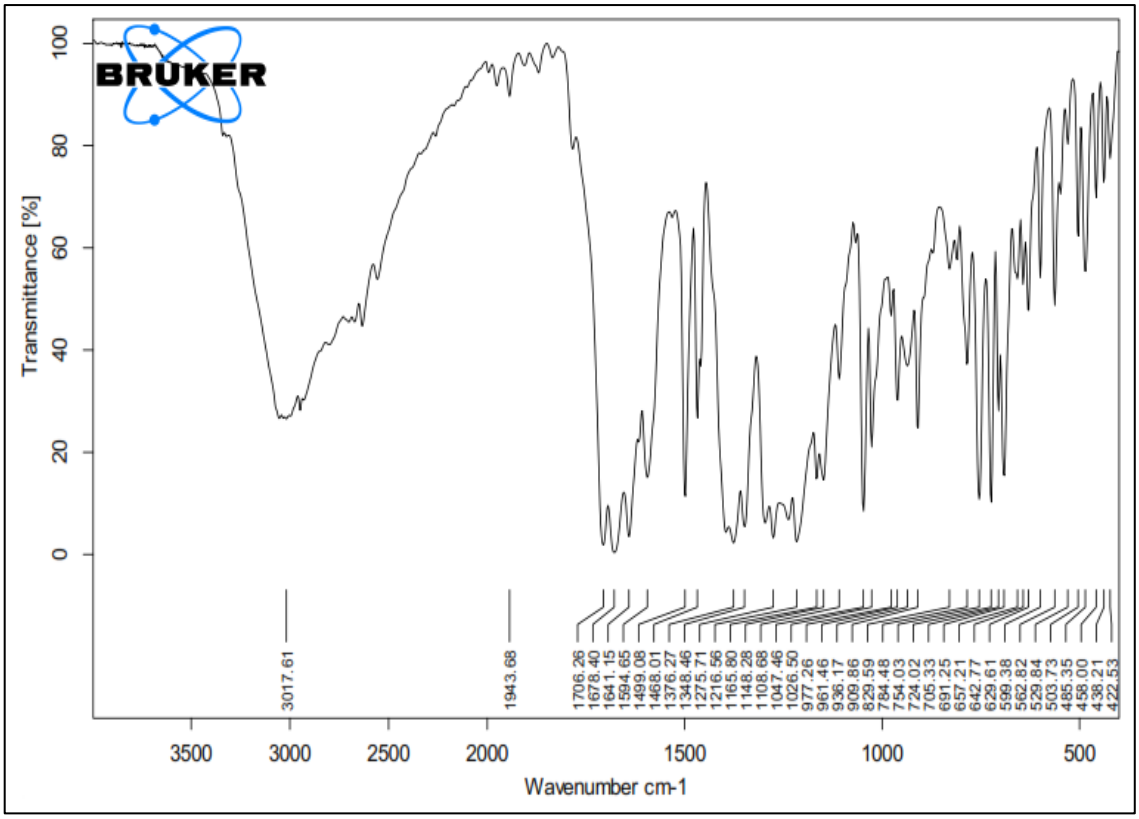

Figure S6.11 FT-IR spectra of 4c

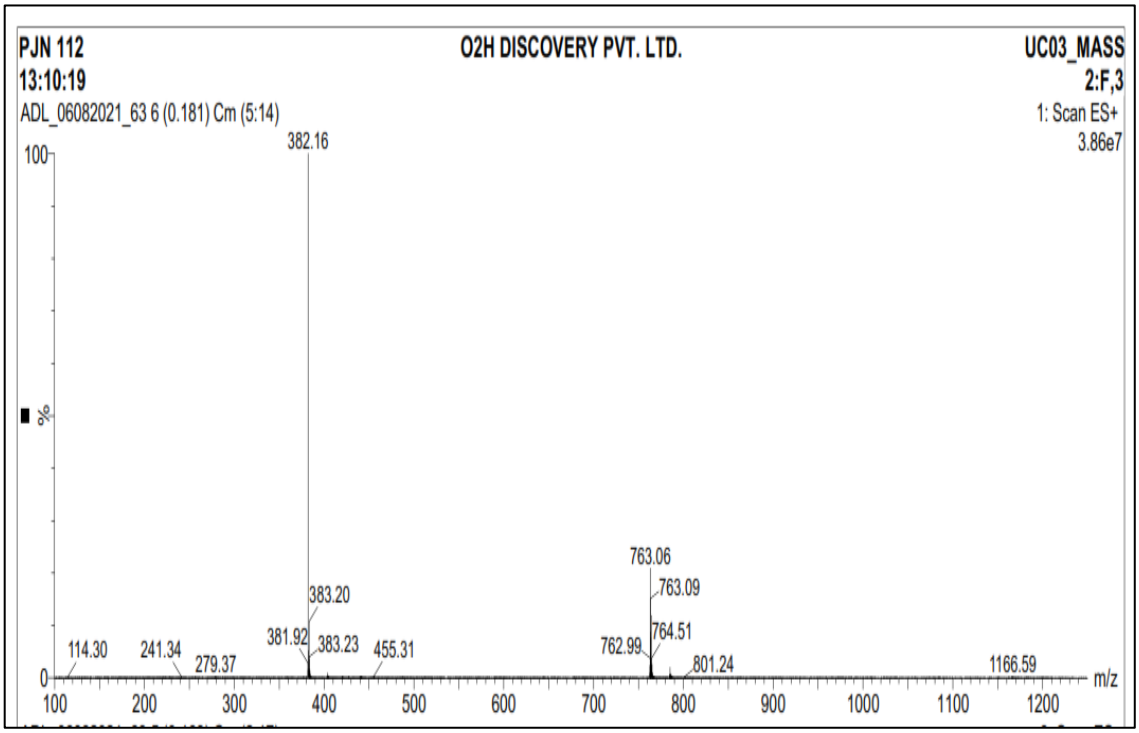

Figure S6.12 ESI-MS spectra of 4c

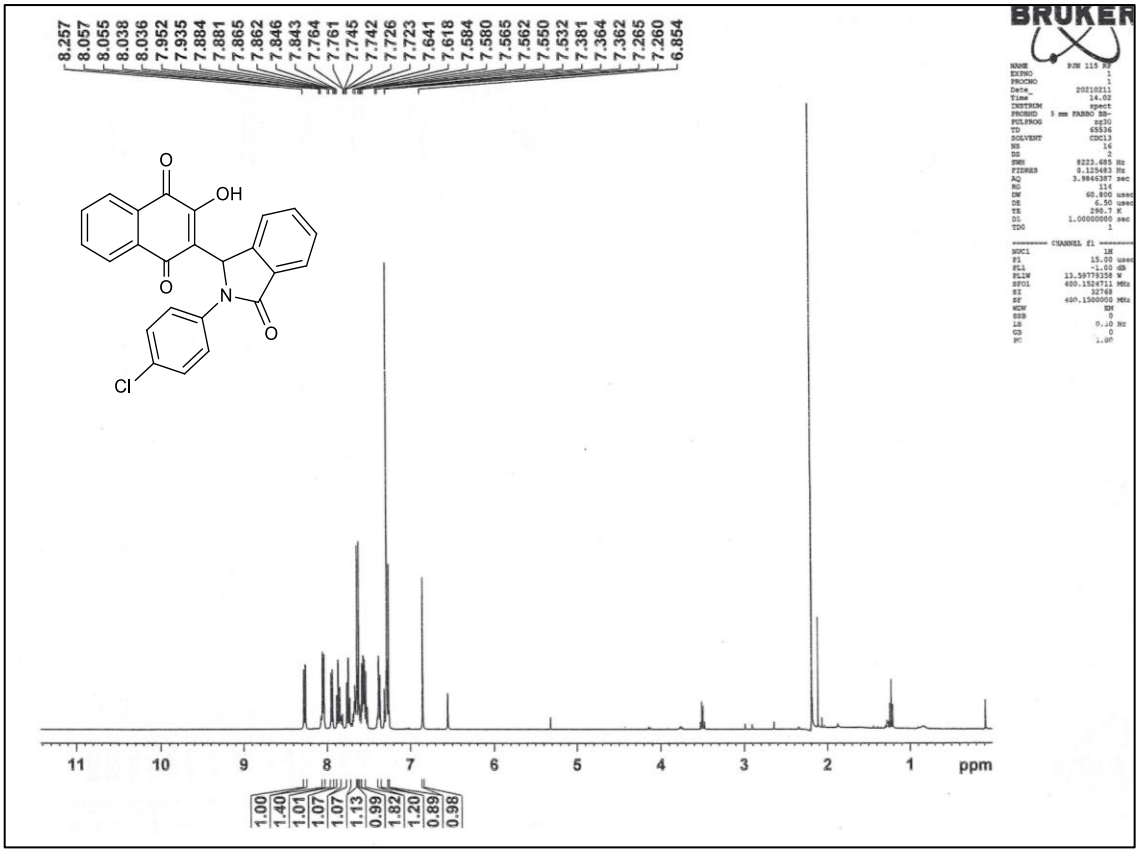

Figure S6.13 ^{1}H NMR spectra 4d

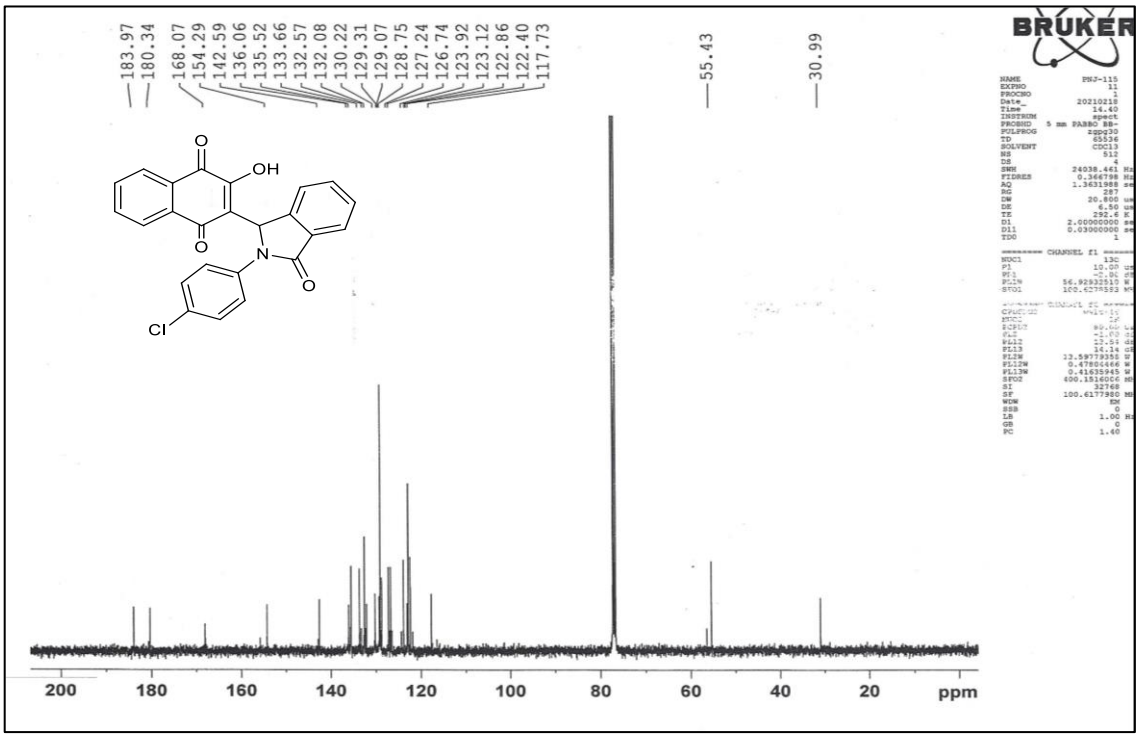

Figure S6.14 ^{13}C NMR spectra of 4d

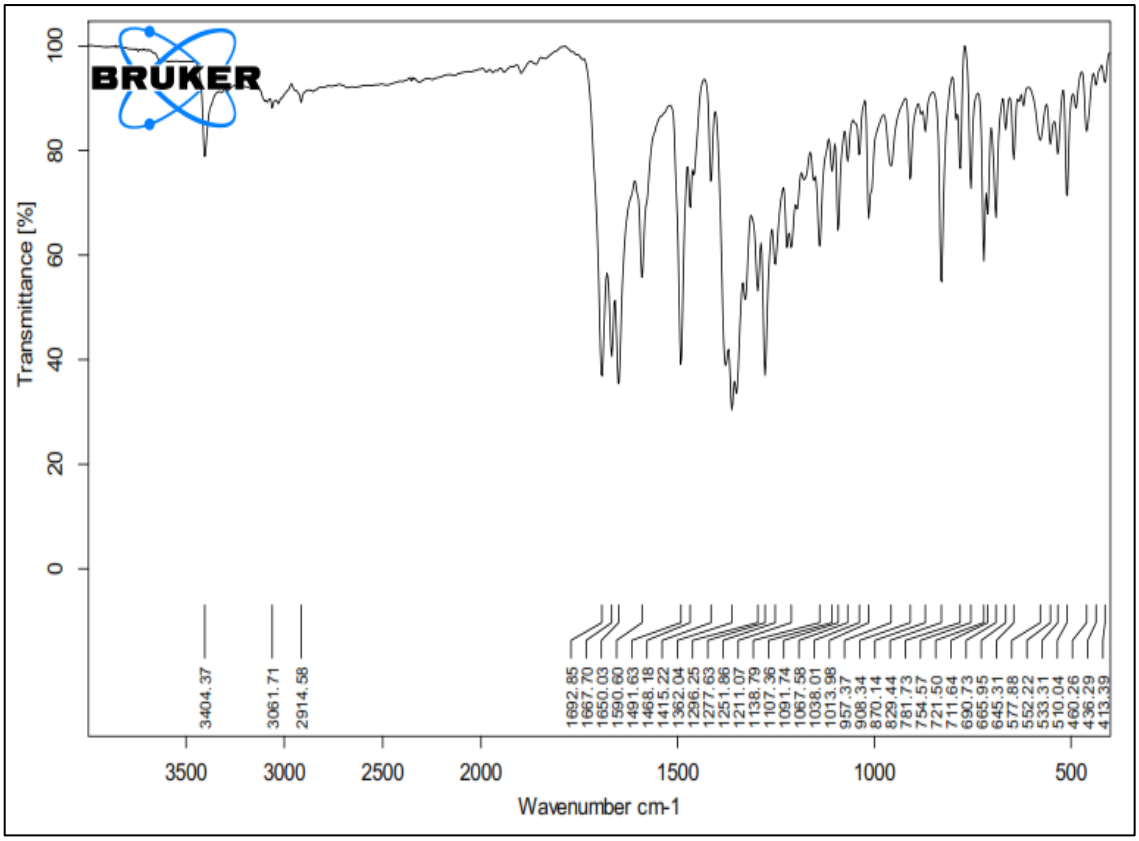

Figure S6.15 FT-IR spectra 4d

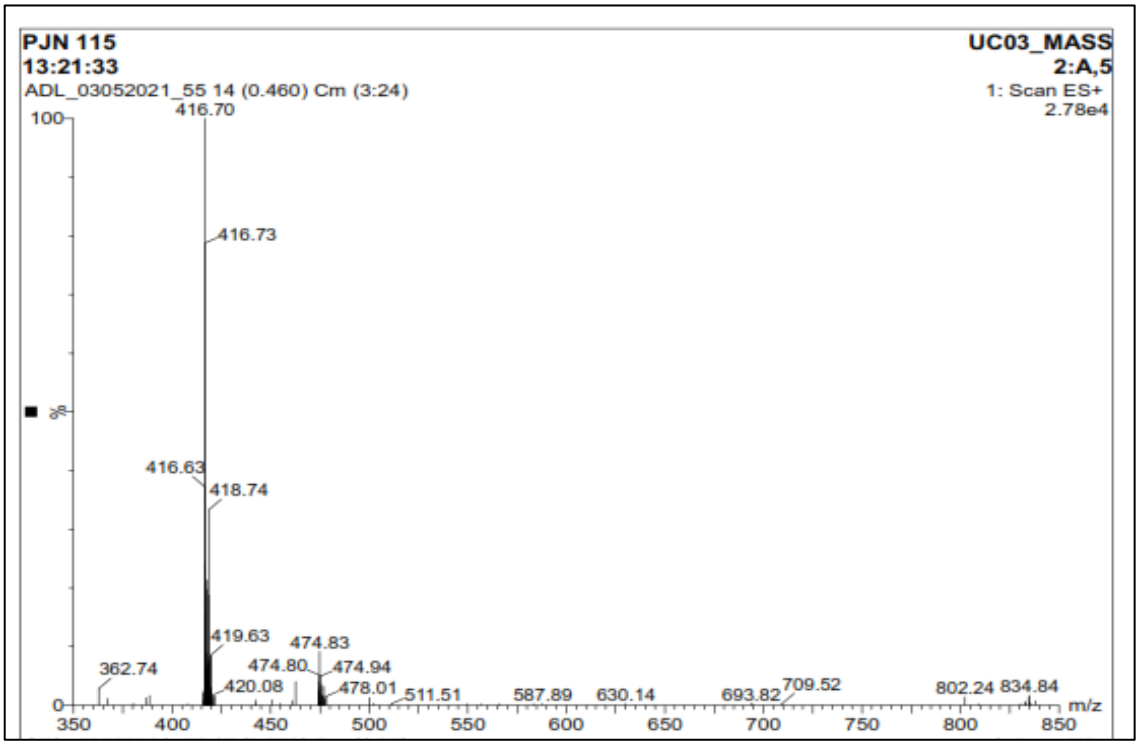

Figure S6.15 ESI-MS spectra of 4d

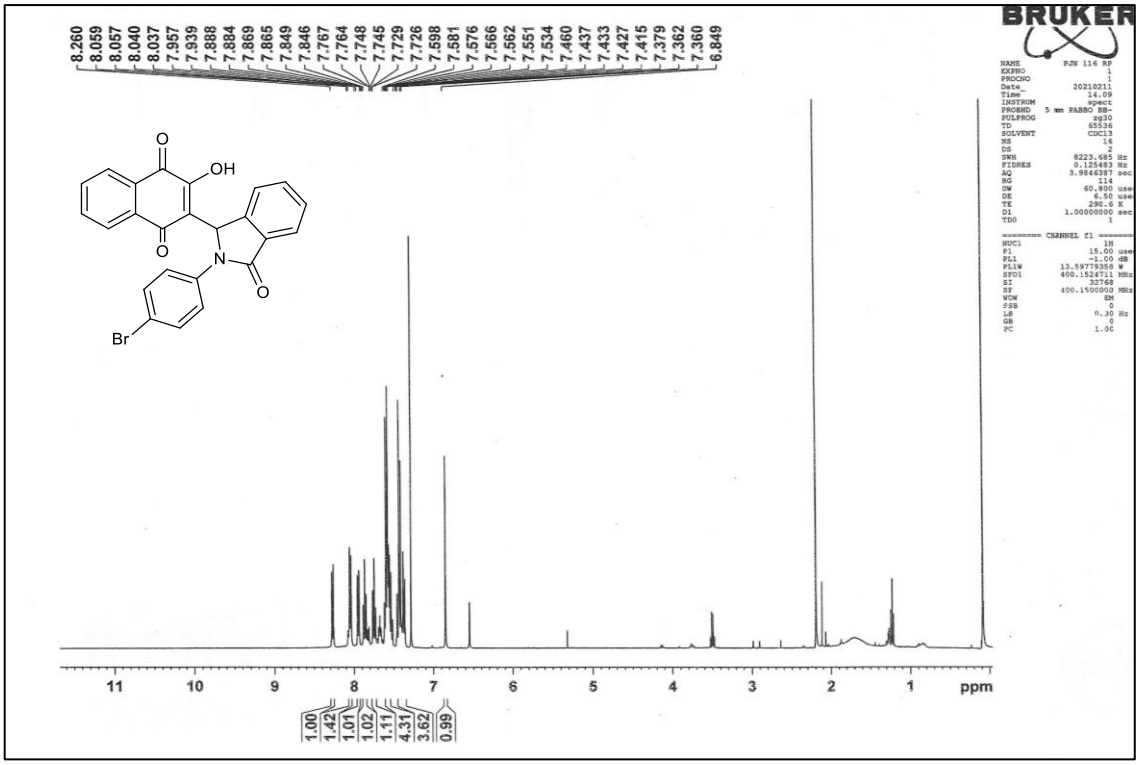

Figure S6.17 ^{1}H NMR spectra of 4e

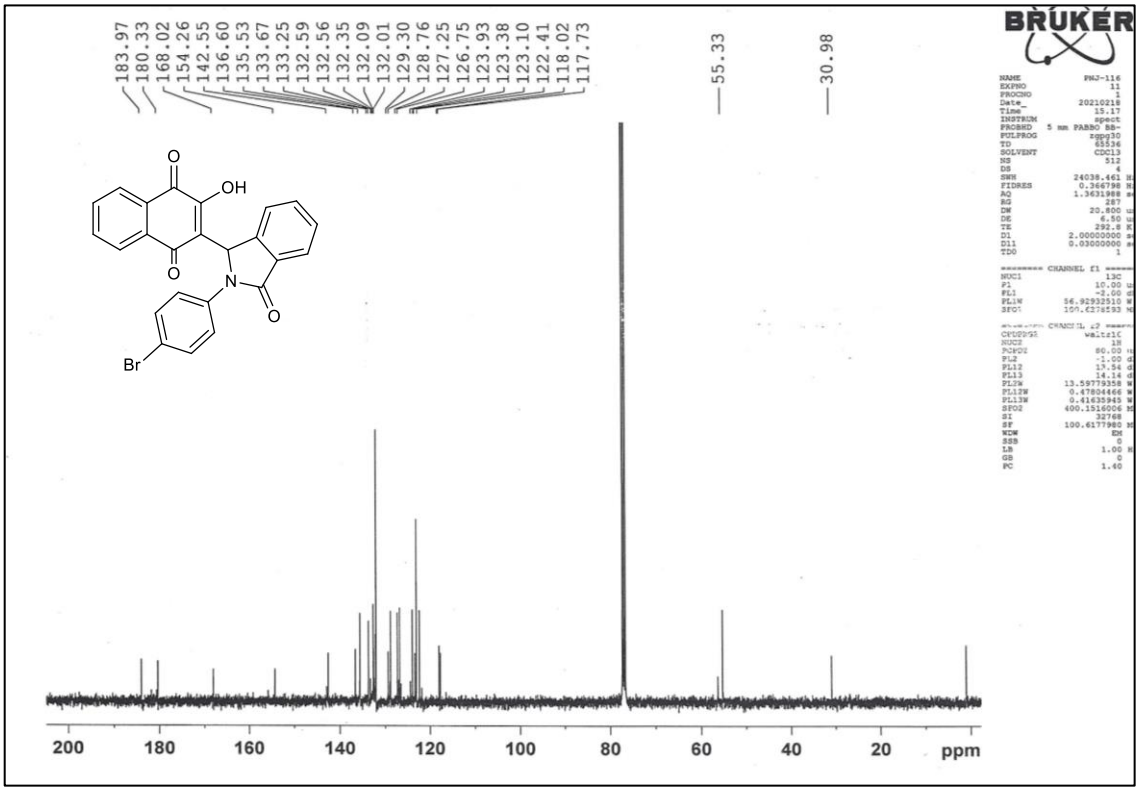

Figure S6.18 ^{13}C NMR spectra of 4e

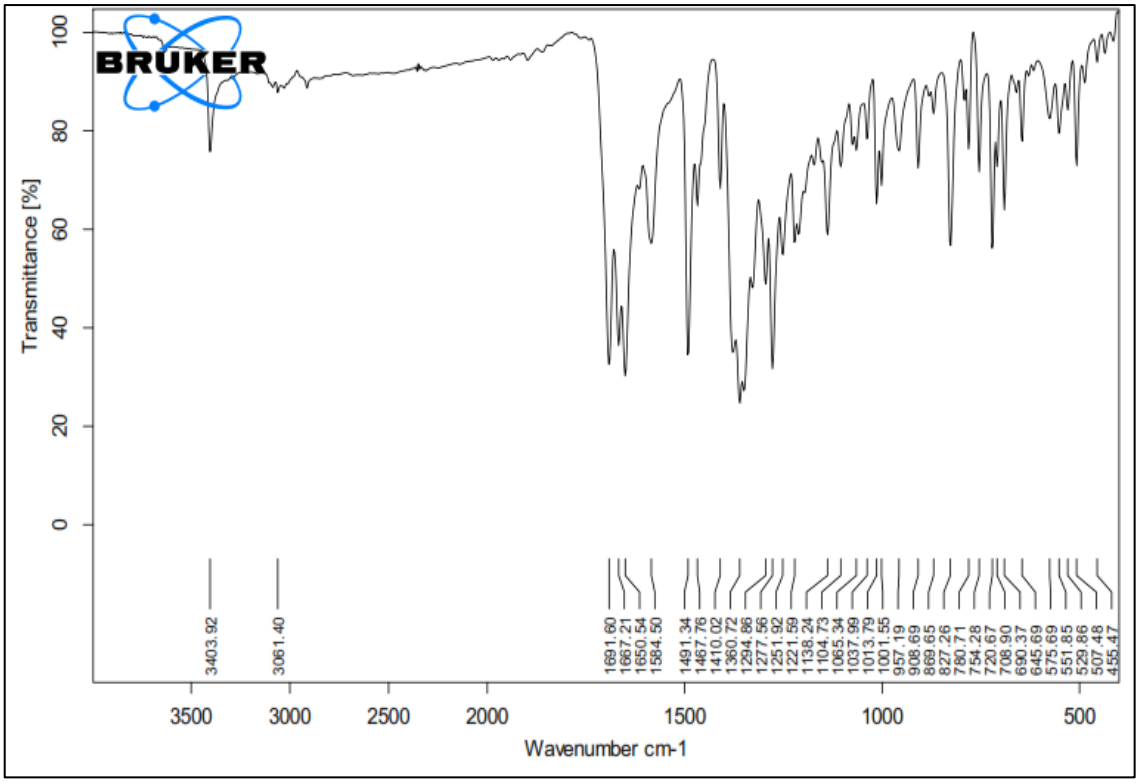

Figure S6.19 FT-IR spectra of 4e

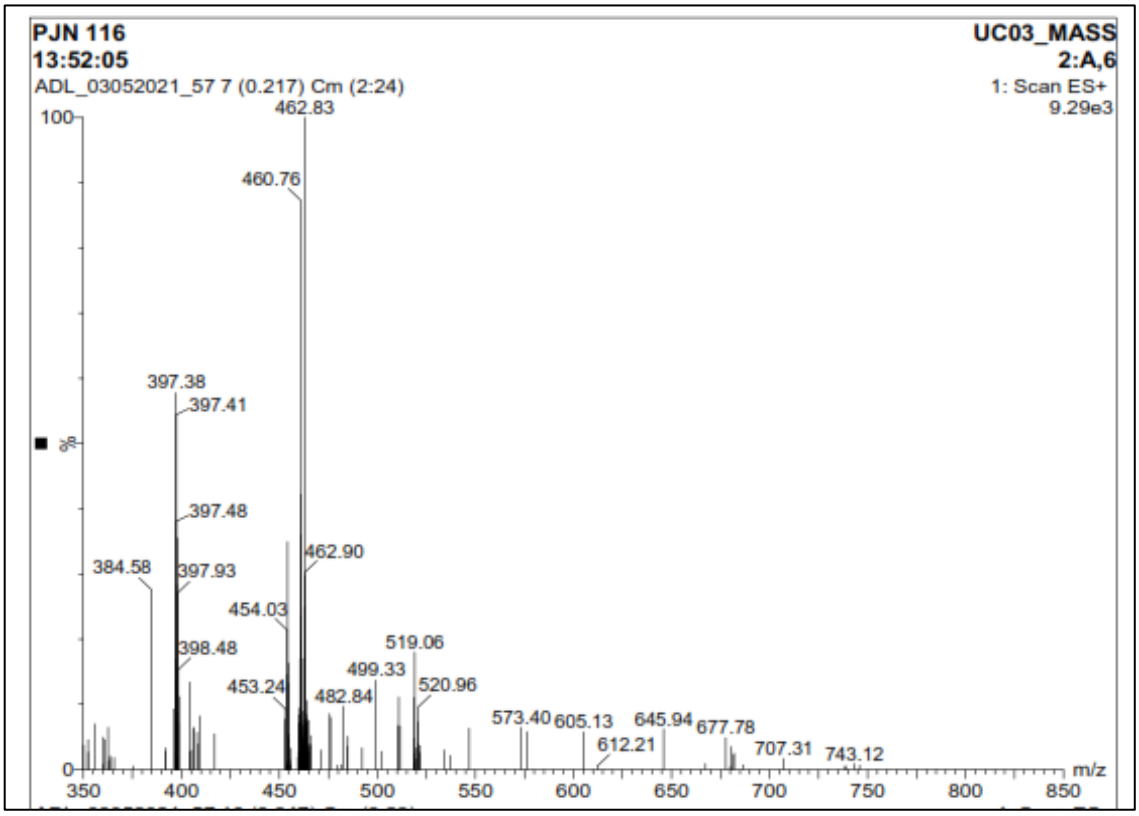

Figure S6.20 ESI-MS spectra of 4e

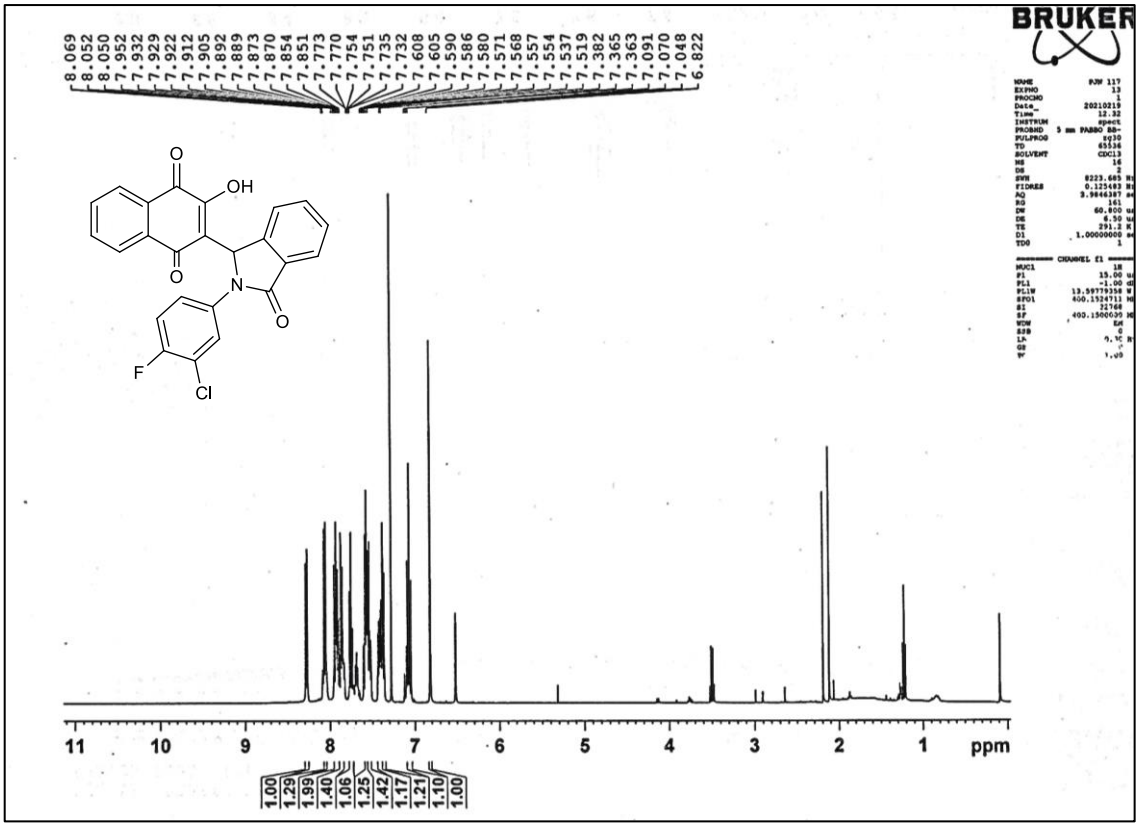

Figure S6.21 ^{1}H NMR spectra of 4f

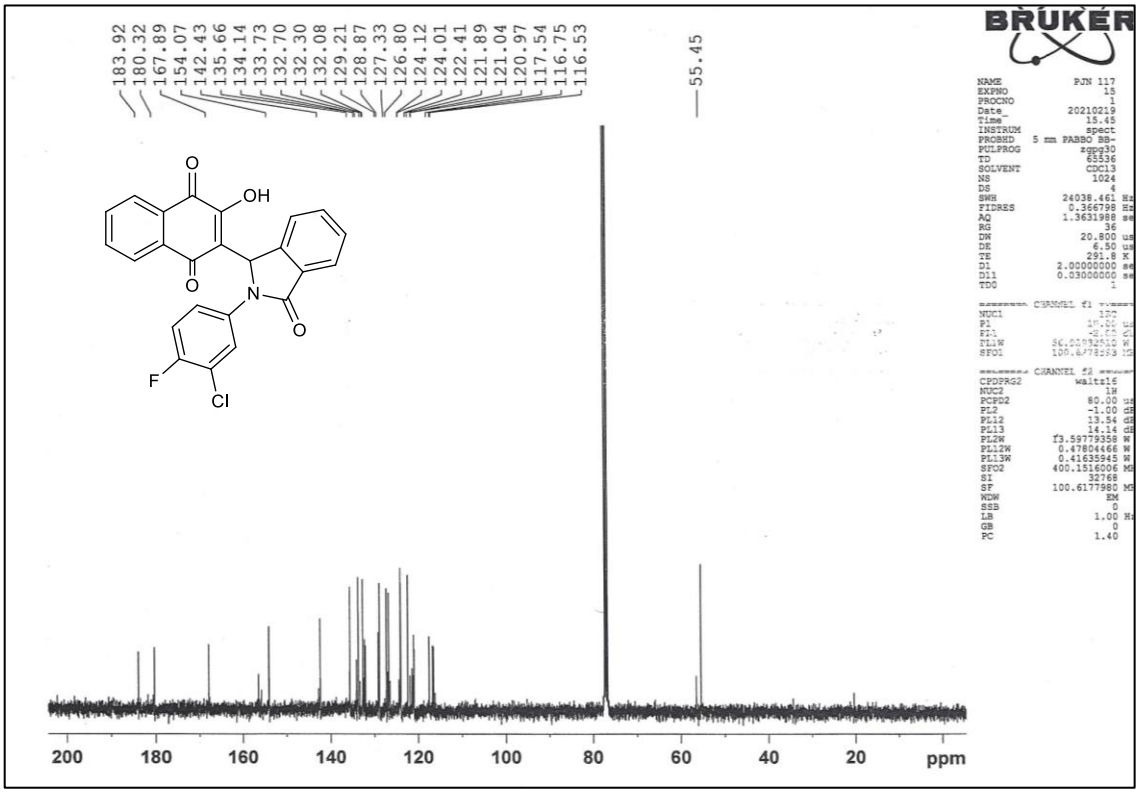

Figure S6.22 ^{13}C NMR spectra of 4f

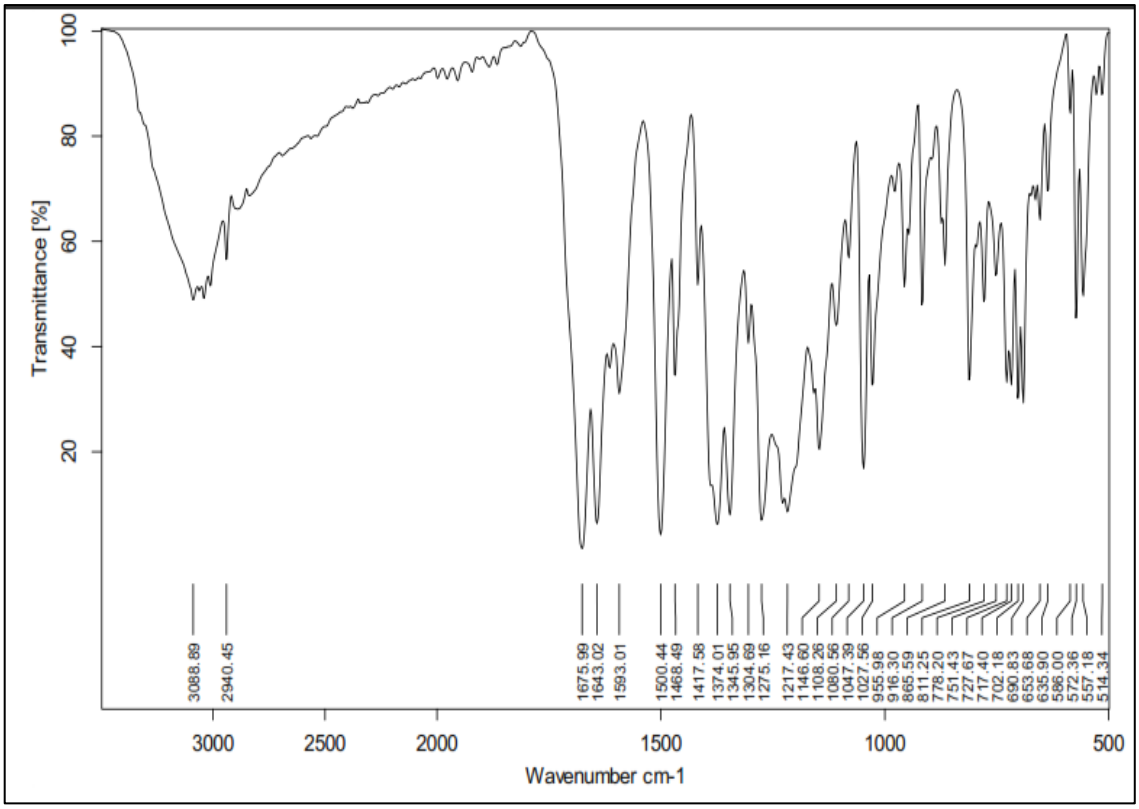

Figure S6.23 FT-IR spectra of 4f

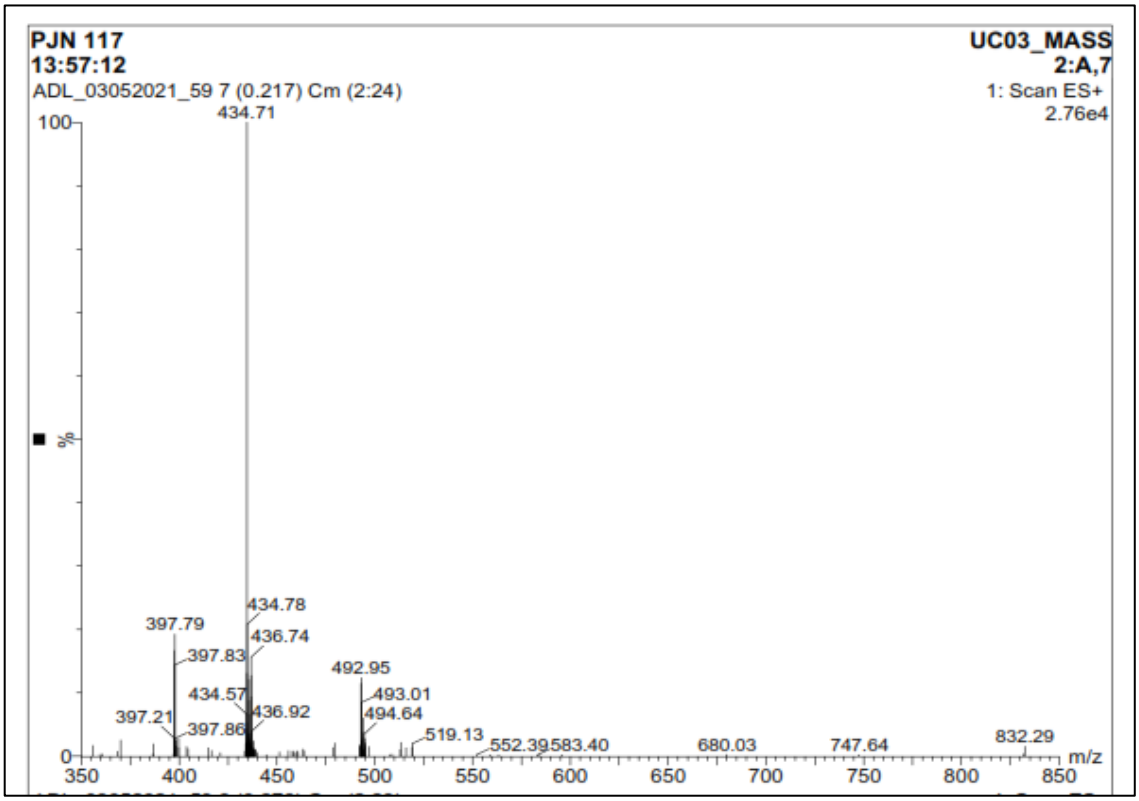

Figure S6.24 ESI-MS spectra of 4f

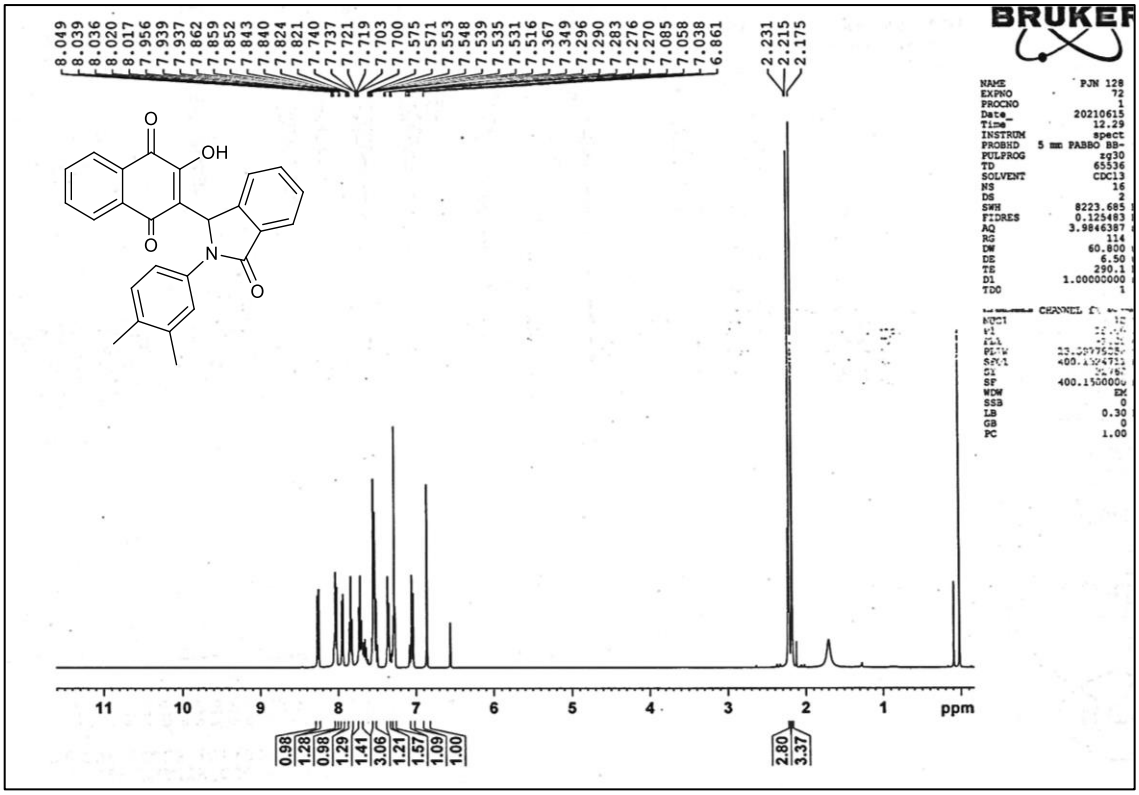

Figure S6.25 ^{1}H NMR spectra of 4g

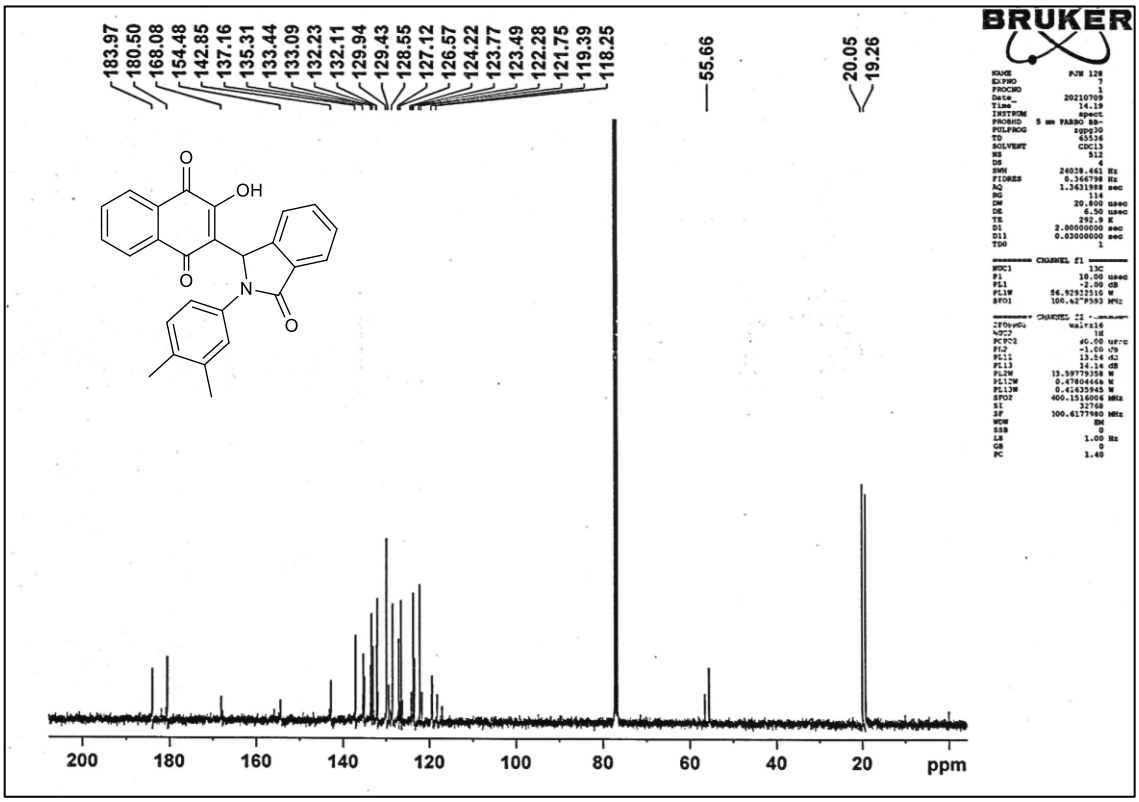

Figure S6.26 ^{13}C NMR spectra of 4g

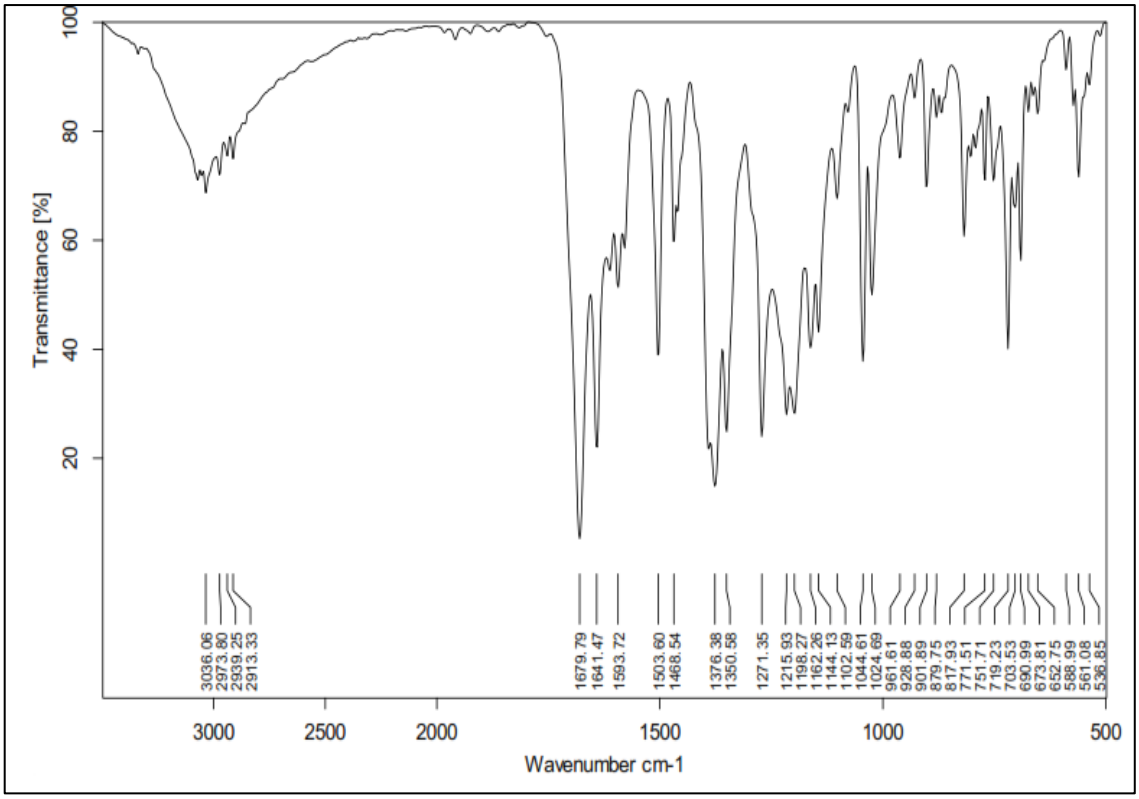

Figure S6.27 FT-IR spectra of 4g

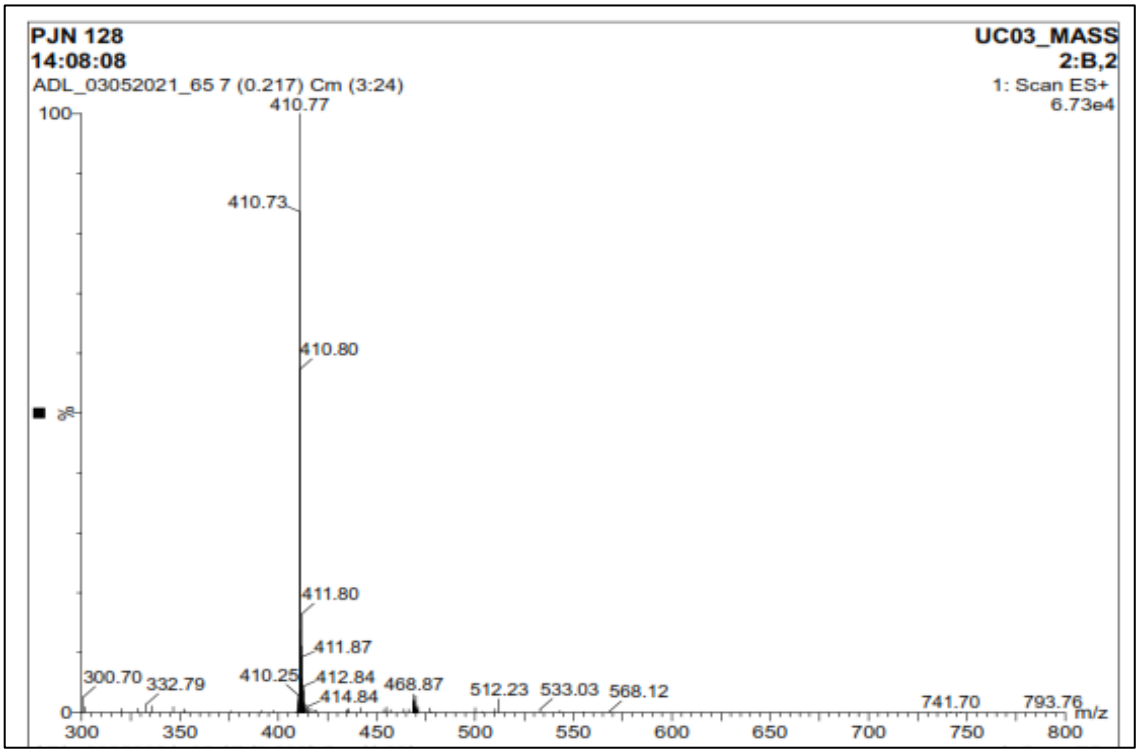

Figure S6.28 ESI-MS spectra of 4g

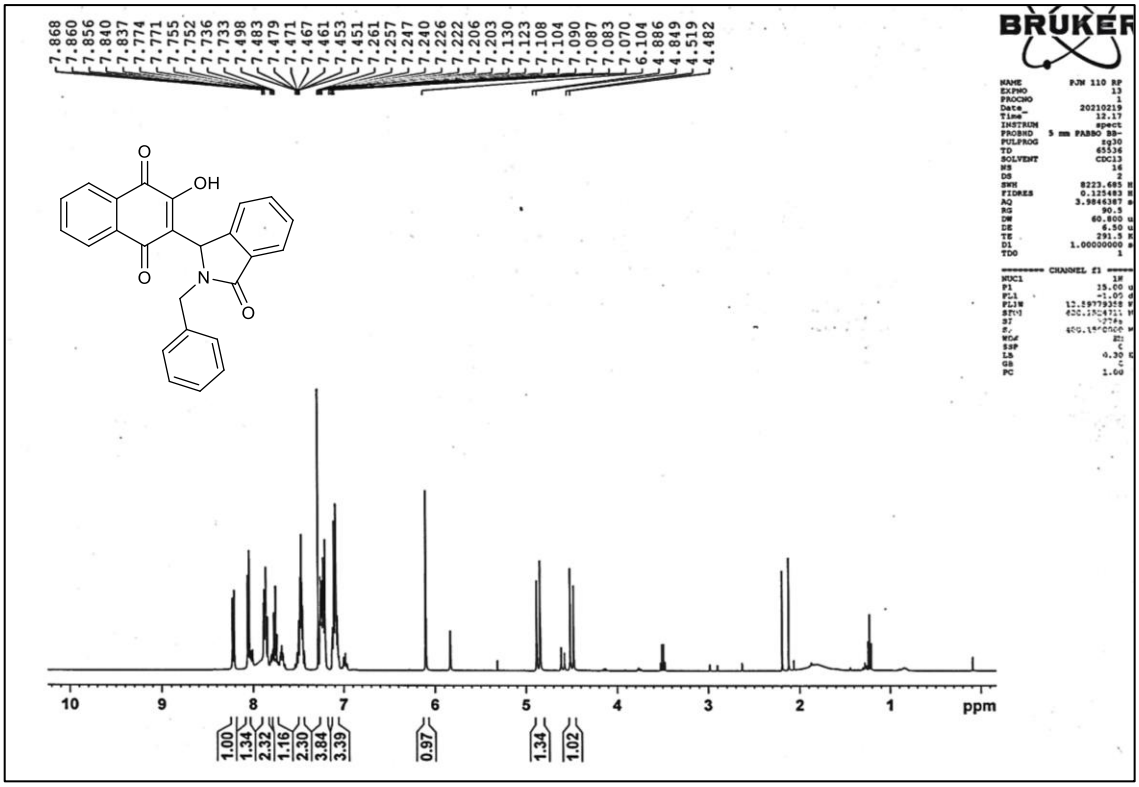

Figure S6.29 ^{1}H NMR spectra of 4h

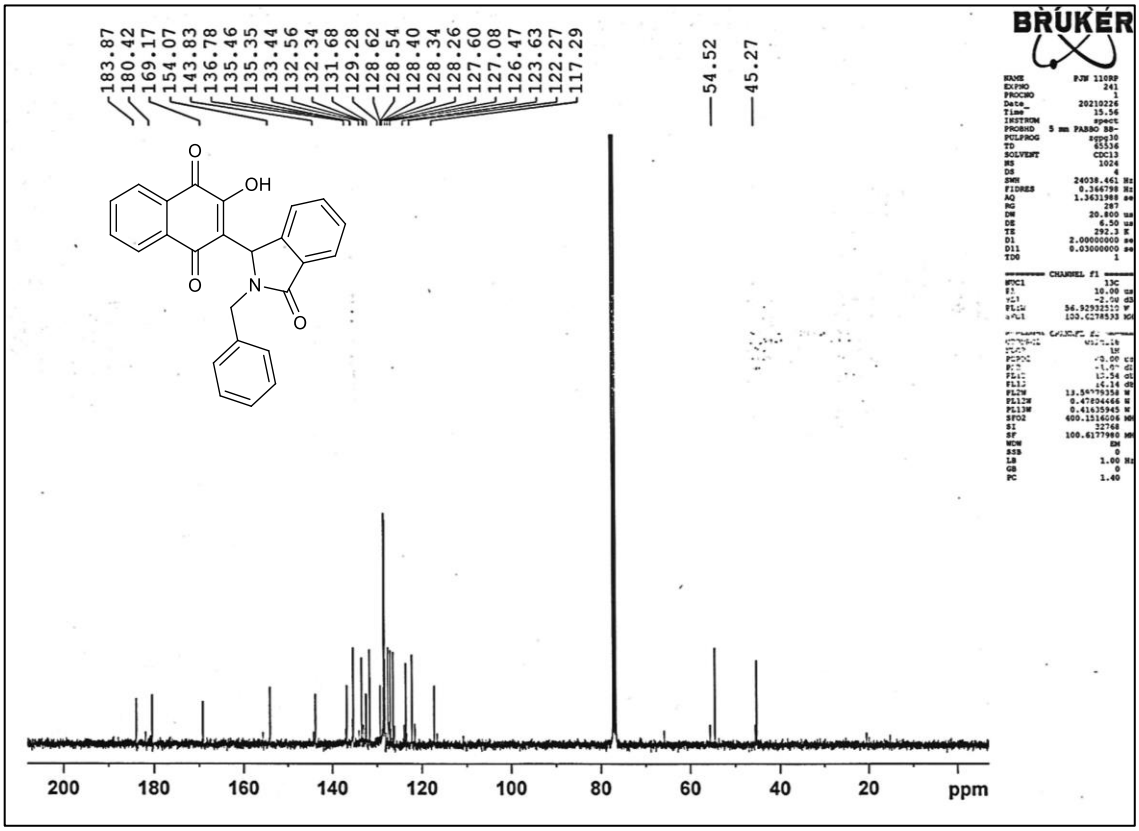

Figure S6.30 ^{13}C NMR spectra of 4h

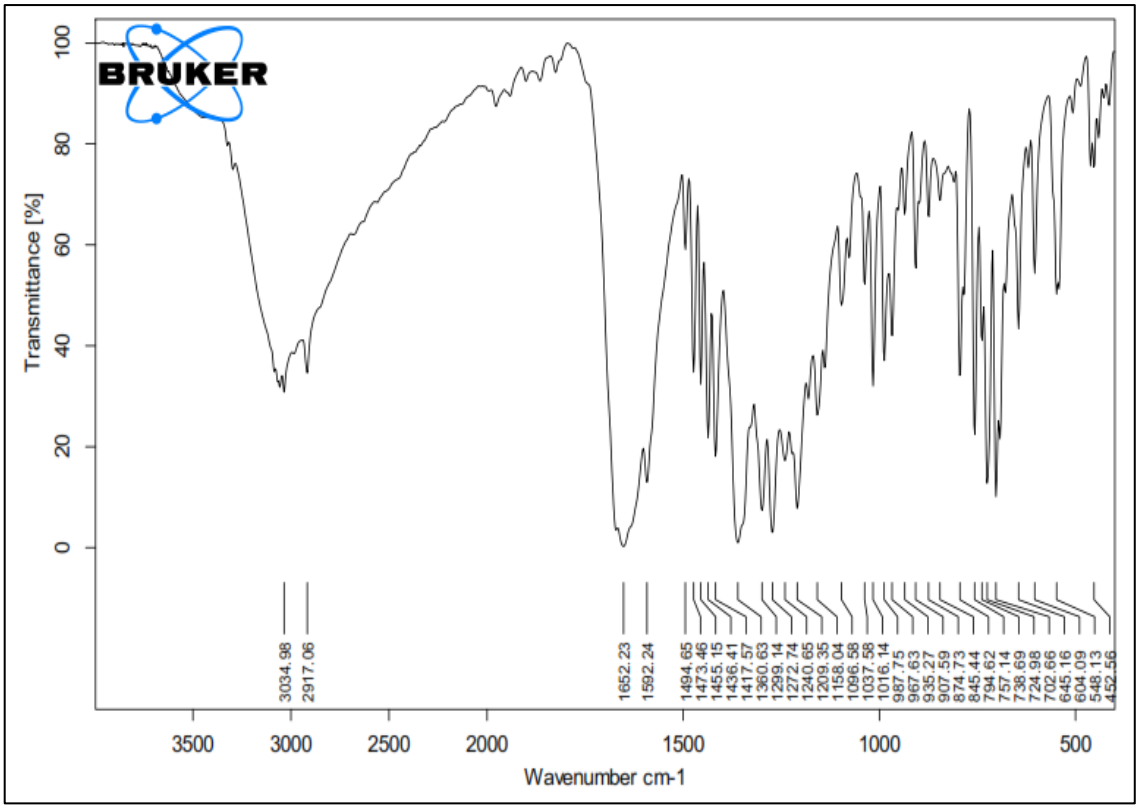

Figure S6.31 FT-IR spectra of 4h

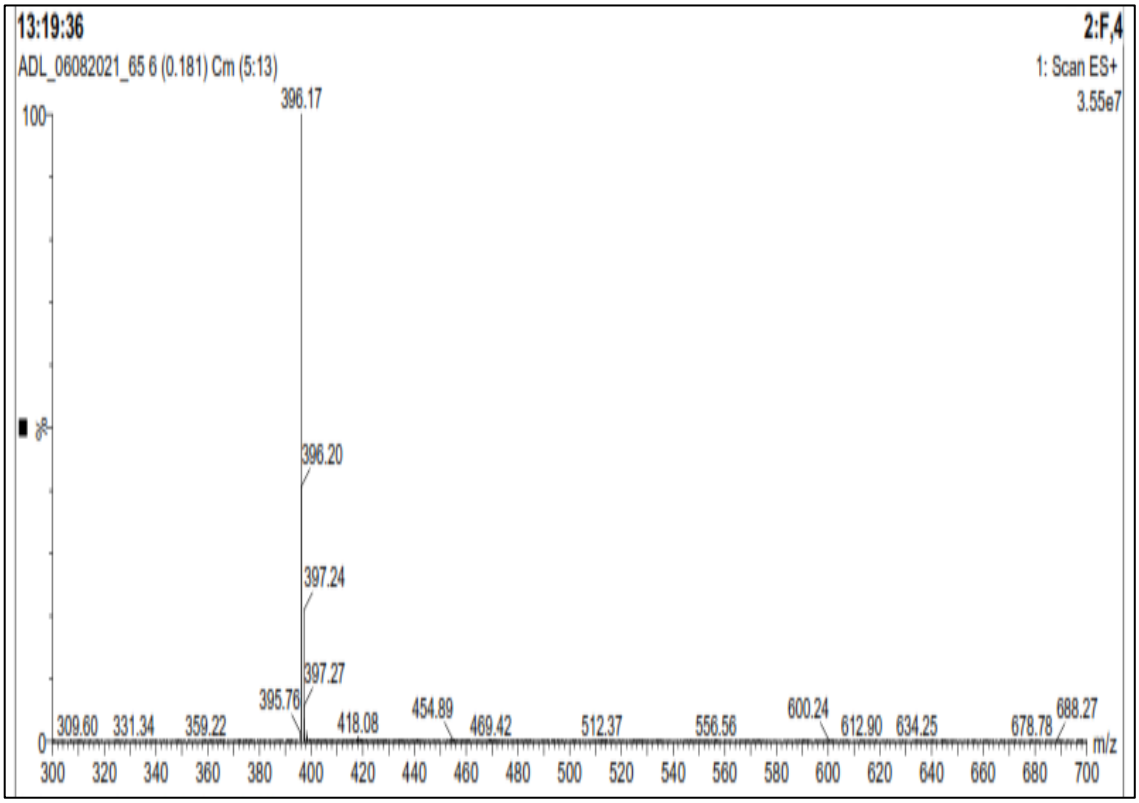

Figure S6.32 ESI-MS spectra of 4h

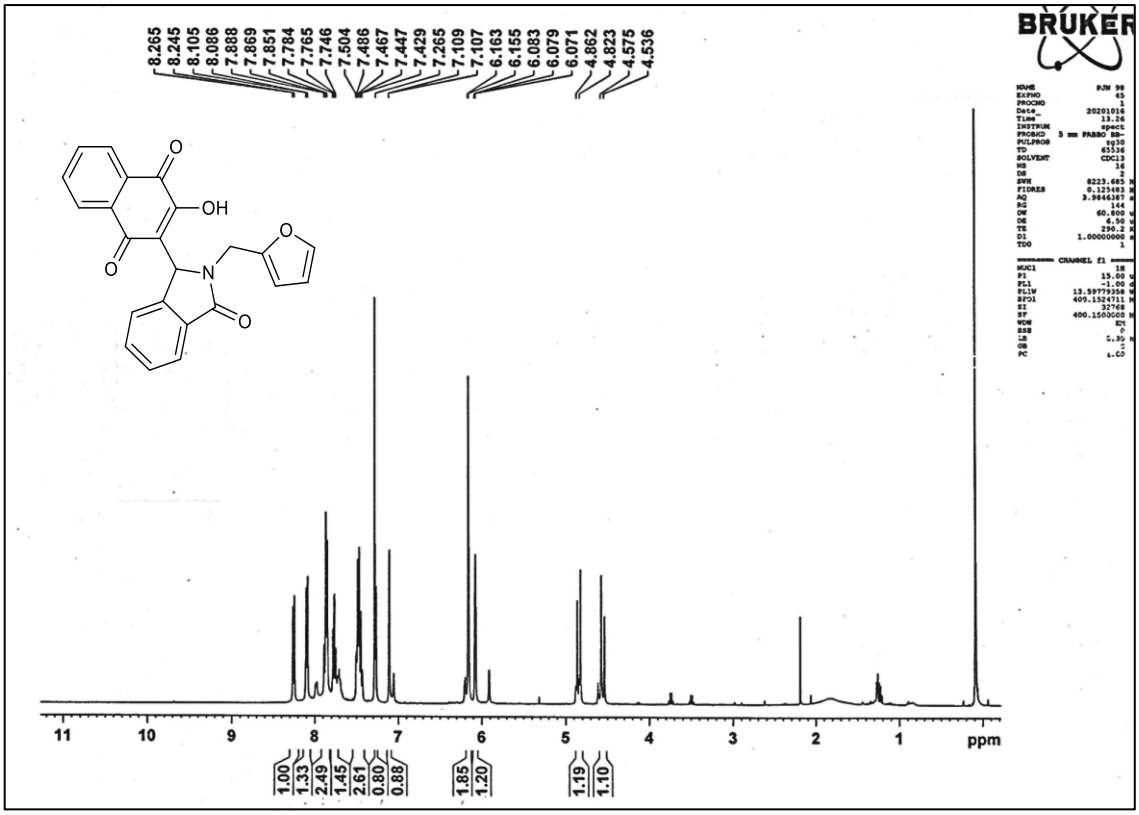

Figure S6.33 ^{1}H NMR spectra of 4i

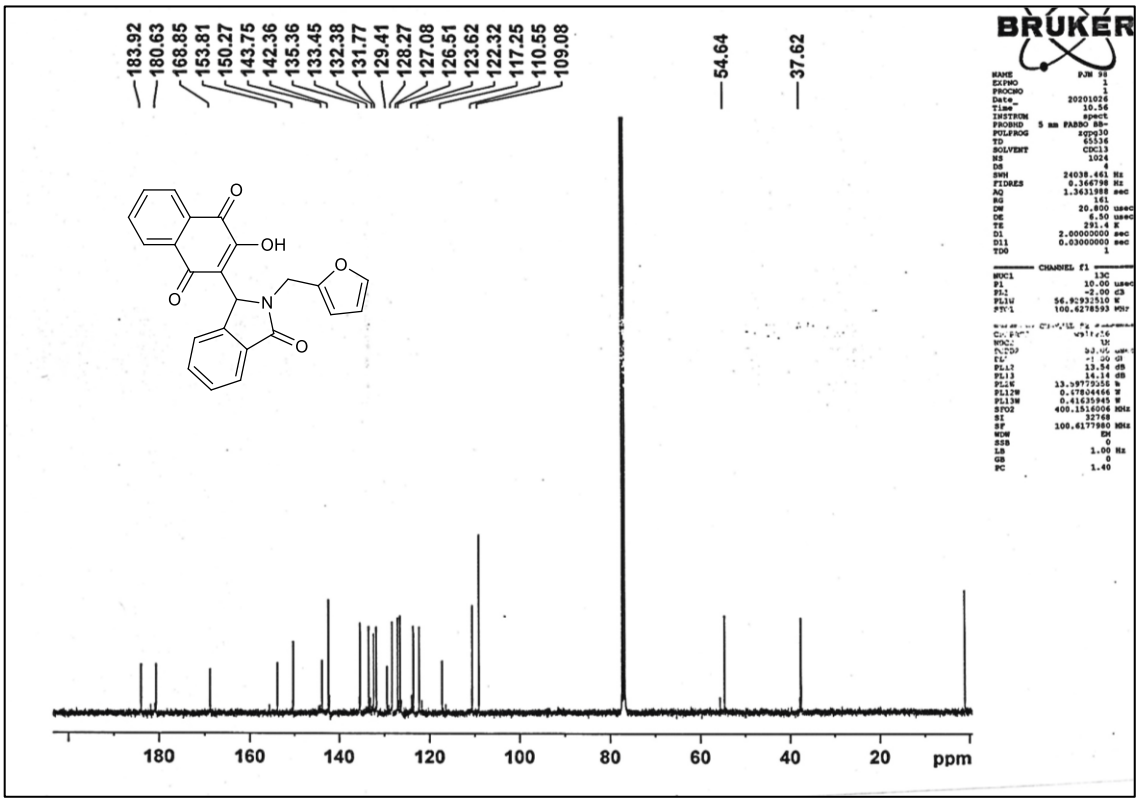

Figure S6.34 ^{13}C NMR spectra of 4i

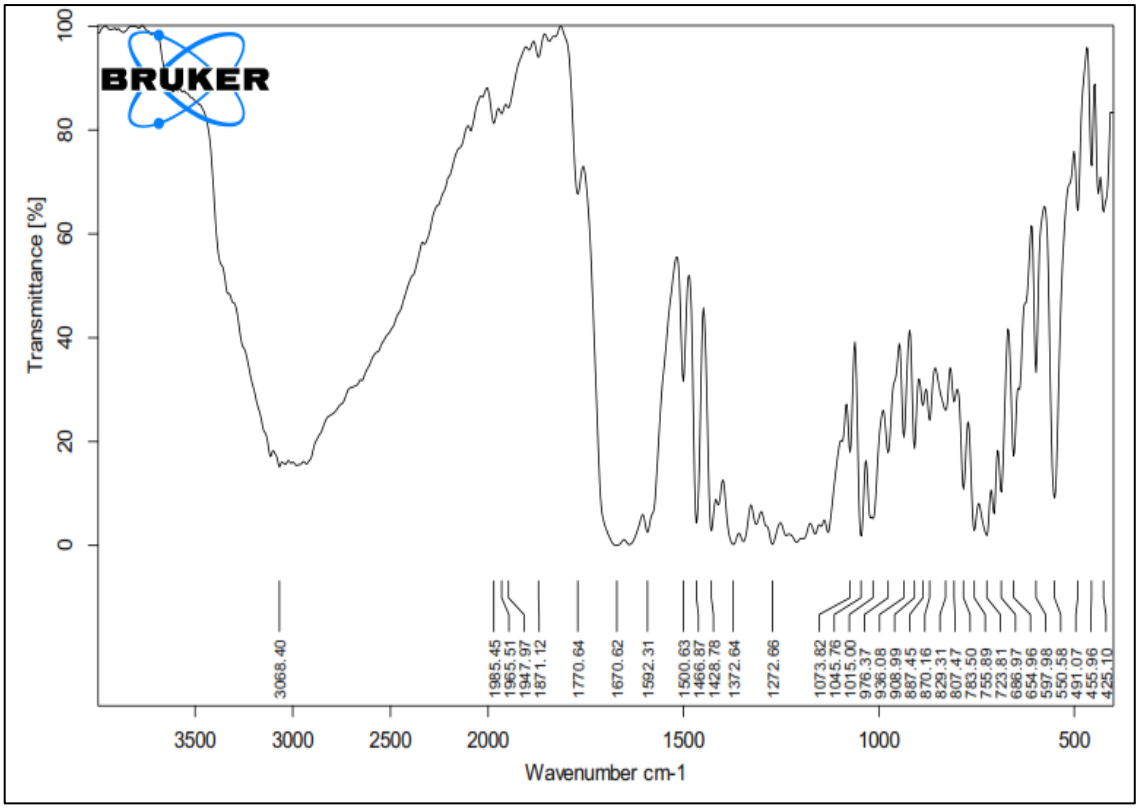

Figure S6.35 FT-IR spectra of 4i

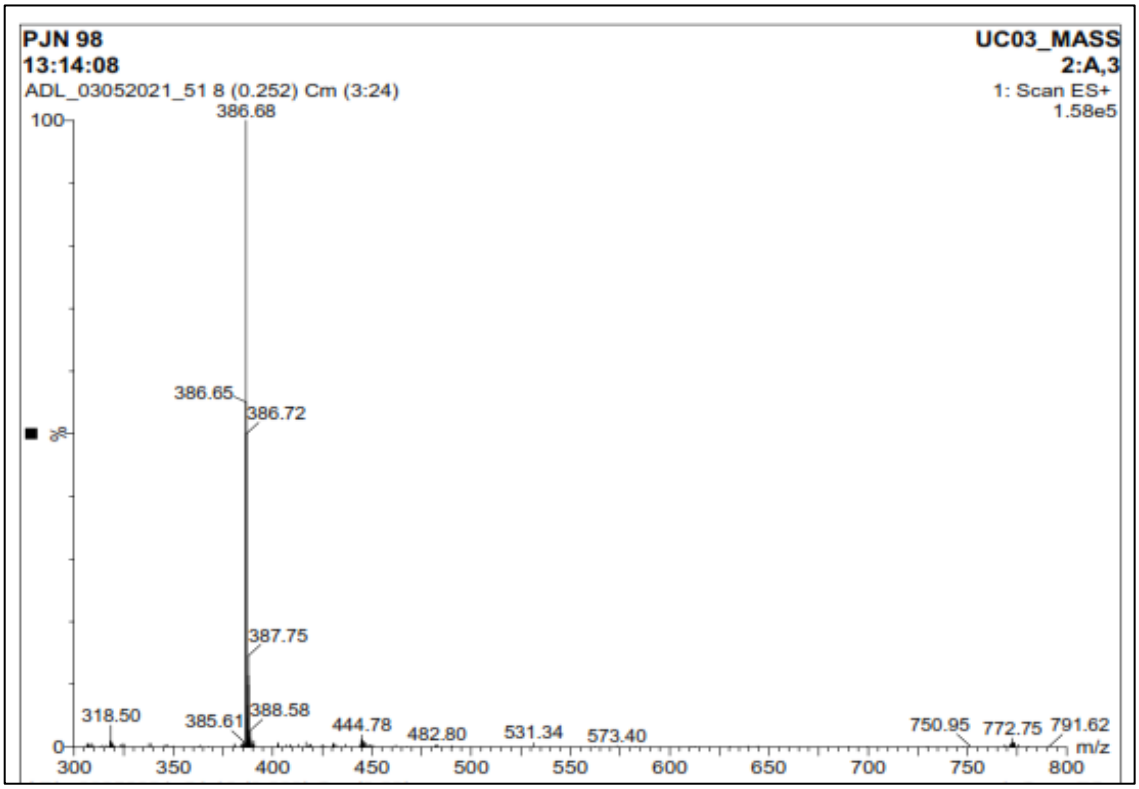

Figure S6.36 ESI-MS spectra of 4i

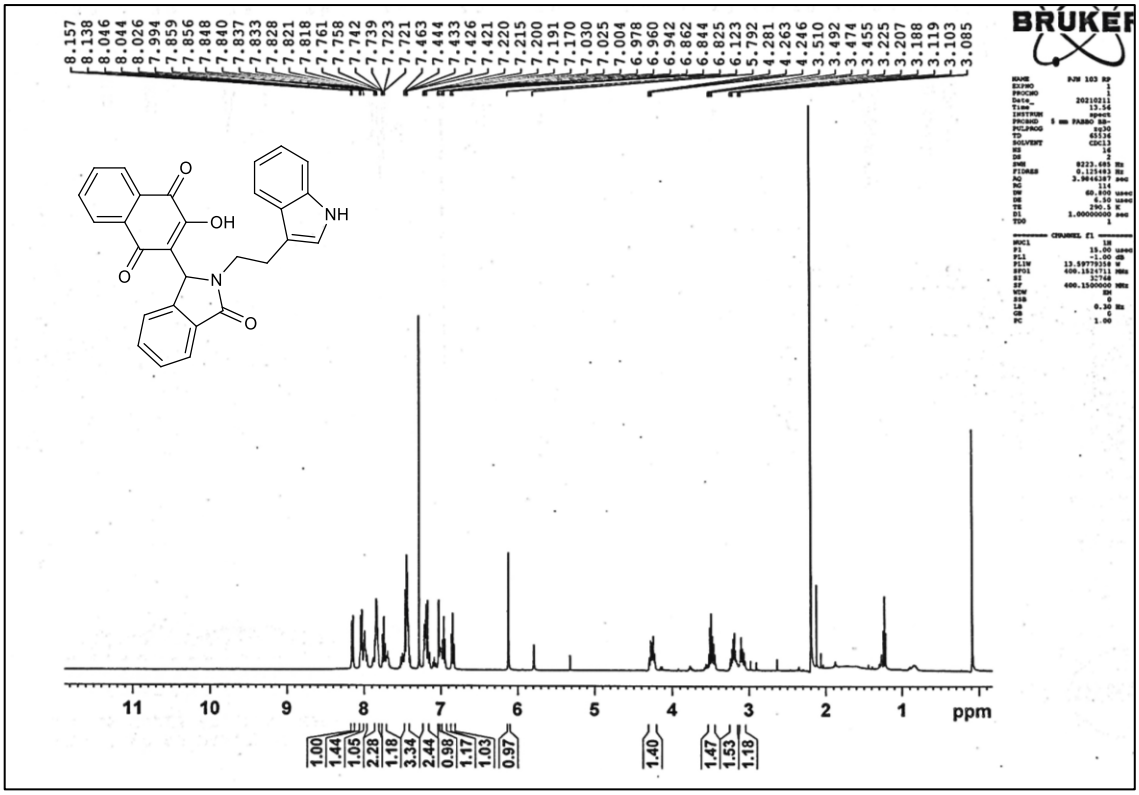

Figure S6.37: ^{1}H NMR spectra of 4j

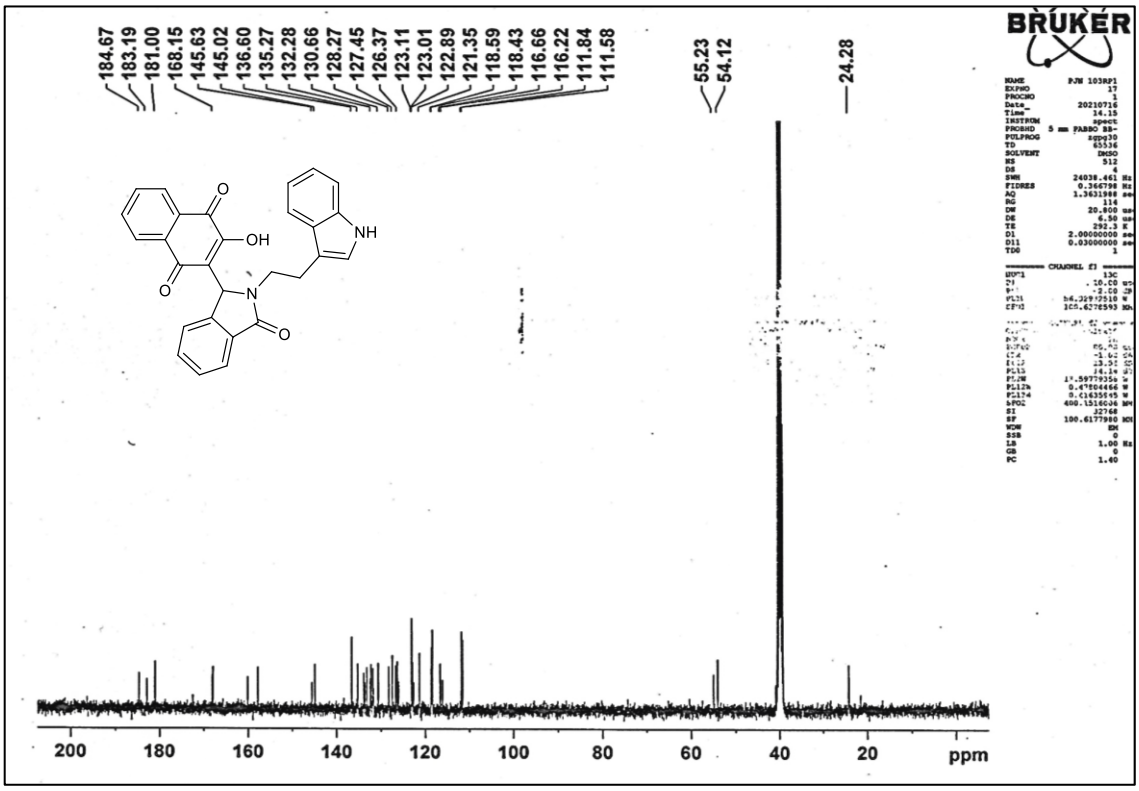

Figure S6.38 ^{13}C NMR spectra of 4j

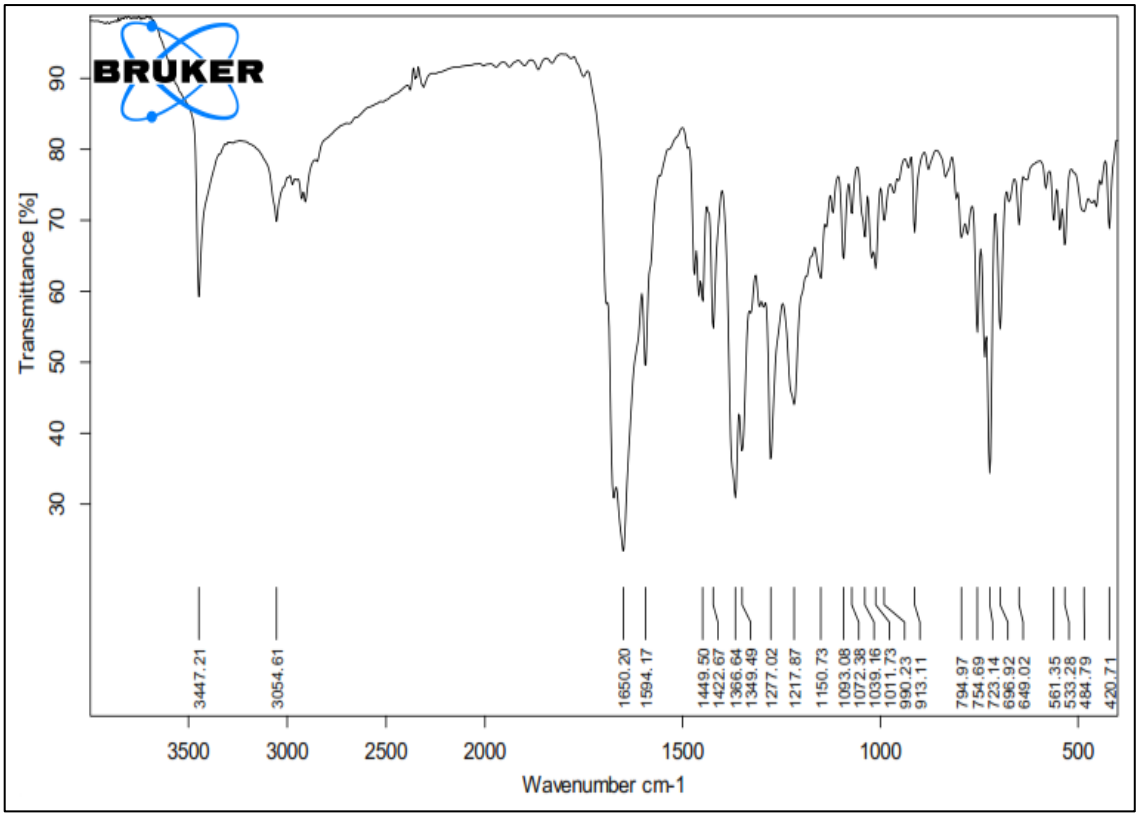

Figure S6.39 FT-IR spectra of 4j

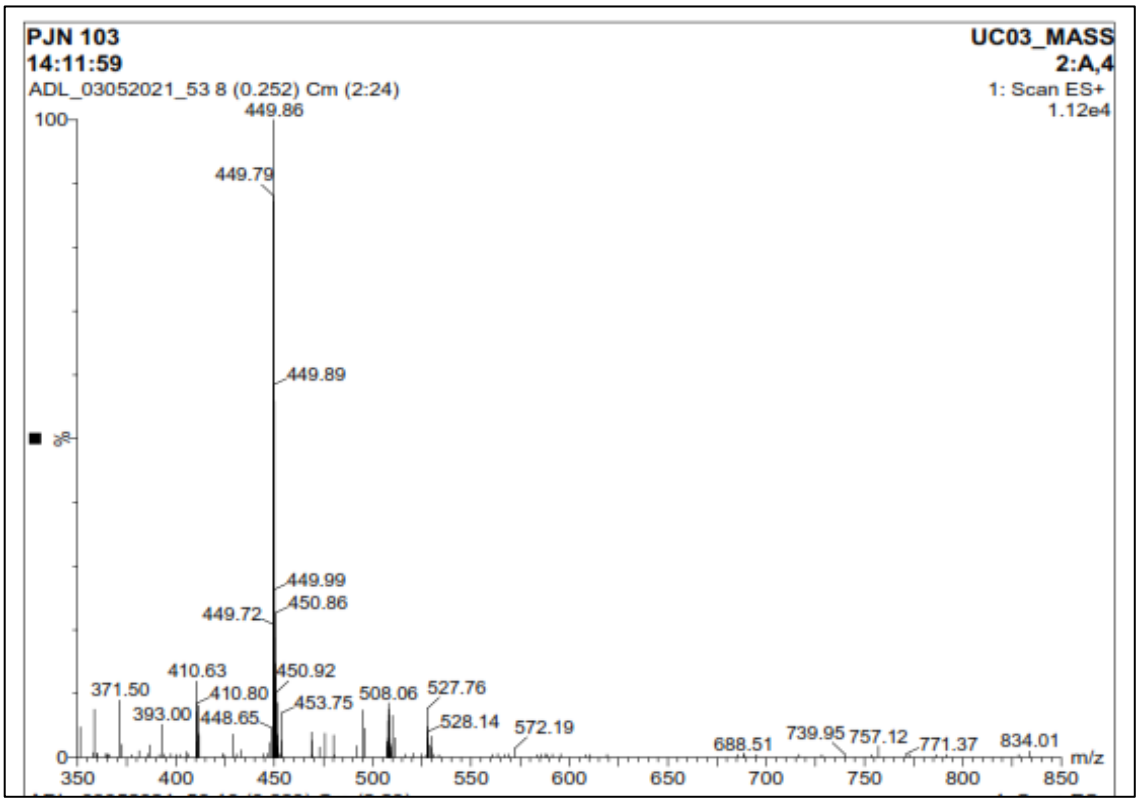

Figure S6.40 ESI-MS spectra of 4j

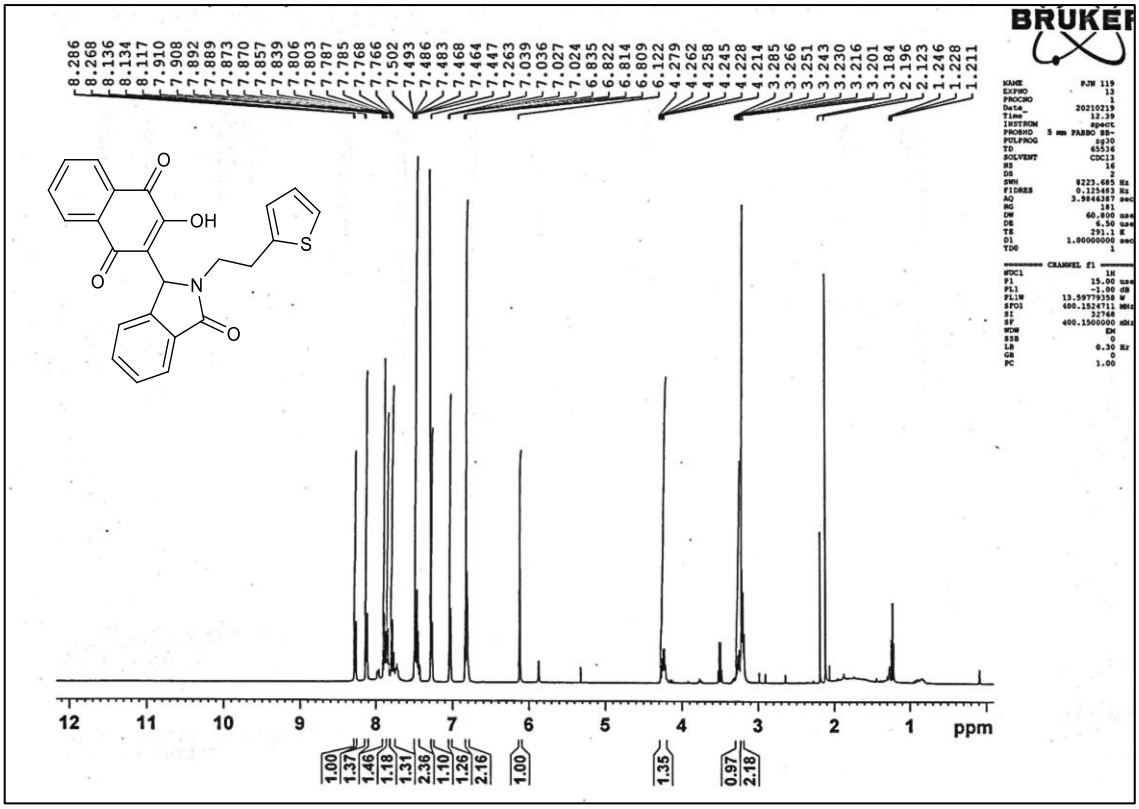

Figure S6.41 ^{1}H NMR spectra of 4k

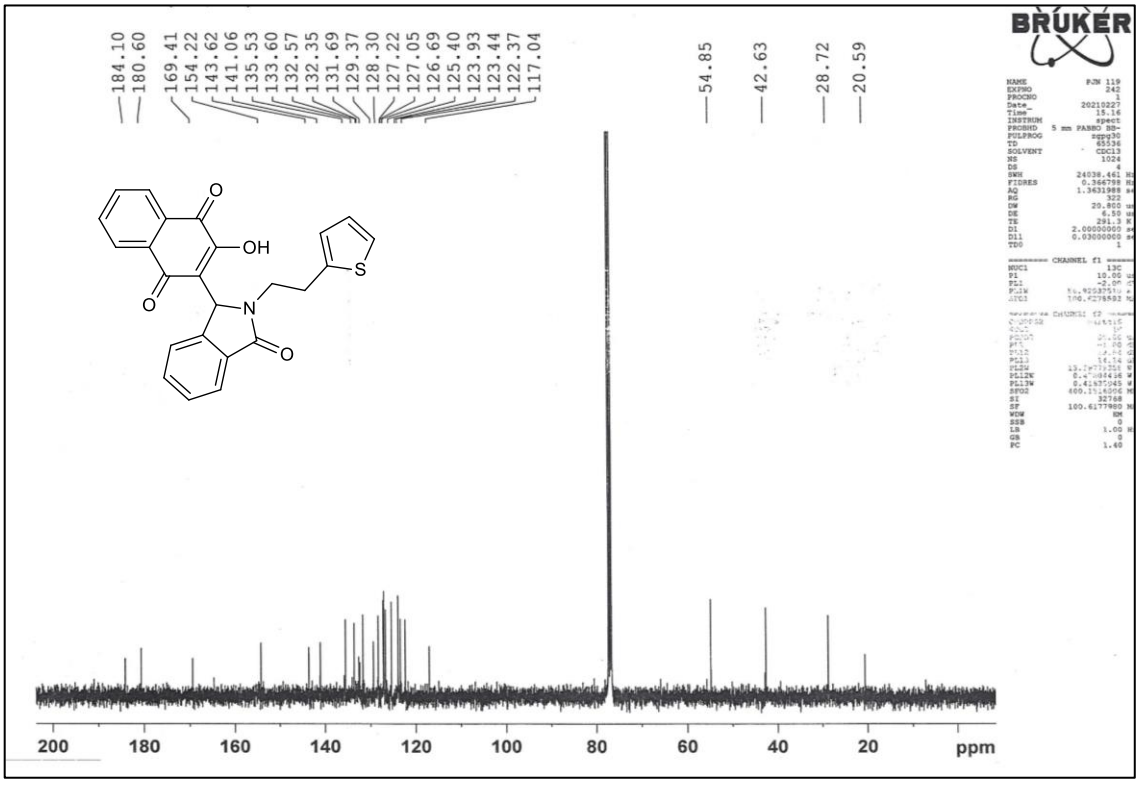

Figure S6.42 ^{13}C NMR spectra of 4k

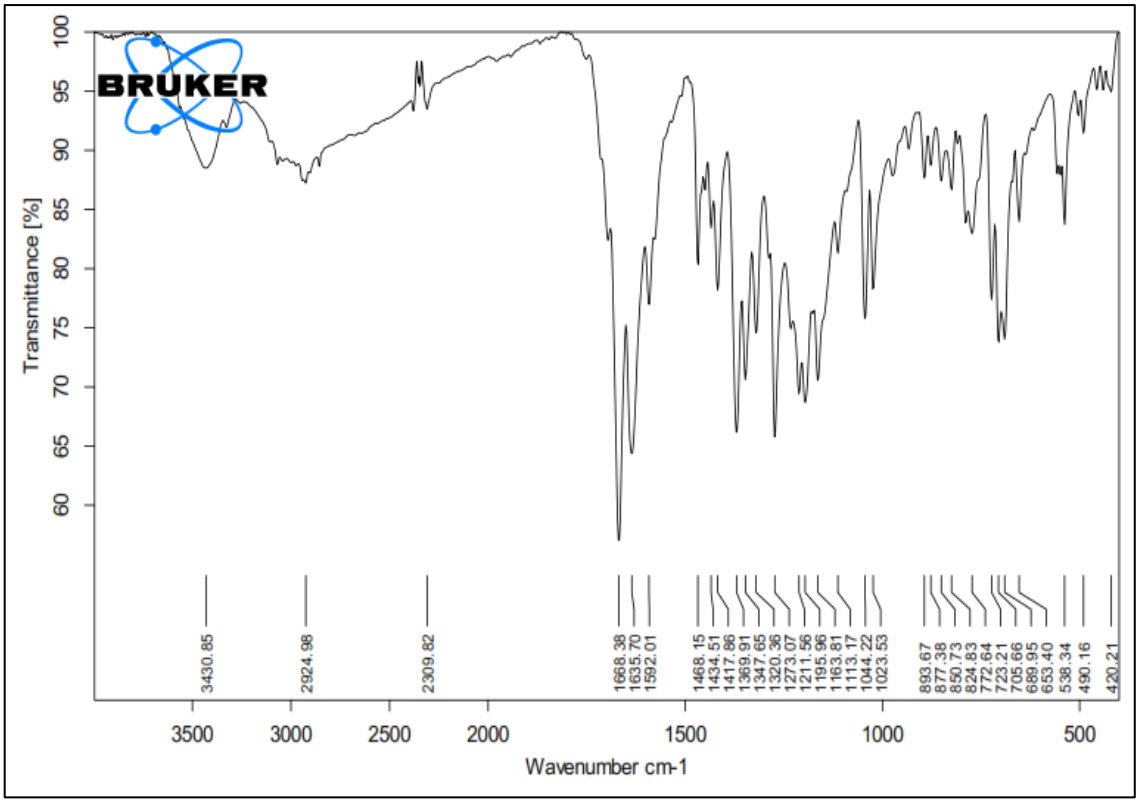

Figure S6.43 FT-IR spectra of 4k

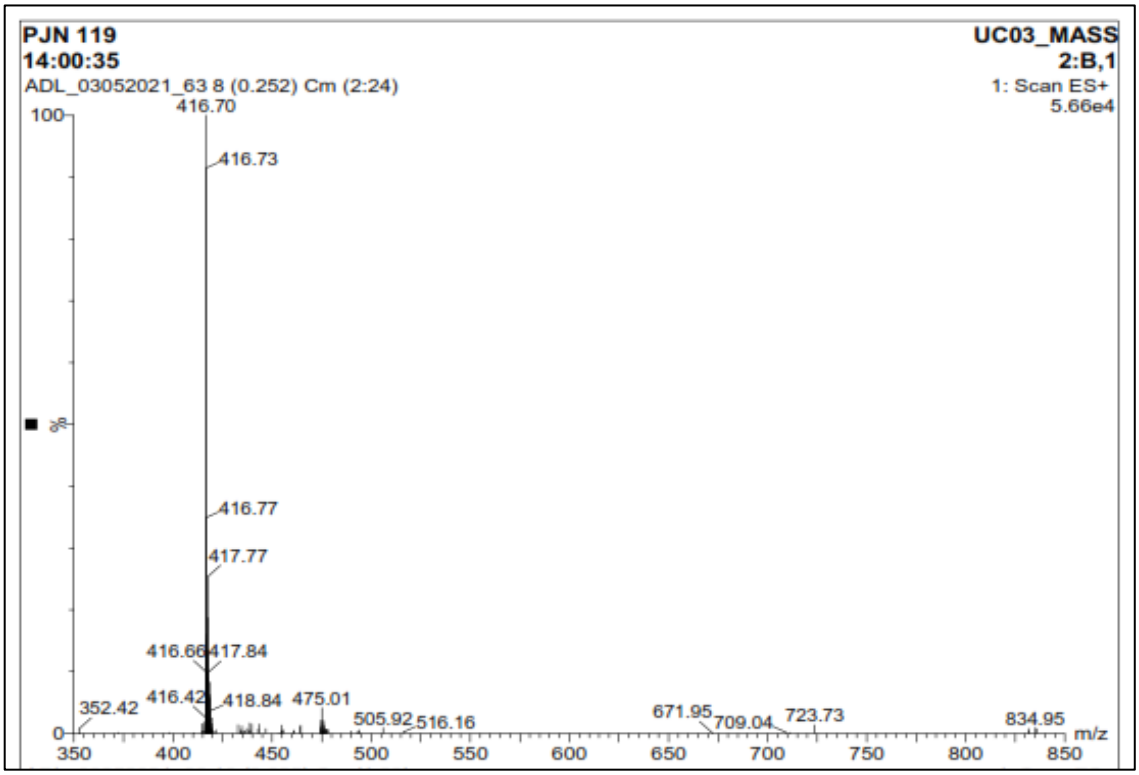

Figure S6.44 FT-IR spectra of 4k

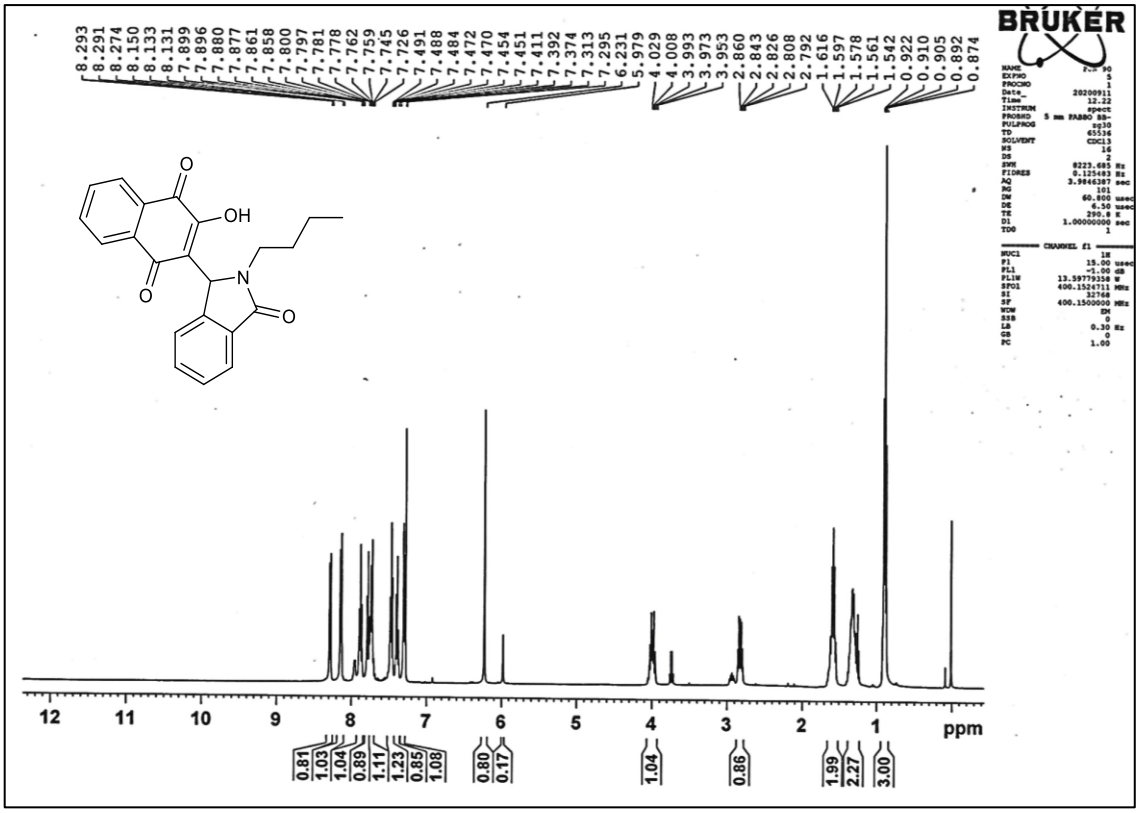

Figure S6.45 ^{1}H NMR spectra of 4l

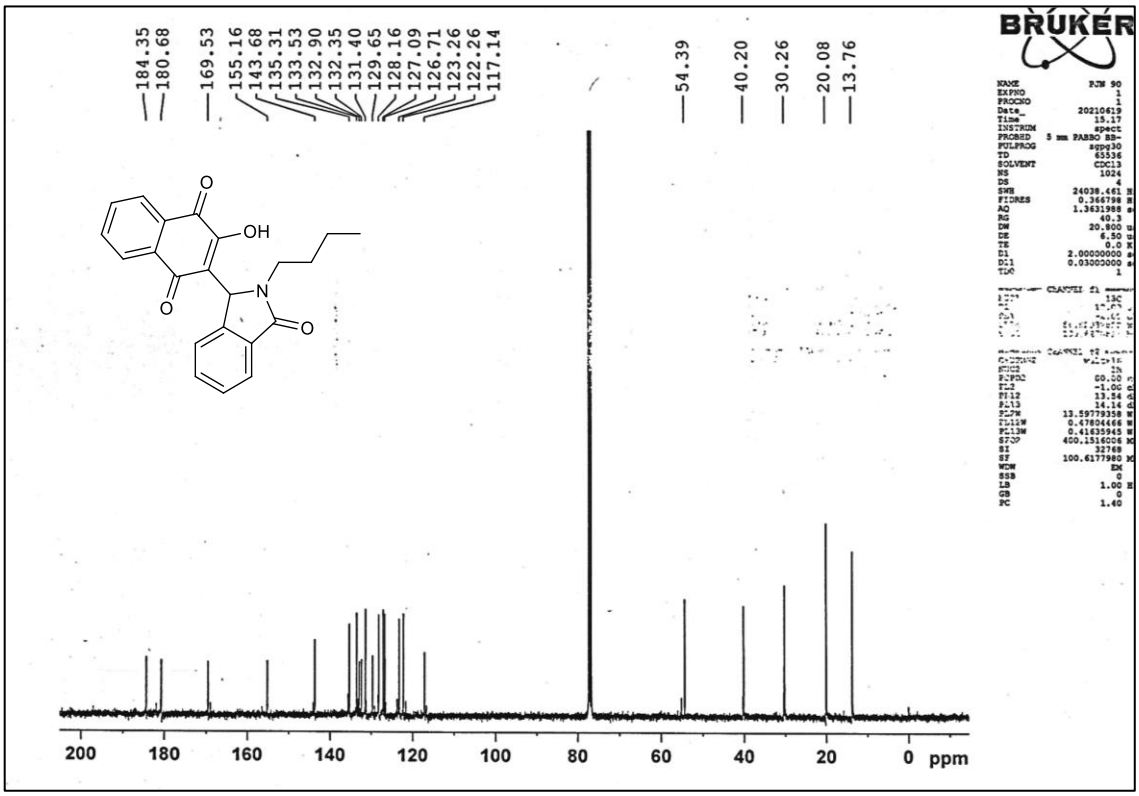

Figure S6.46 ^{13}C NMR spectra of 4l

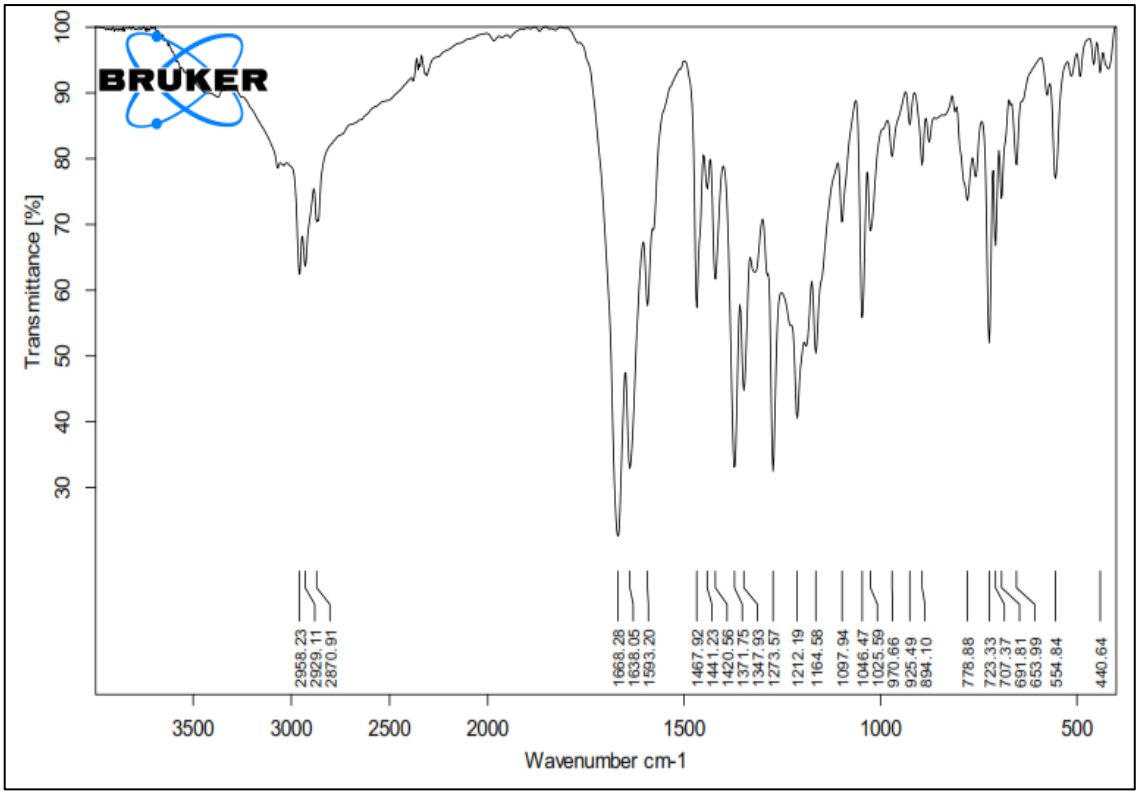

Figure S6.47 FT-IR spectra of 4l

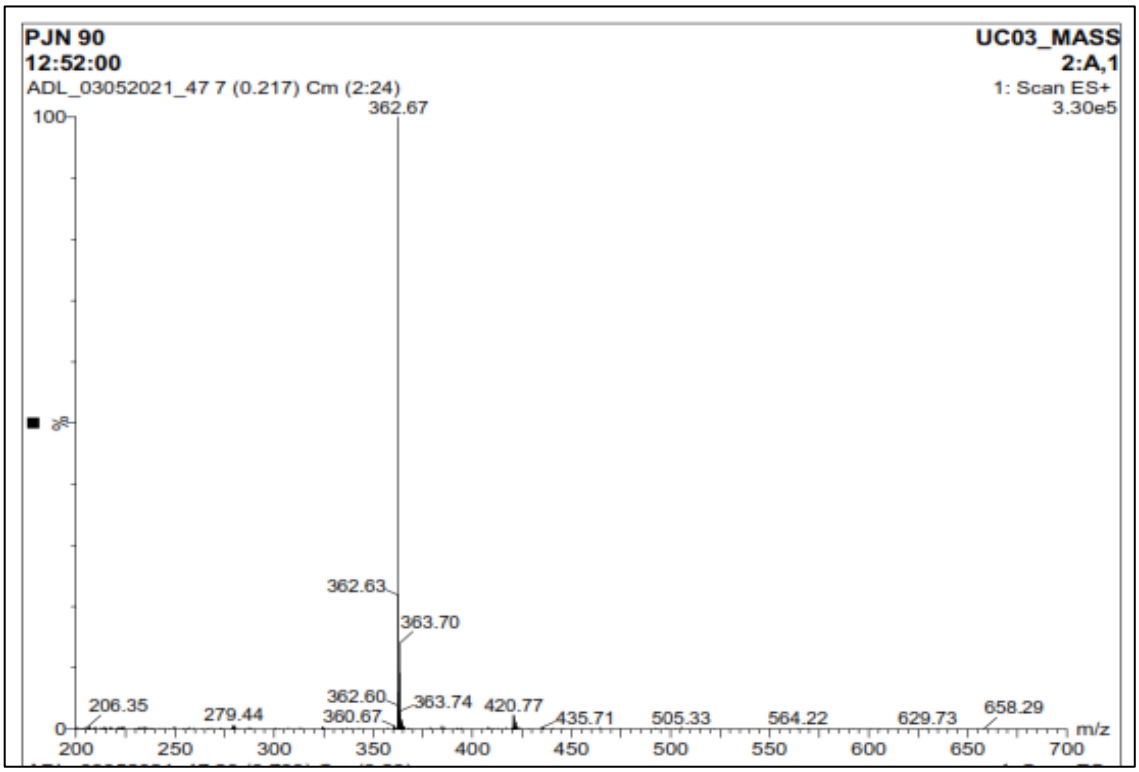

Figure S6.48 ESI-MS spectra of 4l

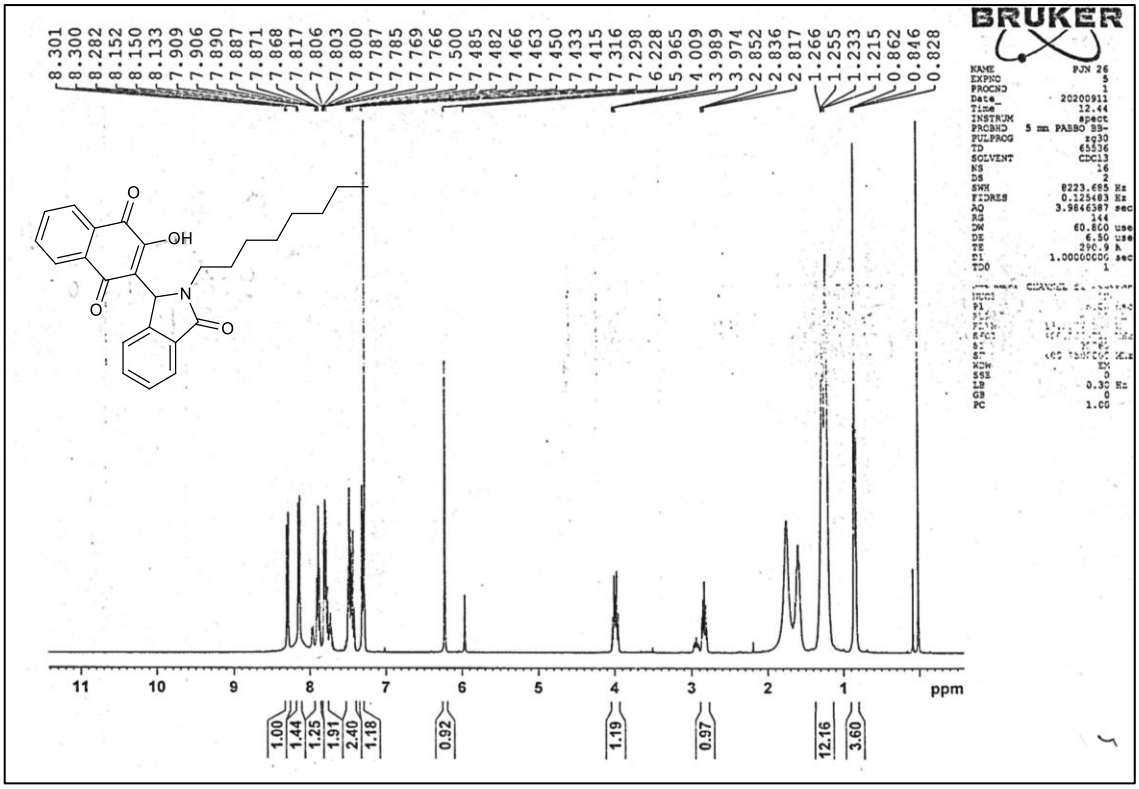

Figure S6.49 ^{1}H NMR spectra of 4m

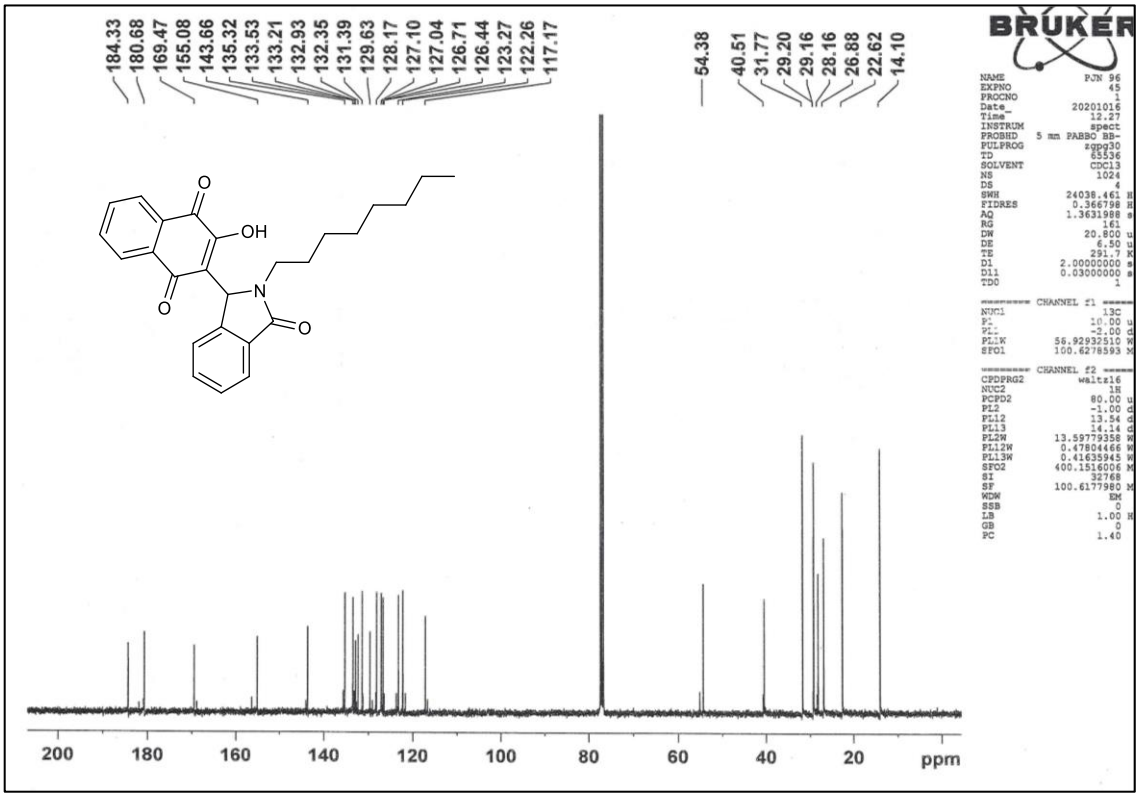

Figure S6.50 ^{13}C NMR spectra of 4m

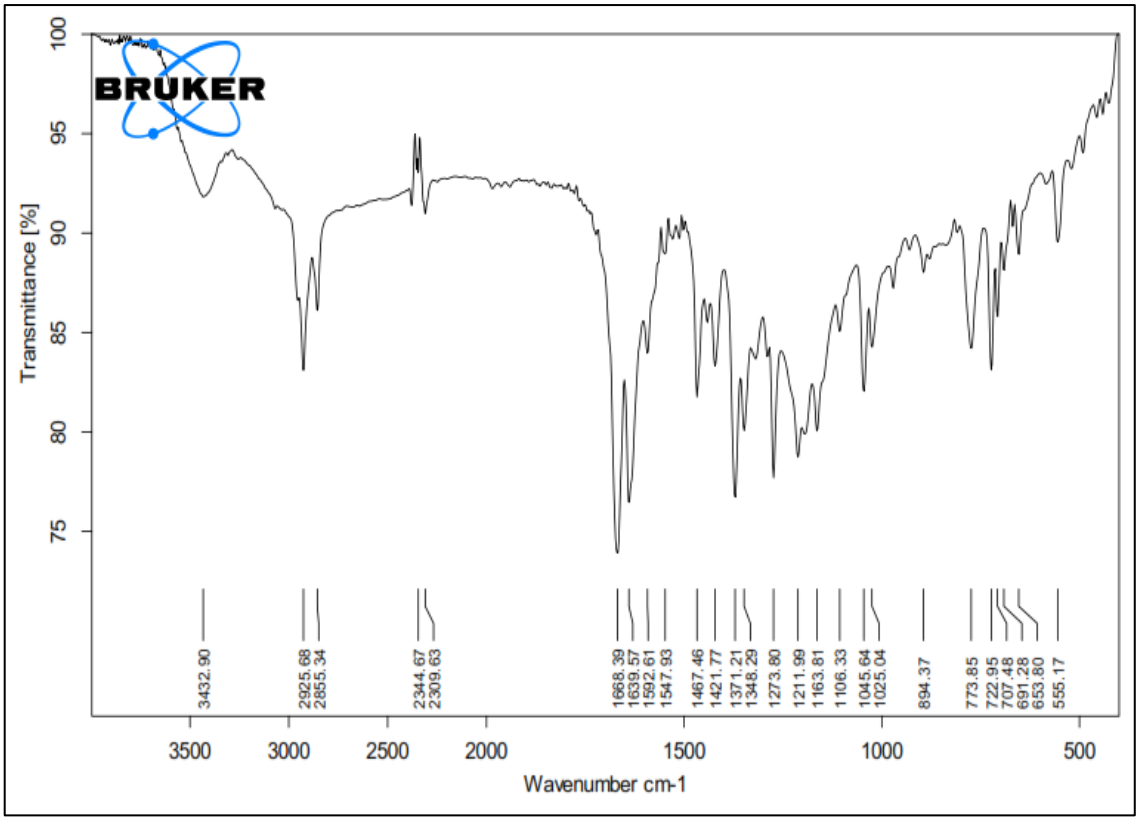

Figure S6.51 FT-IR spectra of 4m

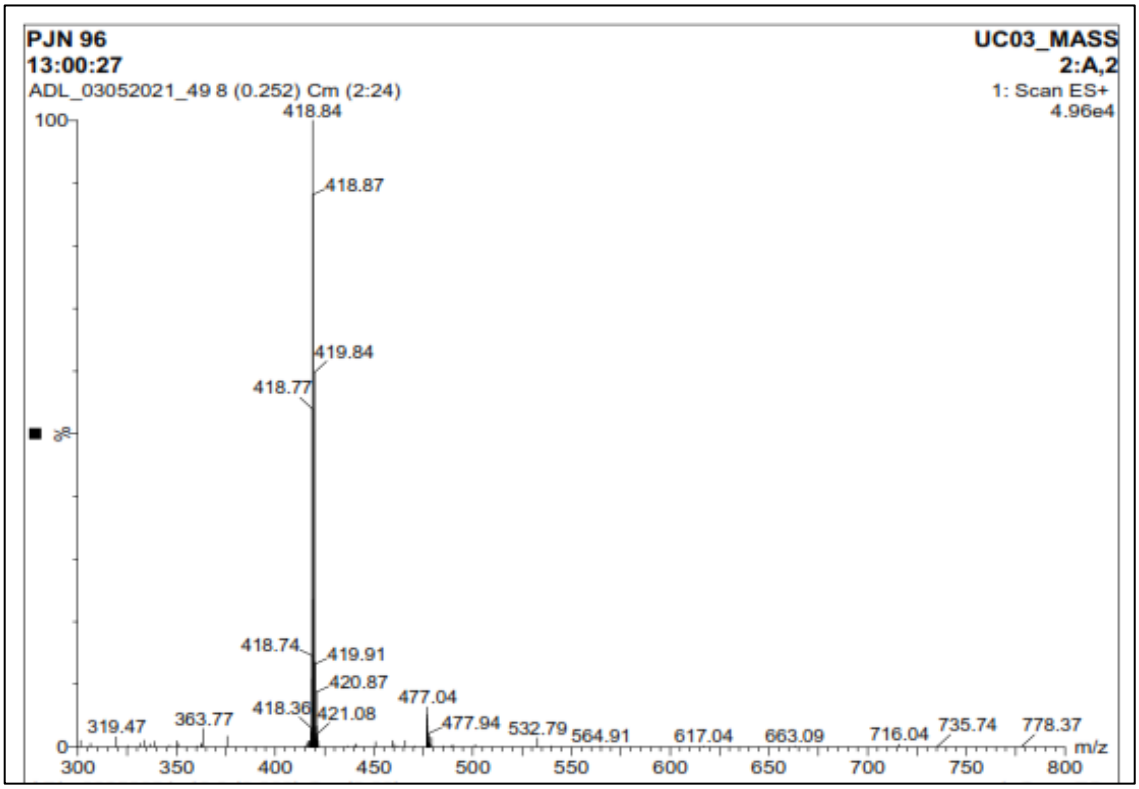

Figure S6.52 ESI-MS spectra of 4m

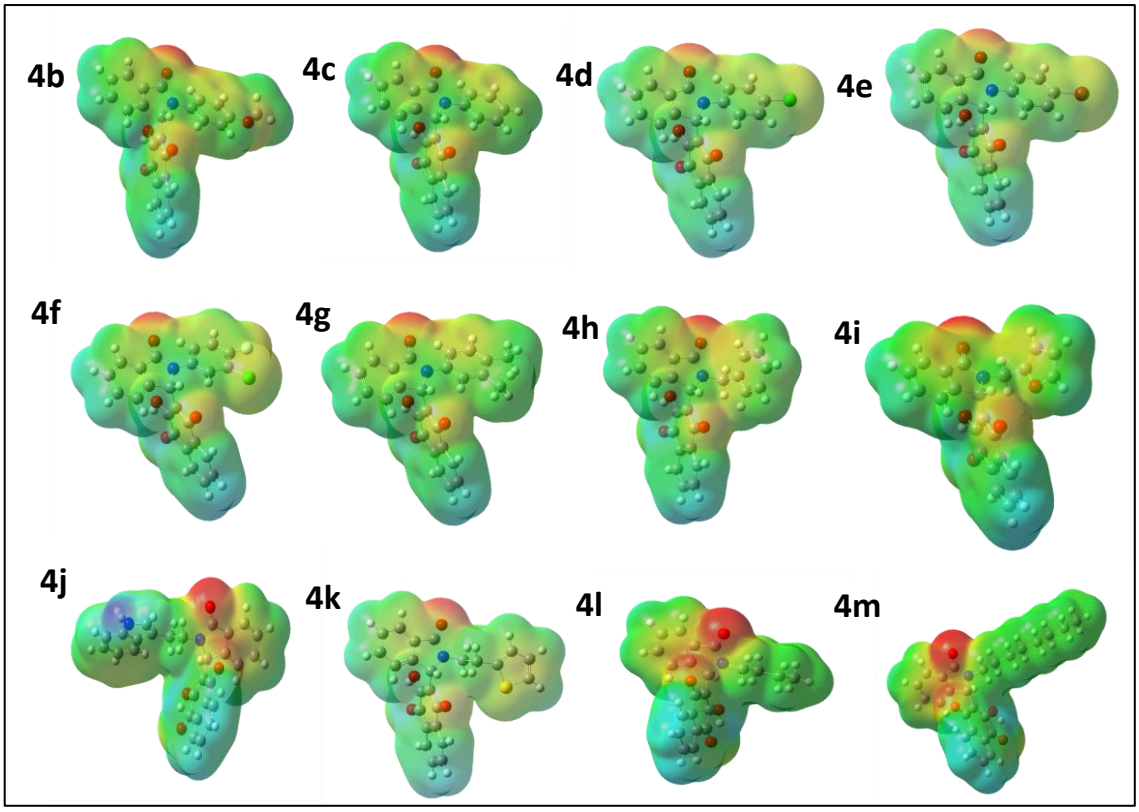

Figure S6.53 MEP surface diagram of 4b-4m.

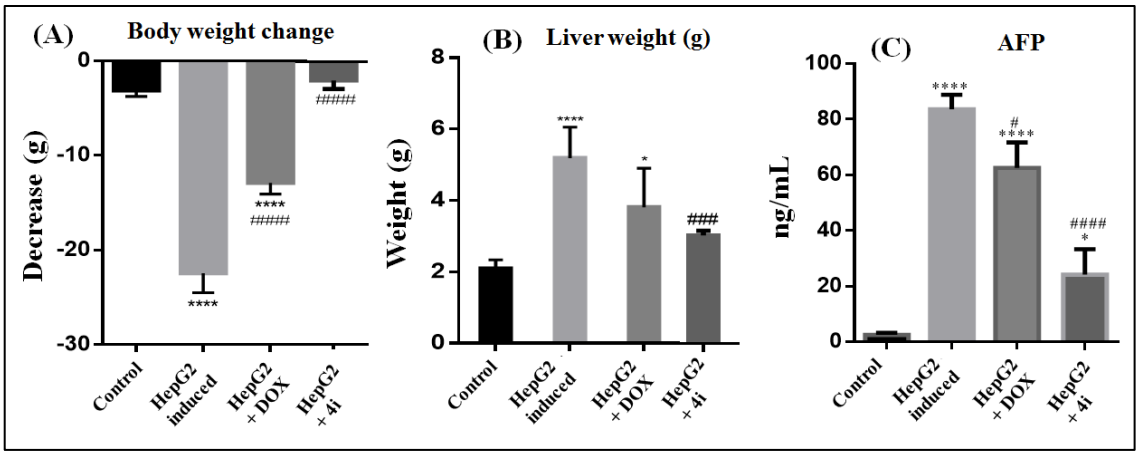

Figure S6.54 (A) changes in body weight, (B) weight of the liver and (C) AFP profile observed in animals.

Table S5.1 HOMO, LUMO, energy gap, global electronegativity, global hardness and softness, global electrophilicity index and dipole moment of 4b-4m.

Parameters	B3LYP/6-31G (d, p) (eV)											
	4b	**4c**	**4d**	**4e**	**4f**	**4g**	**4h**	**4i**	**4j**	**4k**	**4l**	**4m**
HOMO	-5.244	-5.711	-5.808	-5.776	-5.911	-5.48	-6.222	-5.983	-5.325	-5.931	-6.187	-6.179
LUMO	-3.384	-3.42	-3.519	-3.518	-3.522	-3.396	-3.419	-3.326	-3.335	-3.421	-3.354	-3.352
ΔE	-1.859	-2.291	-2.289	-2.258	-2.389	-2.084	-2.803	-2.656	-1.989	-2.509	-2.833	-2.828
Ionization potential (I)	5.244	5.711	5.808	5.776	5.911	5.48	6.222	5.983	5.325	5.931	6.187	6.179
Electron affinity (A)	3.384	3.42	3.519	3.518	3.522	3.396	3.419	3.326	3.335	3.421	3.354	3.352
Chemical potential (μ)	-4.314	-4.5655	-4.663	-4.647	-4.7165	-4.438	-4.8205	-4.6545	-4.33	-4.676	-4.7705	-4.7655
Hardness (η)	0.93	1.1455	1.144	1.129	1.1945	1.042	1.4015	1.3285	0.995	1.255	1.4165	1.4135
Electronegativity (χ)	4.314	4.5655	4.663	4.647	4.7165	4.438	4.8205	4.6545	4.33	4.676	4.7705	4.7655
Softness (S)	0.465	0.5727	0.572	0.5645	0.5972	0.521	0.7007	0.6642	0.4975	0.6275	0.7082	0.70675
Electrophilicity index (ω)	8.653	11.938	12.44	12.190	13.286	10.261	16.283	14.390	9.327	13.720	16.118	16.050
Dipole moment (Debye)	5.498	6.331	7.262	7.23	6.657	6.367	6.216	5.723	5.436	5.783	5.867	5.832

Table S5.2 Physicochemical Properties of the compounds 4a-4m

Comp. No.	Fraction C SP^3 [a]	No. of rotatable bond	HBA [b]	HBD [c]	*i* log P [d]	Molar refractivity	Log S [e]	TPSA [f]
4a	0.08	2	4	1	2.80	115.20	PS	74.68
4b	0.08	3	5	1	2.89	116.73	PS	83.91
4c	0.04	2	4	1	2.55	110.24	PS	74.68
4d	0.04	2	4	1	2.90	115.25	PS	74.68
4e	0.04	2	4	1	2.95	117.94	PS	74.68
4f	0.04	2	5	1	2.88	115.21	PS	74.68
4g	0.12	2	4	1	2.94	120.17	PS	74.68
4h	0.08	3	4	1	2.58	114.49	PS	74.68
4i	0.09	3	5	1	2.33	106.75	PS	87.82
4j	0.11	4	4	2	2.56	131.15	PS	90.47
4k	0.12	4	4	1	2.89	117.17	PS	102.92
4l	0.23	4	4	1	2.73	104.42	PS	74.68
4m	0.35	8	4	1	3.40	123.65	PS	74.68

[a] The ratio of sp^3 hybridized carbons over the total carbon count of the molecule. [b] Number of hydrogen bond acceptors. [c] Number of hydrogen bond donors. [d] Lipophilicity. [e] Water solubility (SILICOS-IT [PS = poorly soluble]). [f] TPSA ($Å^2$).

Table S5.3 Pharmacokinetic/ADME properties of the compounds 4a-4m

Comp. No.	GI abs [a]	BBB Permeant [b]	P-gpsubstrate[c]	CYP1A2 Inhibitor [d]	CYP2C19 Inhibitor [e]	CYP2C9 Inhibitor [f]	CYP2D6 Inhibitor [g]	CYP3A4 Inhibitor [h]	Log K_p [i]
4a	high	yes	no	yes	yes	yes	no	yes	-5.90
4b	high	no	no	no	no	yes	no	yes	-6.27
4c	high	yes	no	yes	yes	yes	no	yes	-6.07
4d	high	yes	no	yes	yes	yes	no	yes	-5.83
4e	high	no	no	yes	yes	yes	no	yes	-6.06
4f	high	no	no	yes	yes	yes	no	yes	-5.87
4g	high	yes	no	no	yes	yes	no	yes	-5.72
4h	high	yes	no	yes	yes	yes	no	yes	-6.21
4i	high	no	no	yes	no	yes	no	yes	-6.78
4j	high	no	no	yes	yes	yes	no	yes	-6.11
4k	high	no	no	yes	yes	yes	no	yes	-6.20
4l	high	yes	no	yes	yes	yes	no	yes	-6.17
4m	high	no	yes	no	yes	yes	no	yes	-4.97

[a] Gastrointestinal absorption. [b] Blood brain barrier permeant. [c] P-gp substrate. [d] CYP1A2: cytochrome P450 family 1 subfamily A member 2 (PDB: 2HI4). [e] CYP2C19: cytochrome P450 family 2 subfamily C member 19 (PDB: 4GQS). [f] CYP2C9: cytochrome P450 family 2 subfamily C member 9 (PDB: 1OG2). [g] CYP2D6: cytochrome P450 family 2 subfamily D member 6 (PDB: 5TFT). [h] CYP3A4: cytochrome P450 family 3 subfamily. A member 4 (PDB: 4K9T). [i] Skin permeation in cm.

6.7 References

1. Boger, D. L., Lee, J. K., Goldberg, J. & Jin, Q. Two comparisons of the performance of positional scanning and deletion synthesis for the identification of active constituents in mixture combinatorial libraries. *J. Org. Chem.* **65**, 1467–1474 (2000).
2. Comins, D. L., Schilling, S. & Zhang, Y. Asymmetric synthesis of 3-substituted isoindolinones: Application to the total synthesis of (+)-lennoxamine. *Org. Lett.* **7**, 95–98 (2005).
3. Speck, K. & Magauer, T. The chemistry of isoindole natural products. *Beilstein J. Org. Chem.* **9**, 2048–2078 (2013).
4. Augner, D., Gerbino, D. C., Slavov, N., Neudörfl, J. M. & Schmalz, H. G. N-Capping of primary amines with 2-Acylbenzaldehydes to give isoindolinones. *Org. Lett.* **13**, 5374–5377 (2011).
5. Augner, D. *et al.* On the antibiotic and antifungal activity of pestalone, pestalachloride a, and structurally related compounds. *J. Nat. Prod.* **76**, 1519–1522 (2013).
6. Lawrence, N. J., Liddle, J., Bushell, S. M. & Jackson, D. A. A three-component coupling process based on vicarious nucleophilic substitution (VNSAR)-alkylation reactions: An approach to indoprofen and derivatives. *J. Org. Chem.* **67**, 457–464 (2002).
7. Riedinger, C. *et al.* Analysis of chemical shift changes reveals the binding modes of isoindolinone inhibitors of the MDM2-p53 interaction. *J. Am. Chem. Soc.* **130**, 16038–16044 (2008).
8. Zhuang, Z., Kung, M., Mu, M. & Kung, H. F. Isoindol-1-one Analogues of 4- (2 ′ -methoxyphenyl) -1- [2 ′ - [N - (2 ″ -pyridyl) - p -iodobenzamido] ethyl] piperazine (p -MPPI) as 5-HT 1A Receptor Ligands. **2623**, 157–166 (1998).
9. Sovic, I. *et al. Novel phenyl and pyridyl substituted derivatives of isoindolines: Synthesis, antitumor activity and DNA binding features*. *European Journal of Medicinal Chemistry* vol. 87 (Elsevier Ltd, 2014).
10. Tian, Y. *et al.* Catalyst-free Mannich-type reactions in water: Expedient synthesis of naphthol-substituted isoindolinones. *Tetrahedron Lett.* **59**, 1454–1457 (2018).
11. Qian, B. *et al.* Palladium-Catalyzed Benzylic Addition of 2-Methyl Azaarenes to N -Sulfonyl Aldimines via C - H Bond Activation in furnishing the subsequent

nucleophilic addition . 1 Recent studies have alternative method for generating R - M intermediates , which have be. *J. Am. Chem. Soc.* **132**, 3650–3651 (2010).

12. Xia, C., White, A. J. P. & Hii, K. K. M. Synthesis of Isoindolinones by Pd-Catalyzed Coupling between N-Methoxybenzamide and Styrene Derivatives. *J. Org. Chem.* **81**, 7931–7938 (2016).
13. Wrigglesworth, J. W., Cox, B., Lloyd-Jones, G. C. & Booker-Milburn, K. I. New heteroannulation reactions of N-Alkoxybenzamides by Pd(II) Catalyzed C-H activation. *Org. Lett.* **13**, 5326–5329 (2011).
14. Dutta, M., Mandal, S. M., Pegu, R. & Pratihar, S. PdII/AgI-Catalyzed Room-Temperature Reaction of γ-Hydroxy Lactams: Mechanism, Scope, and Antistaphylococcal Activity. *J. Org. Chem.* **82**, 2193–2198 (2017).
15. Li, D. D., Yuan, T. T. & Wang, G. W. Synthesis of isoindolinones via palladium-catalyzed C-H activation of N-methoxybenzamides. *Chem. Commun.* **47**, 12789–12791 (2011).
16. Sashidhara, K. V., Singh, L. R., Palnati, G. R., Avula, S. R. & Kant, R. A Catalyst-Free One-Pot Protocol for the Construction of Substituted Isoindolinones under Sustainable Conditions. *Synlett* **27**, 2384–2390 (2016).
17. Tian, Y., Sun, J., Zhang, K., Li, G. & Xu, F. Catalyst-Free Synthesis of 3-(2-Quinolinemethylene)-Substituted Isoindolinones in Water. *Synth.* **50**, 2255–2265 (2018).
18. Rotstein, B. H., Zaretsky, S., Rai, V. & Yudin, A. K. Small heterocycles in multicomponent reactions. *Chem. Rev.* **114**, 8323–8359 (2014).
19. Cioc, R. C., Ruijter, E. & Orru, R. V. A. Multicomponent reactions: Advanced tools for sustainable organic synthesis. *Green Chem.* **16**, 2958–2975 (2014).
20. Tian, Y., Wei, J., Wang, M., Li, G. & Xu, F. Hantzsch ester triggered metal-free cascade approach to isoindolinones. *Tetrahedron Lett.* **59**, 1866–1870 (2018).
21. Chen, T. & Cai, C. An efficient approach to 3-oxoisoindoline-1-difluoroalkyl derivatives via a metal triflate-catalyzed Mannich/lactamization cascade reaction. *New J. Chem.* **41**, 2519–2522 (2017).
22. Nariya, P., Shukla, F., Vyas, H., Devkar, R. & Thakore, S. Synthesis, characterization, DNA/BSA binding and cytotoxicity studies of Mononuclear Cu(II) and V(IV) complexes of Mannich bases derived from Lawsone. *J. Mol. Struct.* **1248**, 131508 (2022).
23. Nariya, P., Shukla, F., Vyas, H., Devkar, R. & Thakore, S. Synthesis and

characterization of Mannich bases of lawsone and their anticancer activity. *Synth. Commun.* **50**, 1724–1735 (2020).

24. Daina, A., Michielin, O. & Zoete, V. SwissADME: A free web tool to evaluate pharmacokinetics, drug-likeness and medicinal chemistry friendliness of small molecules. *Sci. Rep.* **7**, 1–13 (2017).
25. Al Sheikh Ali, A. *et al.* Design, Synthesis, Molecular Modeling, Anticancer Studies, and Density Functional Theory Calculations of 4-(1,2,4-Triazol-3-ylsulfanylmethyl)-1,2,3-triazole Derivatives. *ACS Omega* **6**, 301–316 (2021).
26. Hussein, Y. T. & Azeez, Y. H. DFT analysis and in silico exploration of drug-likeness, toxicity prediction, bioactivity score, and chemical reactivity properties of the urolithins. *J. Biomol. Struct. Dyn.* **0**, 1–10 (2021).
27. Khalid, M. *et al.* An Efficient Synthesis, Spectroscopic Characterization, and Optical Nonlinearity Response of Novel Salicylaldehyde Thiosemicarbazone Derivatives. *ACS Omega* **6**, 16058–16065 (2021).
28. Ricardo, M. *et al.* Phytochemistry In vitro cytotoxicity and structure-activity relationship approaches of ent - kaurenoic acid derivatives against human breast carcinoma cell line. *Phytochemistry* **156**, 214–223 (2018).
29. Rachedi, K. *et al.* Synthesis, DFT and POM analyses of cytotoxicity activity of α-amidophosphonates derivatives: Identification of potential antiviral O,O-pharmacophore site. *J. Mol. Struct.* (2019) doi:10.1016/j.molstruc.2019.07.053.
30. Ali, M. S., Farah, M. A., Al-lohedan, H. A. & Al-anazi, K. M. activities of procaine and its binding with calf modelling study †. 9083–9093 (2018) doi:10.1039/c7ra13647a.
31. Joshi, R. *et al.* Synthesis, spectroscopic characterization, DFT studies and antifungal activity of (E)-4-amino-5-[N'-(2-nitro-benzylidene)-hydrazino]-2,4-dihydro-[1,2,4]triazole-3-thione. *J. Mol. Struct.* (2018) doi:10.1016/j.molstruc.2018.03.081.
32. Hagar, M., Ahmed, H. A. & Alnoman, R. Mesophase behavior and DFT conformational analysis of new symmetrical diester chalcone liquid crystals. *J. Mol. Liq.* (2019) doi:10.1016/j.molliq.2019.04.083.
33. Kumar, S. S., Athimoolam, S. & Sridhar, B. Structural, spectral, theoretical and anticancer studies on new co-crystal of the drug 5- Fluorouracil. *J. Mol. Struct.* (2018) doi:10.1016/j.molstruc.2018.07.079.
34. Khodair, A. I., Awad, M. K., Gesson, J. & Elshaier, Y. A. M. M. New N -ribosides

and N -mannosides of rhodanine derivatives with anticancer activity on leukemia cell line : Design , synthesis , DFT and molecular modelling studies. *Carbohydr. Res.* **487**, 107894 (2020).

35. Grover, M., Singh, B., Bakshi, M. & Singh, S. Quantitative structure – property relationships in pharmaceutical research – Part 1. **3**, (2000).
36. Abdel-Rahman, L. H. *et al.* Synthesis, spectral characterization, DFT calculations, pharmacological studies, CT-DNA binding and molecular docking of potential N, O-multidentate chelating ligand and its VO(II), Zn(II) and ZrO(II) chelates. *Bioorg. Chem.* **114**, 105106 (2021).
37. El-Azab, A. S. *et al.* DFT and experimental (FT-IR and FT-Raman) investigation of vibrational spectroscopy and molecular docking studies of 2-(4-oxo-3-phenethyl-3,4-dihydroquinazolin-2-ylthio)-N-(3,4,5-trimethoxyphenyl) acetamide. *J. Mol. Struct.* **1113**, 133–145 (2016).
38. Solomon, R. V., Bella, A. P., Vedha, S. A. & Venuvanalingam, P. Designing benzosiloles for better optoelectronic properties using DFT & TDDFT approaches. *Phys. Chem. Chem. Phys.* **14**, 14229–14237 (2012).
39. Parr, R. G., Szentpály, L. V. & Liu, S. Electrophilicity index. *J. Am. Chem. Soc.* **121**, 1922–1924 (1999).
40. Devi, K. S. *et al.* Synthesis, spectra, electronic structure, molecular docking and cytotoxicity investigation on 2-(piperidin-1-ylmethyl)-isoindoline-1,3-dione – A Mannich base system. *J. Mol. Struct.* **1224**, (2021).
41. Khalid, M. *et al.* First principles study of electronic and nonlinear optical properties of A–D–p–A and D–A–D–p–A configured compounds containing novel quinoline–carbazole derivatives. *RSC Adv.* **10**, 22273–22283 (2020).
42. Khalid, M. *et al.* An efficient synthesis, structural (SC-XRD) and spectroscopic (FTIR, 1HNMR, MS spectroscopic) characterization of novel benzofuran-based hydrazones: An experimental and theoretical studies. *J. Mol. Struct.* **1216**, 1–12 (2020).
43. Deghady, A. M. Density Functional Theory and Molecular Docking Investigations of the Chemical and Antibacterial Activities for 1-(4-Hydroxyphenyl)-3-phenylprop-2-en-1-one. *molecules* **26**, (2021).
44. Murugavel, S., Ravikumar, C., Jaabil, G. & Alagusundaram, P. Synthesis, crystal structure analysis, spectral investigations (NMR, FT-IR, UV), DFT calculations, ADMET studies, molecular docking and anticancer activity of 2-(1-benzyl-5-

methyl-1H-1,2,3-triazol-4-yl)-4-(2-chlorophenyl)-6-methoxypyridine – A novel poten. *J. Mol. Struct.* **1176**, 729–742 (2019).

45. Lipinski, C. A., Lombardo, F., Dominy, B. W. & Feeney, P. J. Experimental and computational approaches to estimate solubility and permeability in drug discovery and development settings. *Adv. Drug Deliv. Rev.* **64**, 4–17 (2012).
46. Veber, D. F. *et al.* Molecular properties that influence the oral bioavailability of drug candidates. *J. Med. Chem.* **45**, 2615–2623 (2002).
47. Egan, W. J., Merz, K. M. & Baldwin, J. J. Prediction of drug absorption using multivariate statistics. *J. Med. Chem.* **43**, 3867–3877 (2000).
48. Pascale, F., Bedouet, L., Baylatry, M., Namur, J. & Laurent, A. Comparative chemosensitivity of VX2 and HCC cell lines to drugs used in TACE. *Anticancer Res.* **35**, 6497–6504 (2015).
49. Galle, P. R. *et al.* Biology and significance of alpha-fetoprotein in hepatocellular carcinoma. *Liver Int.* **39**, 2214–2229 (2019).
50. Wang, X. & Wang, Q. Alpha-Fetoprotein and Hepatocellular Carcinoma Immunity. *Can. J. Gastroenterol. Hepatol.* **2018**, 1–8 (2018).
51. Gupta, A., Singh, P., Kamble, B., Kulkarni, A. & Joghee Nanjan Chandrasekar, M. Synthesis, Docking and Biological Evaluation of Some Novel 5-bromo-2- (5-aryl-1,3,4-thiadiazol-2-yl)isoindoline-1,3-dione Derivatives Targeting ATP-binding Site of Topoisomerase II. *Lett. Drug Des. Discov.* **9**, 668–675 (2012).
52. Llovet, J. M. *et al.* Hepatocellular carcinoma. *Nat. Rev. Dis. Prim.* **7**, (2021).
53. Morini, M. *et al.* The α3β1 integrin is associated with mammary carcinoma cell metastasis, invasion, and gelatinase B (MMP-9) activity. *Int. J. Cancer* **87**, 336–342 (2000).
54. Klopfleisch, R. Macrophage reaction against biomaterials in the mouse model – Phenotypes, functions and markers. *Acta Biomater.* **43**, 3–13 (2016).
55. El-Helby, A. G. A. *et al.* Design, synthesis, molecular modeling, in vivo studies and anticancer activity evaluation of new phthalazine derivatives as potential DNA intercalators and topoisomerase II inhibitors. *Bioorg. Chem.* **103**, 104233 (2020).
56. Kumar, A., Narayan, V., Prasad, O. & Sinha, L. Monomeric and dimeric structures, electronic properties and vibrational spectra of azelaic acid by HF and B3LYP methods. *J. Mol. Struct.* **1022**, 81–88 (2012).
57. Trott, O. & Olson, A. J. AutoDock Vina: Improving the speed and accuracy of

docking with a new scoring function, efficient optimization, and multithreading. *J. Comput. Chem.* 455–461 (2010) doi:10.1002/jcc.21334.

58. Patel, M. *et al*. Coumarin-carbazole based functionalized pyrazolines: Synthesis, characterization, anticancer investigation and molecular docking. *RSC Adv.* **11**, 27627–27644 (2021).

59. Das, M. *et al*. Carbon nanotube embedded cyclodextrin polymer derived injectable nanocarrier: A multiple faceted platform for stimulation of multi-drug resistance reversal. *Carbohydr. Polym.* **247**, 116751 (2020).